THE DETERMINATION OF AN UPPER CRUSTAL MODEL FOR THE RIO GRANDE RIFT NEAR SOCORRO, NEW MEXICO, EMPLOYING S-WAVE REFLECTIONS PRODUCED BY LOCAL MICROEARTHQUAKES

by

Eric J. Rinehart

Submitted in Partial Fulfillment of
the Requirements for the Degree of
Doctor of Geoscience

NEW MEXICO INSTITUTE OF MINING AND TECHNOLOGY

Socorro, New Mexico

July 1979

ABSTRACT

The primary purpose of this study was to determine a model of the upper crust for the Rio Grande rift near Socorro, New Mexico. To achieve this purpose, the upper surface of a known extensive magma body injected at mid-crustal levels was extensively mapped and used as a known reflector of microearthquake S-waves. The observed S to S (S_zS) reflections effected a crustal velocity structure and accurate microearthquake depths of focus. These and other geophysical observations were combined into a consistent crustal model.

Reflection data came primarily from a very local microearthquake study, initiated in May, 1975, that used a five to eight station movable seismic network and provided both analog and high quality digital seismograms. From 316 recording days, 99 individual shocks which were laterally located to within ±0.5 km (s.d.) allowed mapping of 214 unmistakable S_zS reflection points. The least squares inversion location program employed a homogeneous half-space having a 5.8 km/sec P-wave velocity and a 3.35 km/sec S-wave velocity. Station corrections were derived and applied to every arrival time; corrections account for the diversity in the local near surface geology and ranged from +0.28 to -0.20 second.

The impulsive nature of the S_zS and the S to P reflections (S_zP), the single energy pulse recorded for many S_zP phases and the identical frequency contents of both the direct S-wave and the S_zS reflections indicate that the upper surface of the magma body is singular and sharp to S-wave energy. S_zP/S_zS amplitude ratios indicate that the material beneath the discontinuity has very little rigidity. Specific values of impedances cannot be estimated. Other evidence indicates that the magma is probably basaltic. S_zS reflection points show that the magma body is continuous

and has, when deep P-wave reflection data are included, an areal extent of at least 1700 km^2. The body extends from 10 km south of Socorro to possibly more than 50 km to the north. Data do not indicate more than 0.8 km of surface relief and to a first approximation it is horizontal. It lies beneath surface rift structures having as much as 3 to 5 km of displacement.

S_zS reflection travel times were inverted with recording station locations and epicenter locations to determine an S-wave velocity structure. Results, assuming an horizontal magma layer, indicate that the best average crustal velocity is 3.405 ± 0.05 km/sec. Using this velocity the best depth to the magma is 19.2 ± 0.6 km. A two-layered model supported by microearthquake distributions has a velocity of 3.35 km/sec in a 10 km thick upper layer and a velocity of 3.44 ± 0.05 km/sec in a lower 9.2 km thick layer. No anisotropies have been noted; however, a six percent lower than average velocity in south central La Jencia basin was found. Data also allowed two degrees of northward dip on the magma body which places it in concordance with the Moho.

Using the final crustal velocity model, accurate depths of focus (±1.4 km) were determined for more than 150 microearthquakes. Cross sections of these hypocenters show that the seismic activity is diffusely centered over the magma body and cannot be associated with prominent faults exposed at the surface. The activity is normally distributed between 3 and 13 km in depth and is not substantially different than seismic activity found in other geothermal areas exhibiting similar tectonics.

The flat relief of the upper surface of the magma body, the S-wave velocity structure, and the hypocentral locations of the microearthquakes suggests a two-layer crustal model: (1) the first layer extends

from the surface to 10 km, has an S-wave velocity of 3.35 km/sec and allows brittle rock failure; (2) a transition zone from 10 to 13 km where the brittle upper crust changes to a ductile lower crust; and (3) the lower layer extending from 10 km to the magma body, or 19.2 km, has an S-wave velocity of 3.44 km/sec and is ductile to long-term strains. The mid-crustal position of the magma body appears to be controlled by the lower boundary of the third layer (the Conrad discontinuity).

ACKNOWLEDGEMENTS

I am very much indebted to Dr. Allan R. Sanford, who was my advisor and committee chairman, for urging the continuance of investigation of the extensive magma body. In addition, special thanks are due to him for his extensive discussions and manuscript critiques. I would also like to acknowledge the helpful suggestions and time spent on this project by the other members of my committee. They are Dr. Antonius Budding, Dr. Charles Chapin and Dr. John Schlue.

Thanks are due to the original team of graduate students, undergraduate students and technician who helped initiate and maintain the operational logistics of the seismic array. Especially valuable assistance was received from R. Mott, P. Shuleski, R. Ward, T. C. Wallace and K. West.

Special thanks are due my family for their encouragement and patience. In particular, I would like to thank my wife, Leslie, for support throughout the project and her patience in understanding the socioeconomic implications of a graduate student's wife.

The research described in this paper was sponsored jointly by the National Science Foundation (Grant Number EAR77-23166) and the Energy Resource Board of the State of New Mexico (Grant Number ERB77-2312). In addition, one year of support was generously given to me through the Gulf Oil Graduate Fellowship. Practically indefinite support was given to me by New Mexico Tech's Computer Science Department and was very much appreciated.

TABLE OF CONTENTS

Introduction	1
Purpose and Scope	1
Geological and Geophysical Background	2
Data	7
Instrumentation	7
Hypocentral Locations	10
Reflection Data	18
Other Data	18
Magma Body	20
Introduction	20
Properties of the Upper Surface	20
Lateral Extent of the Magma Body	30
Surface Relief on the Magma Body	34
Depth to the Magma Body	38
Thickness of the Magma Body	40
Inversion of S_zS Reflection Data	41
Introduction	41
Inversion Technique	41
Inversion Models	47
Discussion of the Inversion Results	64
Discussion	69
Epicenters	69
The Magma Body	77
Crustal Model	82
References	87

Appendix 1 Reflection Data 1-1

Appendix 2 Epicenters 2-1

Appendix 3 Computer Programs 3-1

Appendix 4 Outstanding Seismograms 4-1

LIST OF FIGURES

Figure		Page
1.	Physiographic provinces and the Rio Grande rift in New Mexico.	3
2.	Magnification response curves for the MEQ-800 seismographs using either an L4-C or Willmore geophone.	9
3.	Major physical features near Socorro.	11
4.	Two well recorded microearthquakes with clearly defined S_zP and S_zS reflections.	21
5.	Reproduction of two strong microearthquakes with clearly defined S_zP and S_zS reflections.	22
6.	Spectral density functions obtained for direct S-waves and S_zS reflections recorded at stations SC and WT.	24
7.	Observed S_zP/S_zS amplitude ratios versus angles of incidence.	28
8.	Cross section of the crust showing ray paths and distances.	31
9.	A map of Class A and B reflection points and the outline of the magma body.	32
10.	Ray paths for microearthquakes which helped define the relief on the upper surface of the magma body.	36
11.	Simplified diagram of COCORP Line 1A showing the two major P-wave reflectors.	37
12.	Cross section and areal view of inversion model M1.	51
13.	Simultaneous plot of the calculated average S-wave velocity of model M1 and the goodness of fit factor versus the iteration step.	53

Figure		Page
14.	A comparison of inversion model M2 with model M3.	55
15.	Logarithmic sum of the squared residuals of micro-earthquake depths of focus obtained in two ways.	59
16.	Travel time of Class A S_zS relfections versus distance.	65
17.	Travel time of S_zS reflections versus distance using a restricted data set.	67
18.	Map of Class A and B epicenters of microearthquakes in relation to major faults, the margins of the extensive magma layer and the intra-rift Socorro-Lemitar uplift.	70
19.	Four west to east cross sections of microearthquake hypocenters located in the local Socorro area.	72
20.	Four west to east cross sections of microearthquake hypocenters determined for a crustal volume extending from just south of Socorro to approximately 50 km to the north.	73
21.	Histogram of microearthquake depths of focus.	75
22.	A diagram of the postulated model of the upper crust near Socorro, New Mexico.	83

LIST OF TABLES

Table		Page
1.	Portable Seismograph Station Location and Station Corrections.	12
2.	Qualitatively Analysed Frequency Content of the S_ZS Reflections.	26
3.	S-Wave Velocities, Average Depth of Focus, and Depth to Reflector of Four Studies.	39
4.	Velocities Calculated Using Model M3 and a Restricted Data Set.	63

INTRODUCTION

Purpose and Scope

The primary purpose of this study was to determine an upper crustal geophysical model for the Rio Grande rift near Socorro, New Mexico, employing microearthquake seismic signals. To achieve this purpose the upper surface of an extensive magma body contained within the upper crust beneath Socorro was first extensively mapped and was then used as a known reflector of microearthquake S-waves. The S-wave reflection travel times were combined with recording station locations and microearthquake epicenters to yield both a viable crustal velocity model, via a least squares inversion, and accurate microearthquake depths of focus. All three geophysical observations -- i.e. the shape of the magma body, the improved depths of focus and the velocity model -- were combined to give a compatible, although nonunique, crustal model. The model as determined can help account for some of the observed and postulated features of the rift; for example, differential depths to basement rock of up to 3 to 5 km (Sanford, 1968; Chapin et al., 1978, and Brown et al., 1979); recent Quaternary faults (Sanford et al., 1972); low P-wave and S-wave upper crustal velocities (Sanford et al., 1973); detachment of the lower upper crust from the upper brittle crust (this study) and recent crustal extension (Chapin and Seager, 1975; Eaton, 1979).

Evidence for an extensive magma body comes from many seismograms of local microearthquakes which contain two sharp arrivals following the direct S-wave by about 2.5 and 5.0 seconds. These were identified as S to P reflections (S_zP) and S to S reflections (S_zS) from the upper surface of the extensive magma body (Sanford and Long, 1963; and Sanford

et al., 1973). These early analyses of the reflection amplitudes and arrival times also placed a minimum value on the areal extent of the reflector, restricted its depth and determined something about its physical properties.

To obtain greater detailed knowledge about the magma body and to study in some detail the geophysical properties of the upper crust in the Socorro area, a very localized microearthquake study was initiated in May, 1975 (Sanford et al., 1977). From more than 1200 microearthquakes recorded during 316 recording days, 99 very select shocks producing unmistakable S_zS reflections and having very accurate epicentral locations were winnowed. From this restricted data set 214 accurately determined reflection points were obtained. Inasmuch as a completely new data set was thus available for this present study, early interpretations concerning the magma body, presented in three previous papers (Sanford and Long, 1965; Sanford et al., 1973; and Sanford et al., 1977), were re-evaluated and, when acceptable, were refined by the new data set; on the other hand, unacceptable interpretations have been replaced with more viable options. Substantial improvements in the knowledge of the areal extent, surface relief, orientation with known crustal horizons and depth to the magma body provided much of the needed data to determine a quite complete crustal model of the Rio Grande rift.

Geological and Geophysical Background

To set the stage for this study, a very brief description of the Rio Grande rift near Socorro, New Mexico, will be attempted. Figure 1 (from Sanford et al., 1977) is a generalized map of the rift which includes the main physiographic features surrounding the rift as it is seen within New Mexico. The Rio Grande rift is a nearly north to south

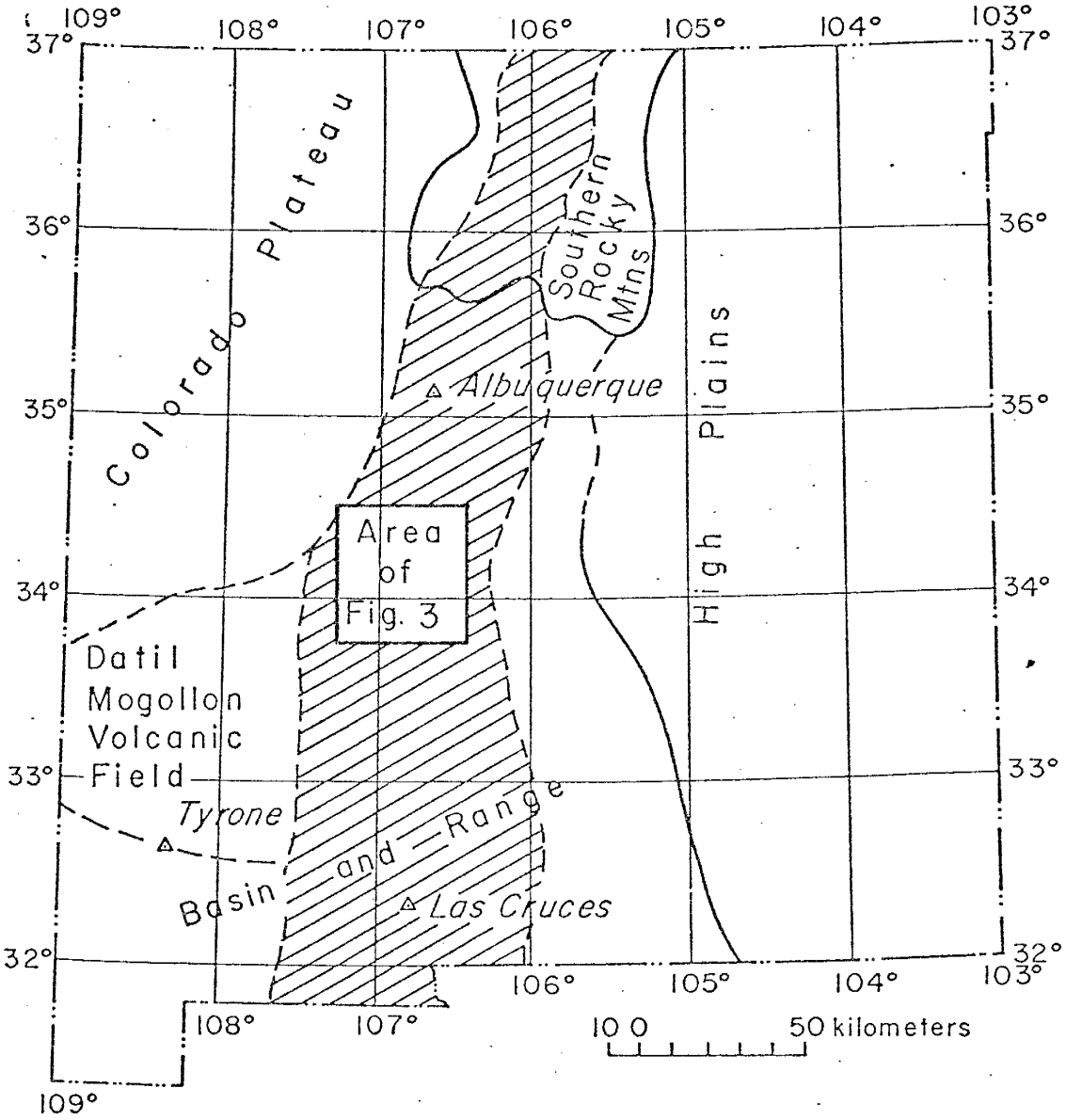

Figure 1. Physiographic provinces and the Rio Grande rift in New Mexico (after Chapin, 1971). Also shown is the approximate area contained in Figure 3.

linear feature extending from just north of Leadville, Colorado, to Chihuahua, Mexico (Chapin, 1971). The rift appears to be comprised of three separate segments: (1) the northern rift which ends near the Colorado and New Mexico boundary, (2) the central rift extending from the state boundary to near Socorro, NM, and (3) the southern rift extending from Socorro, NM, southward (Ramberg et al., 1978).

This study is concerned primarily with a 100 km long section of the central Rio Grande rift extending from approximately 30 km south of Albuquerque, New Mexico, to approximately 20 km south of Socorro (see Figure 3). To the east of this portion of the rift exists the Great Plains province; to the northwest and west exists the Colorado Plateau and to the southwest exists the Basin and Range province and the intervening Datil-Mogollon volcanic field. The best identifying features of this portion of the rift are (1) 3 to 5 km deep alluvial basins (Sanford, 1968; and Chapin and Seager, 1975), (2) bounding Quaternary faults that strike northnortheast or northnorthwest (Sanford et al., 1972), (3) raised structural margins, especially on the eastern side of the rift (Chapin, 1971) and (4) several intrarift uplifts (Chapin and Seager, 1975). The important intra-rift uplift in this study is the Socorro-Lemitar Mountain block which begins approximately 10 km southwest of Socorro, strikes northnorthwest, visually ends 40 km north of Socorro and can be geophysically traced for at least another 10 km toward the north (Brown et al., 1979).

Rifting began about 32 m.y. ago (Chapin, 1979) as determined by radiometric dating of the change from intermediate calc-alkalic volcanic rocks to ~~ba~~ bimodal rhyolite-basaltic andesite suite and by dating of volcanic rocks above and below an angular unconformity. In the Socorro

area, there was a lull in volcanism between about 20 and 13 m.y. ago (Chapin, 1979) during which 1000 to 1500 m of fanglomerate-playa deposits accumulated in a broad early rift basin. This basin, the Popotosa basin, was broken up into a series of parallel grabins separated by intra-rift uplifts during a strong pulse of eperrogenic uplift between about 7 and 4 m.y. ago (Chapin, 1979). The rate of extension and uplift have apparently slowed since 4 m.y. ago as evidenced by nearly flat lying Pliocene basalt flows that rest on strongly uplifted and tilted older rocks.

The youngest rhyolitic intrusions in the Socorro area have been dated at about 6 m.y. (Chapin, personal communication, 1979). The youngest basaltic flows in the Socorro area have been dated at 4 m.y. (Bachman and Mennert, 1978).

However, recent basaltic flows as young as 0.14 m.y. old have been identified (Kudo, 1976) 70 km north of Socorro. The Socorro area is also a point of intersection of two volcanic lineaments -- one postulated to be a deep seated transverse shear zone (Chapin et al., 1978) -- which could very well allow for the local magmatic activity including the deep extensive magma body.

Geophysically, recent, extremely rapid (2 to 6 mm/yr) uplift centered over the extensive magma body has been identified by Reilinger et al. (1979) using level line data. Also, the Socorro area is an area of concentrated seismic swarming that is also centered over the magma body and is between portions of the rift that are almost aseismic (Sanford et al., 1979).

The above discussion is admittedly short. It serves for a very quick review and more importantly, lists most of the important references

that contain extensive information about the rift, especially for the Socorro area. In addition to the above references, very comprehensive reviews, interpretations and further references are contained in Rio Grande Rift: Tectonics and Magmatism edited by Riecker (1979) and the Guidebook to Rio Grande Rift in New Mexico and Colorado compiled by Hawley (1978).

DATA

A very localized, high resolution microearthquake array initiated in May, 1975, provided most of the S_zS and S_zP reflection data necessary to obtain greater knowledge about the extensive magma body and the upper crust of the Rio Grande rift. In this section the instrumentation and array deployment will be discussed. In addition, the microearthquake location procedure and criteria used to differentiate between two different classes of data will be presented.

Instrumentation

The microearthquake seismograms used in this report were primarily recorded with a movable array of five to six Sprengnether MEQ-800 seismic recording systems. This basic network was supplemented after April, 1977, by two Sprengnether DR-100 digital recording systems. For qualitatively determining the frequency content of the reflections, MEQ-800 records were compared with those from an LRSM (Long Range Seismic Monitoring) system located at SNM. Real time data from telemetered signals were available from Albuquerque Seismological Laboratory (U.S.G.S.) for stations LAD and LPM starting in 1977.

MEQ-800 Seismograph. The MEQ-800 is a self-contained portable analog seismic recording system with a wide sensitivity range. The amplifiers for the system, which have gain settings ranging from 60 to 120 db in discrete 6 db intervals, are stable to ± 1 db. Filtering of the seismic signal is possible for both low frequencies (below 5 or 10 Hz) and high frequencies (above 5, 10 or 30 Hz). For this study, only the 30 Hz setting on the high frequency filter was ever used. This filtering was necessary to reduce noise caused by near surface atmospheric disturbances. Only especially quiet stations located in mines (e.g. WT

or DM) or caves (e.g. IC or CC) were recorded unfiltered. Predominant frequencies of the P phases of the recorded microearthquakes (19.7±1.5 Hz; Johnson, 1978) and the S phases (see Figure 4) are well within the filtered or unfiltered frequency range of the seismographs. Helical recording on smoked paper at a rate of 120±1.0 mm/min was used to record the seismic signal.

Self-contained, quartz crystal chronometers produced time marks at 60 second intervals. These clocks were synchronized at the beginning of each recording week with the WWV standard time signal by simultaneously recording signals from both the clock and the WWV. To correct for clock drift the two time signals were again simultaneously recorded at the end of each recording week.

To complete the MEQ-800 system, a Mark Products vertical L4-C geophone (1.0 Hz natural frequency) or, when necessary, a Willmore vertical geophone (1.5 Hz natural frequency), was used. Magnification response curves for the usual field settings are shown in Figure 2. A peak magnification of around 1.6×10^6 is achieved at 40 Hz (with the high filter set on 30 Hz).

DR-100 Seismograph. The DR-100 system is a precision 12-bit digital seismic recorder. It continually samples the seismic signal until triggered by a particular event whose beginning short-term average is larger, by a prescribed amount, than the long-term signal average. At this time, the signal producing the large short-term average is recorded on magnetic tape. Allowances are made for recording the beginning of the triggering signal and timing information, supplied by a quartz crystal chronometer. The amplification and available filter settings are identical to the MEQ-800 system as is the geophone, a Marks Products

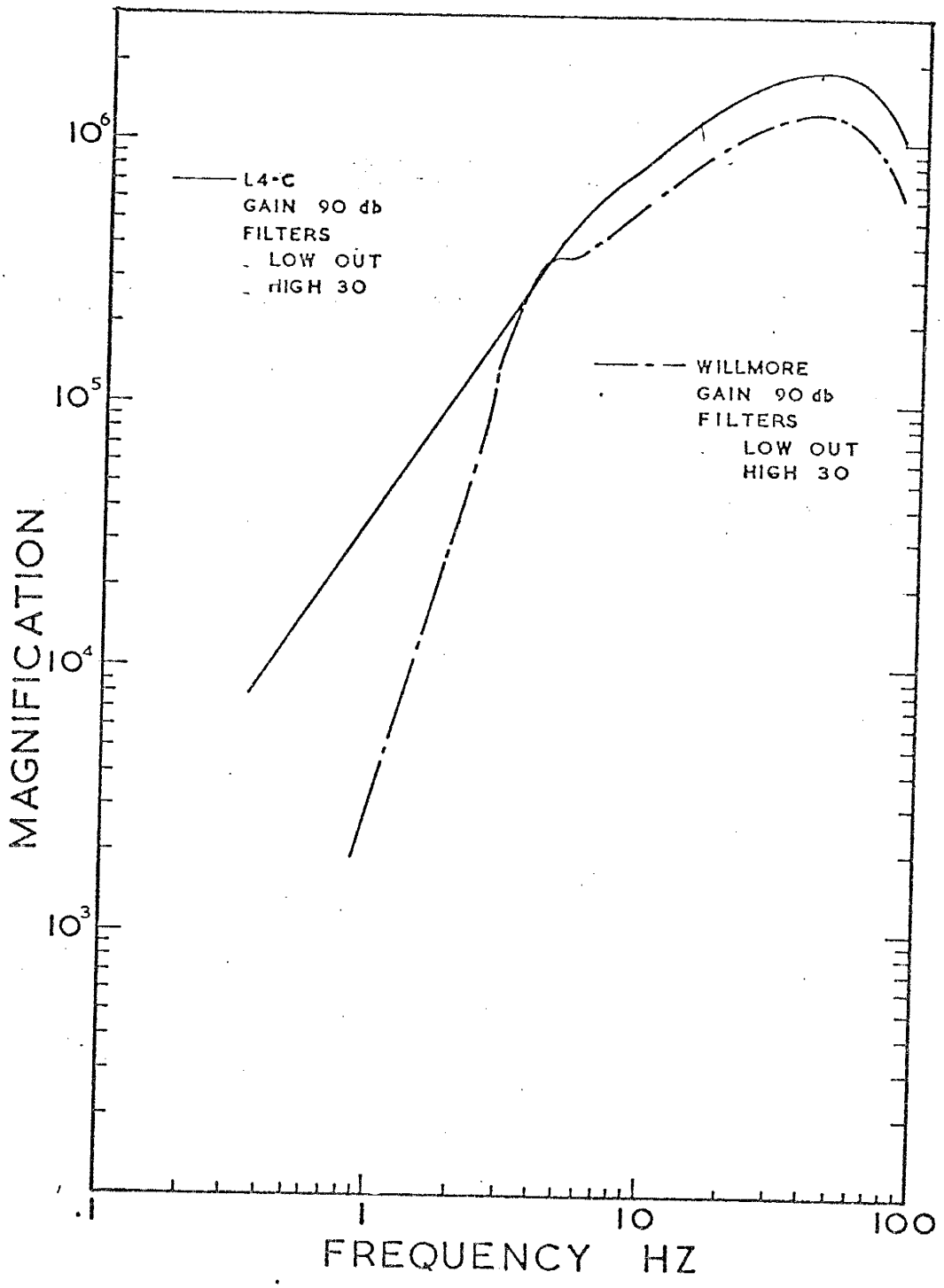

Figure 2. Magnification response curves for the MEQ-800 seismographs using either an L4-c or Willmore geophone. Curves are for the usual field settings.

L4-C. For the microearthquake study, the digital recording was done at 100 samples per second. A companion play back system (DP-100) provided both analog and digital outputs for subsequent data processing and analysis.

LRSM System. The station at SNM has a Long Range Seismic Monitoring (LRSM) system. The system employs one vertical and two horizontal (N-S and E-W) short period Benioff seismometers. The signal, after amplification is recorded on a helical 35 mm film recorder at a rate of 0.25 mm/sec. The magnification has a peak value of 140 k at 3.3 Hz.

Arrays. The five to eight Sprengnether systems were available for use in a movable array which could occupy any of the 26 station sites shown in Figure 3 and listed in Table 1. Protection from atmospheric noise was a main prerequisite for site selection. In most cases caves and abandoned mines were used; however, nine stations (BB, CK, CU, HC, TD MY, NG, SL and TA) were only protected by rock overhangs. When possible, the geophone at the station was buried. In all cases, the underlying material of the station is solid rock, reducing as much as possible, seismic signals arriving nearly vertically because of refraction through low velocity surface material. The majority of the recording time was spent with arrays in the southern portion of the area until Fall, 1977, when the instruments were moved to the more northerly stations.

The MEQ-800 seismographs were deployed on Mondays and retrieved on Fridays. The DR-100 units were placed in the field for longer periods of time. They proved reliable enough to provide continuous sampling and individual event recording for periods of up to 4 weeks.

Hypocentral Locations

Microearthquakes were located using a damped least squares inversion

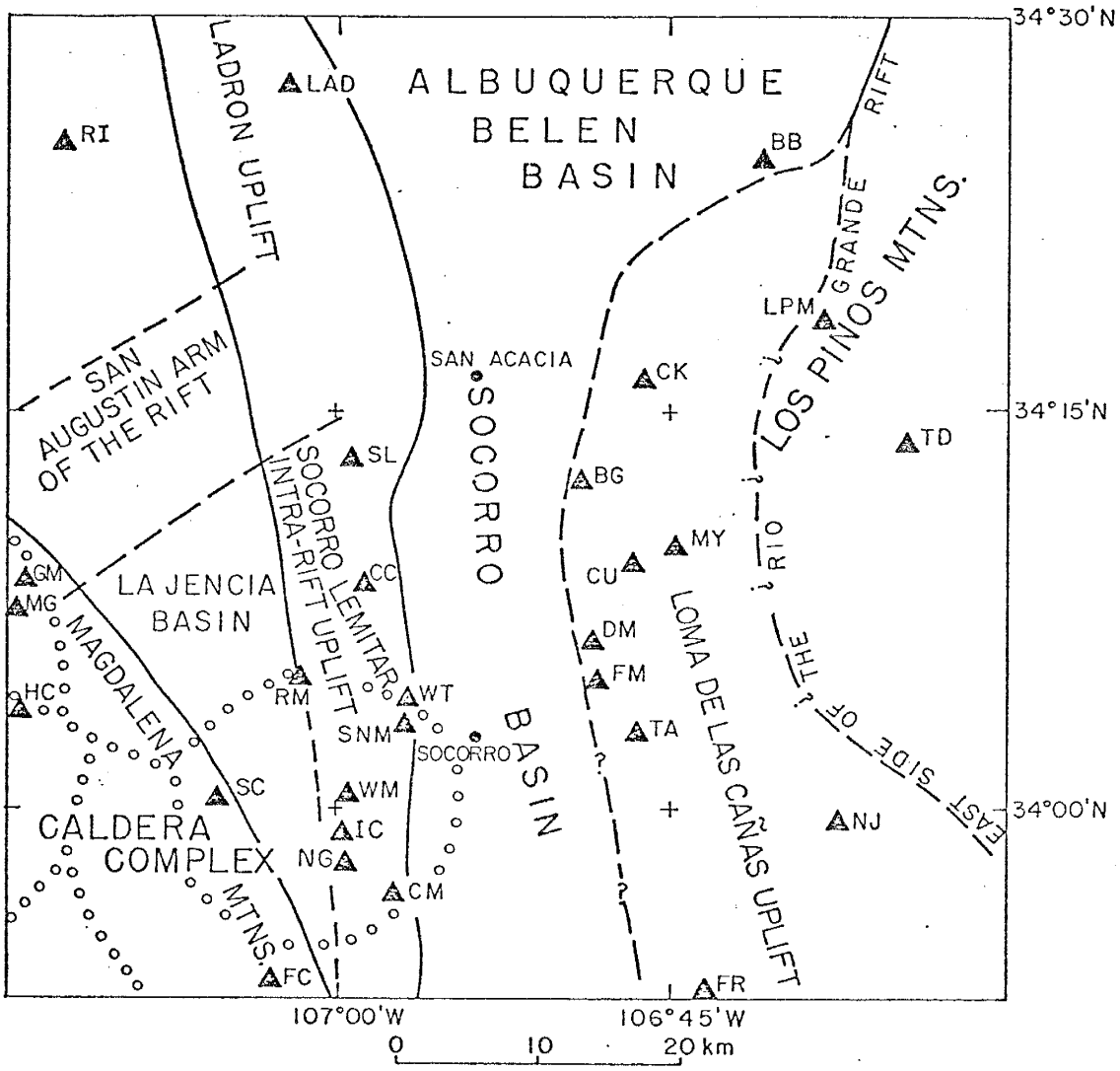

Figure 3. Major physical features near Socorro. Also shown are the locations of the seismic recording stations used.

TABLE 1. Portable Seismograph Station Locations@ and Station Corrections.

Station	Latitude	Longitude	Elevation(m)	Station* Correction(sec)
BB	34.4090	106.6818	1615	-.02
BG	34.2068	106.8205	1516	+.02
CC	34.1442	106.9819	1649	-.09
CK	34.2725	106.7702	1578	#
CM	33.9501	106.9576	1640	+.22
CU	34.1573	106.7785	1585	-.03
DM	34.1075	106.8079	1536	-.09
FC	33.8950	107.0504	1850	-.27
FM	34.0829	106.8047	1537	+.02
FR	33.8747	106.7270	1558	#
GM	34.1454	107.2345	1945	-.09
HC	34.0658	107.2361	2240	+.13
IC	33.9870	106.9967	1730	+.18
LAD	34.4583	107.0375	1768	-.20
LPM	34.3076	106.6336	1737	+.00
MG	34.1305	107.2425	2024	#
MY	34.1667	106.7459	1645	-.08
NG	33.9648	106.9933	1730	+.15
NJ	33.9924	106.6253	1644	#
RI	34.4234	107.2075	1530	+.18
SC	34.0100	107.0894	2073	+.28
SL	34.2234	106.9910	1615	-.09
TA	34.0498	106.7751	1558	-.05
TD	34.2339	106.5778	1850	-.20
WM	34.0120	106.9929	1673	+.12
WT	34.0722	106.9459	1555	-.20

*P-wave corrections. For S-wave corrections multiply by $\sqrt{3}$.

Not determined because of lack of data.

@ Relative latitudes and longitudes.

program written by R. M. Ward (personal communication, 1979). The program provided estimates for hypocentral locations, origin times and errors for these parameters. Because four unknowns (latitude, longitude, depth of focus and origin time) were calculated, five or more P-wave arrival times were required to provide redundancy in the solution. To calculate the four unknowns, a crustal P-wave velocity model, P-wave arrival times and initial estimates of the four unknowns were needed for the program.

The crustal velocity model used for this study was a homogeneous half space with a P-wave velocity of 5.8 km/sec. Three different types of observations substantiate the low P-wave velocity. Sanford et al. (1973) obtained a 5.8 km/sec velocity from the distances and travel times between a U.S.G.S. station at Albuquerque (ALQ) and microearthquakes accurately located in the vicinity of Socorro. Toppozada and Sanford (1976) observed a secondary phase with a velocity of 5.8 km/sec on a refraction profile along the Rio Grande rift which they interpreted as a direct P-phase through the upper crust of the rift. Finally a best least squares value of 5.8 km/sec has been obtained through inversion of the microearthquake P-wave arrival time data (R. M. Ward, personal communication, 1978).

Impulsive P-wave arrival times were measured to ±0.02 seconds with a modified Gaertner traveling microscope. Variations in recording rates were accounted for by measuring the duration of each minute on each record at the time of the arrival of the event. Clock drift, which was no larger than 0.5 sec/week, was corrected for by assuming linear clock drift between times of synchronic recording of the internal clock and

the WWV time signal. Subsequent checks have shown that this assumption was accurate to at least ±0.05 seconds. The best check of the overall error in P-wave arrivals came from comparing arrivals from known manmade explosions. P-wave arrivals from different explosions having identical ray paths from the source to several stations were timed. Although different recording units were used at the stations, different personnel timed the explosions and the events occurred at different times of the recording week, P-wave travel times between the source and stations were reproducible to ±0.03 seconds at the 95% confidence interval.

Initial estimates of the origin times for the microearthquakes were obtained from Wadati plots, i.e. graphs of S-P intervals versus P-wave arrival times. The Wadati origin time is the P-phase arrival time at an S-P interval of zero. The slope of the line passing through the data was constrained to 0.73, the value for a Poisson's ratio of 0.25. Initial estimates of the epicentral location were found by using the Wadati origin times to find approximate P-wave travel times. These travel times were then used in a graphical, cord-intersecting technique to determine the coordinates of the epicenter (Richter, 1958, pp. 320-321). Initial estimates for depths of focus were set at 10 km.

Original locations of microearthquakes using the half space velocity model revealed that there were particular crustal zones within which events could not be located well. In addition, there were particular stations that always produced substantial time residuals (observed minus theoretical travel times) when used in the solution of a microearthquake location. For example, microearthquakes located near station CM many

times had average time residuals that were more than twice as great as those for shocks located near WT or SC. Moreover, time residuals for station CM were usually greater than those for other stations. Station CM is within the boundaries of the Socorro Caldera which contains a substantial thickness of low velocity material. Between WT and CM thicknesses of alluvial and ash flow tuff fill of up to 5 km are expected (Chapin et al., 1978). Several other similar anamolous crustal zones and stations having associated large residuals were found.

To account for the large time residuals caused by both known and unknown diverse geologic conditions beneath and/or near recording stations, individual station corrections were calculated. Microearthquake data proved too ambiguous to be the only source of data for calculating the corrections; so for as many stations as possible, corrections were assigned by measuring arrival times of local explosions whose locations and origin times were accurately known. Differences between theoretical and observed travel times for these explosions were attributed to differences in the geologic conditions directly beneath the station. For stations that were too distant to record the explosions, corrections were calculated using the location program in the following manner. A hypocenter was determined for a particular event using those recording stations that had station corrections determined from explosions. The remaining uncorrected arrival times were then inserted into the location program and a new hypocenter was found. Variable station corrections were added to the uncorrected station arrival times until the two locations agreed. All the station corrections were shifted so that the origin time found with the iterative program agreed, on the average, with the origin times obtained from the Wadati plots.

The P-wave station correction, the times to be subtracted from arrival times, are listed in Table 1. The S-wave station corrections to be applied to the S_zS reflection travel times were the P-wave station corrections multiplied by $\sqrt{3}$ which assumes the rock immediately beneath each station has a Poisson ratio of 0.25. The station corrections roughly reflect the near-surface geology (see Figure 3). To the southwest and west of station WT, corrections are largest, greater than 0.20 seconds, because stations in this area are located on thick sequences of intra-caldera fill (Chapin et al., 1978). Stations north of and including station WT have the smallest corrections, less than -0.12 seconds, because they are located on or close to Precambrian rock. Stations located on intra-rift uplifts on the eastern side of the rift also have small corrections, between 0.00 and 0.02 seconds.

The microearthquake origin times were used to determine the S_zS reflection travel times. Because of their importance, origin times determined by the iterative procedure and Wadati procedure were continually compared. Wadati origin times were considered more reliable because they depended only on Poisson's ratio. Iterative origin times depended upon, in addition to the crustal velocity structure, the final microearthquake hypocenters. Erroneous hypocenters, especially for poorly constrained events, oftentimes resulted in origin time errors of up to several seconds. On the other hand, because small changes in Poisson's ratio are probable in the region, some variation in the Wadati origin times is possible. Therefore, the procedure followed was to use the Wadati origin time if it differed from the iterative origin time by 0.45 seconds or more. This restriction helped immensely for poorly constrained locations, the majority of which were for events outside of the

recording array. Origin times were constrained to the Wadati values for less than 20 of the events used. For the remaining events, iterative origin times were used. These differed from the Wadati origin times by less than ±0.25 seconds, on the average.

An estimate of the average error in hypocentral locations is needed before proper errors in resulting reflection points and the S-wave velocity structure can be estimated. The iterative location program calculated a covariance matrix from which estimates of the relative errors could be based. This covariance matrix was based on (1) a P-wave arrival time standard deviation of 0.03 seconds, (2) the geographic distribution of stations and (3) a 5.8 km/sec P-wave velocity half-space crustal model. For events used in this study the covariance matrixes gave average standard deviations of ±0.38 km in latitude, ±0.40 km in longitude and ±0.85 km in depth of focus. Unfortunately, these errors are only relative and depend strongly on the above factors.

For shocks located within a small local array with an area less than approximately 500 km^2 (used extensively in 1975 to early 1977) the estimates of the errors in latitude and longitude are probably accurate. For shocks located outside of the array and for events recorded by a poorly distributed array, lateral errors of up to ±2 km are suspected for many events, especially Class B.

With the particular location program used, depths of focus are very closely allied to origin times and station distribution. There appears to be almost a one to one trade off between origin time estimates and depths. Earlier origin times are associated with deeper depths of focus assuming the same epicentral location. It will be seen in the inversion section that depths of focus errors may be as great as

±5 km. These errors can be reduced by calculating depths of focus using a known reflector, the magma body, and reflection travel times.

Reflection Data

The microearthquakes recorded during the 316 operating days from May, 1975, to January, 1978, were inspected for all S_zS and S_zP reflections. Reflections and their associated shocks were then categorized. Class A reflections always are associated with Class A microearthquakes; however, there can be Class B reflections associated with Class A shocks. The reverse is not true. Reflections and events were categorized using the following specifications.

Class A (all specifications required)

1. Unmistakable S_zS arrival (see Figure 4).
2. Five or more stations recording the microearthquake.
3. Iterative origin time is within ±0.45 seconds of the Wadati origin.
4. Average P-wave residuals are within ±0.09 seconds for events contained in the recording array; residuals are within ±0.2 seconds for events outside the recording array.

Class B

Any reflection, and/or its associated event which does not satisfy all specifications for a Class A status.

Locations for many Class B data were available from Fender (1978). Class A and B data are listed in Appendix 1. All hypocenters are given in Appendix 2.

Other Data

Most of the information on the extent and shape of the upper surface of the magma body was determined from the spatial positions of the

points of reflections; however, important additional controls were obtained from COCORP deep P-wave reflection profiles crossing the Rio Grande rift (Brown et al., 1979)(see Figure 9).

MAGMA BODY

Introduction

From previous studies (Sanford and Long, 1965; Sanford et al., 1973; Sanford et al., 1977) the existence of an extensive magma body approximately 18 to 19 km beneath the Socorro area has been known for several years. In this paper, amplitude ratios of the S_zP to S_zS reflection phases, wave form character and reflection frequency content have all been used to gain insight into the physical properties of the discontinuity and type of material beneath it. In addition, a necessary effort of this study was to map, with confidence and some resolution, the lateral extent and relief of this discontinuity so that it could be used in conjunction with travel times of the S_zS reflections to determine upper crustal S-wave velocities with a linear inversion technique.

Properties of the Upper Surface

Particularly good examples of microearthquake seismograms containing S_zP and S_zS reflections are shown in Figures 4 and 5. Figure 4 contains two digital records from the DR-100 recording units. Although each seismogram was recorded on a separate day, both events occurred near station SC and are believed to be members of the same microearthquake swarm. Figure 5 is reproduced from LRSM seismograms. In addition to these two figures, many well-recorded seismograms reproduced from both MEQ-800 and LRSM records appear in Appendix 4.

On all seismograms reproduced, both the S_zP and S_zS reflections are impulsive implying that the discontinuity is quite sharp (10's of meters). For many shocks, the S_zP consists of a single sharp oscillation followed by a weak or nonexistent coda. The S_zS reflection appears,

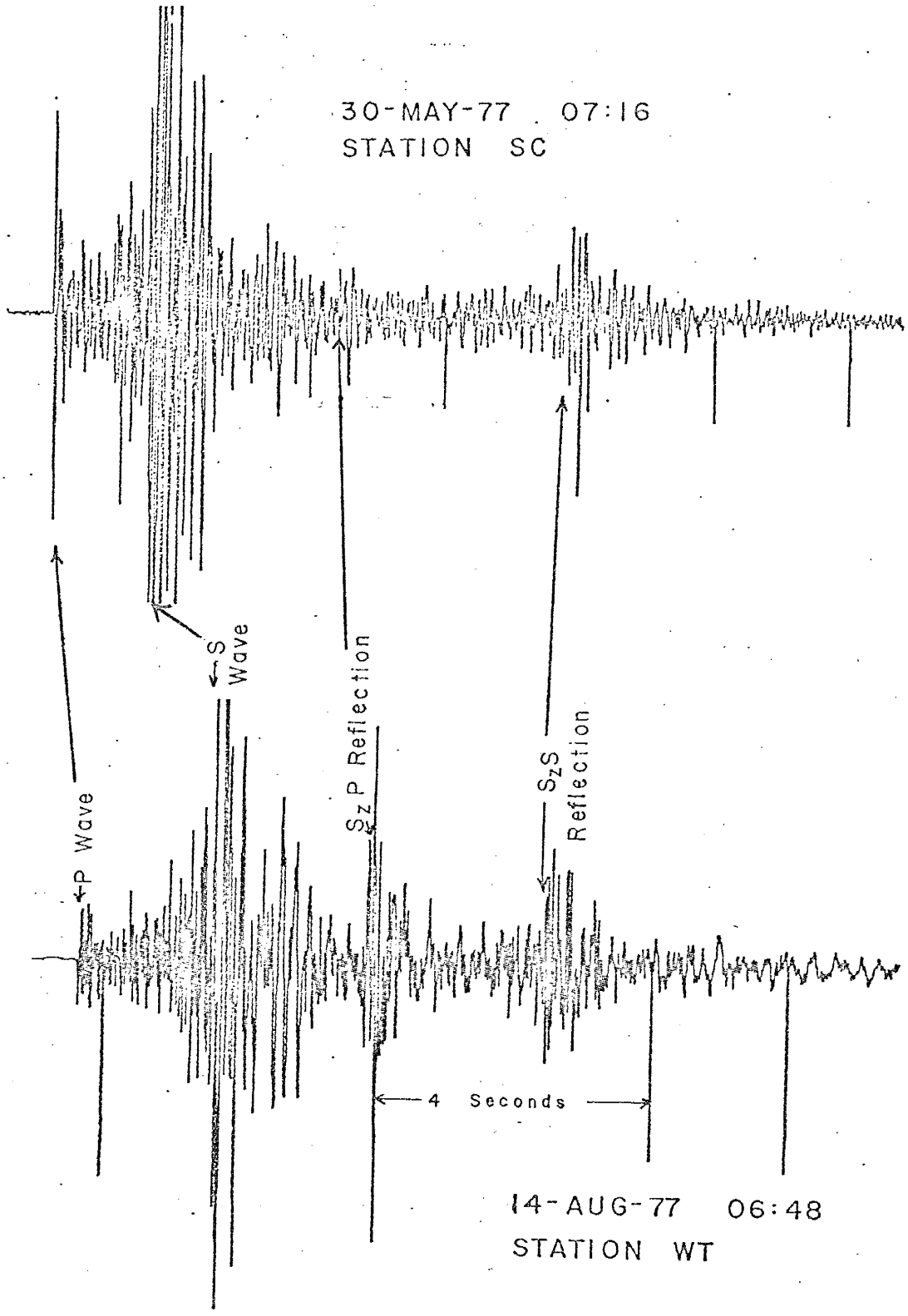

Figure 4. Two well recorded microearthquakes with clearly defined S_zP and S_zS reflections. Recording was done with a short-period DR-100 digital seismographs at stations SC and WT.

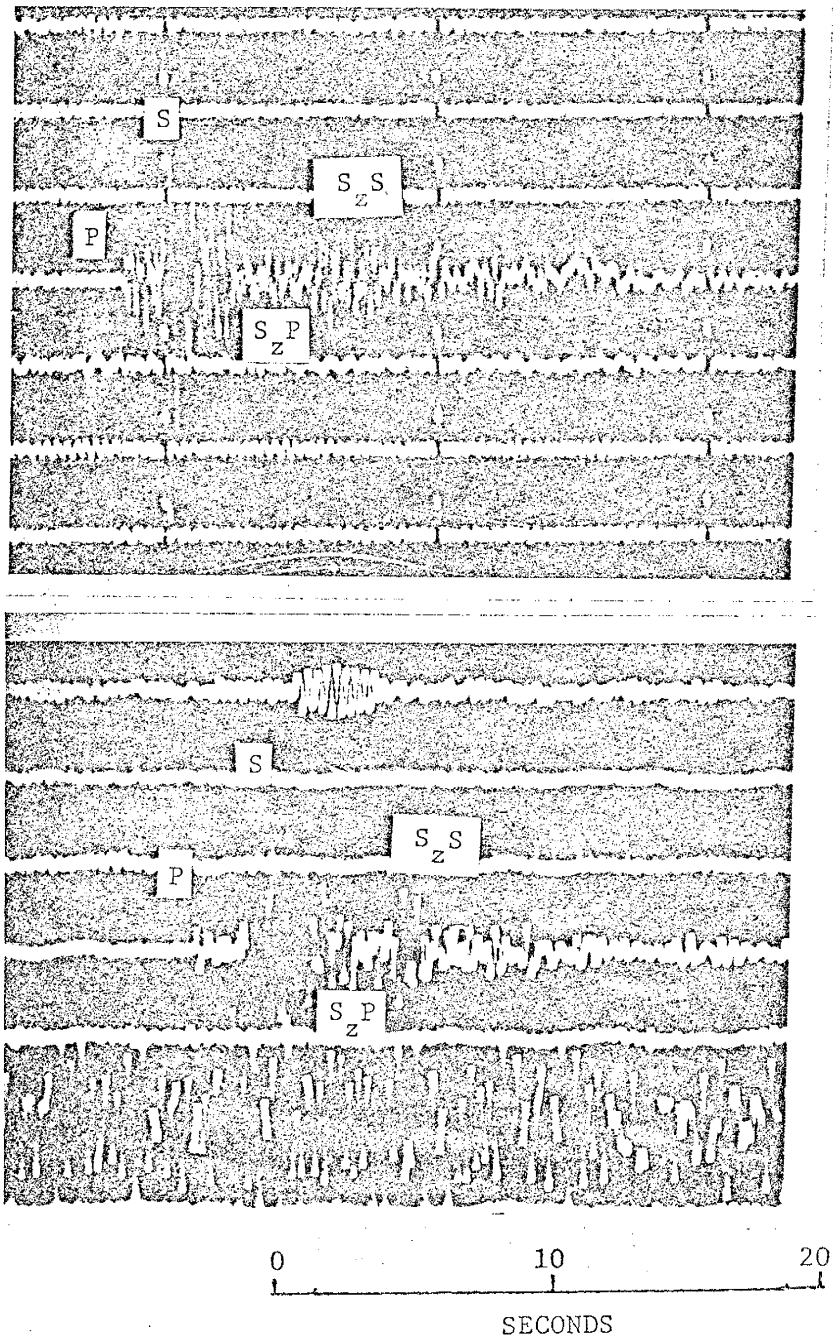

August 12, 1976
O. T. 01:45
Station SNM
(Member of swarm occurring at 04:56)

December 27, 1978
O. T. 09:29
Station SNM
(Not located)

Figure 5. Reproductions of two strong microearthquakes recorded by the LRSM system at station SNM. Reflections show a predominate frequency of from 3 to 4 Hz.

on many records, to be almost an exact copy, at a reduced amplitude, of the direct S-wave.

To determine if the discontinuity equally reflects all frequencies of the direct S-wave as suggested by the similarity between the direct S-wave and the S_zS reflection, spectral analysis of both phases was done by applying the theory of discrete stationary time series (Robinson, 1967 and Jenkins and Watts, 1968). Autocovariances of the signals were calculated and then transformed, via Fourier Transformations, to give spectral density function estimates of the signals. The short duration of individual direct S-waves and S_zS reflections prohibited accurate resolution of the spectrum at closely spaced frequencies. To improve the frequency resolution of the spectral estimates, averages of the spectral density functions were calculated for several recorded signals originating from individual microearthquake swarms.

Three sets of spectral density functions, each set containing estimates for the direct S-wave and the S_zS reflection are seen in Figure 6. The spectrums obtained at station SC are nearly identical. The same is true for the spectrums obtained for northerly events recorded at station WT. The spectral estimate obtained for the S_zS reflection originating from the southwesterly swarm and recorded at WT compares well with the estimates of the spectrums obtained for the northerly swarm; however, the S-wave derived from the southwesterly swarm, as recorded at WT, appears to be lacking substantially in high frequencies. It is noted that this direct S-wave passes through crustal material thought to contain zones of low rigidity (Sanford et al., 1977) which could account for the absence of high frequencies. Nevertheless, the almost identical nature of the other spectrums indicate almost equal S-wave reflection

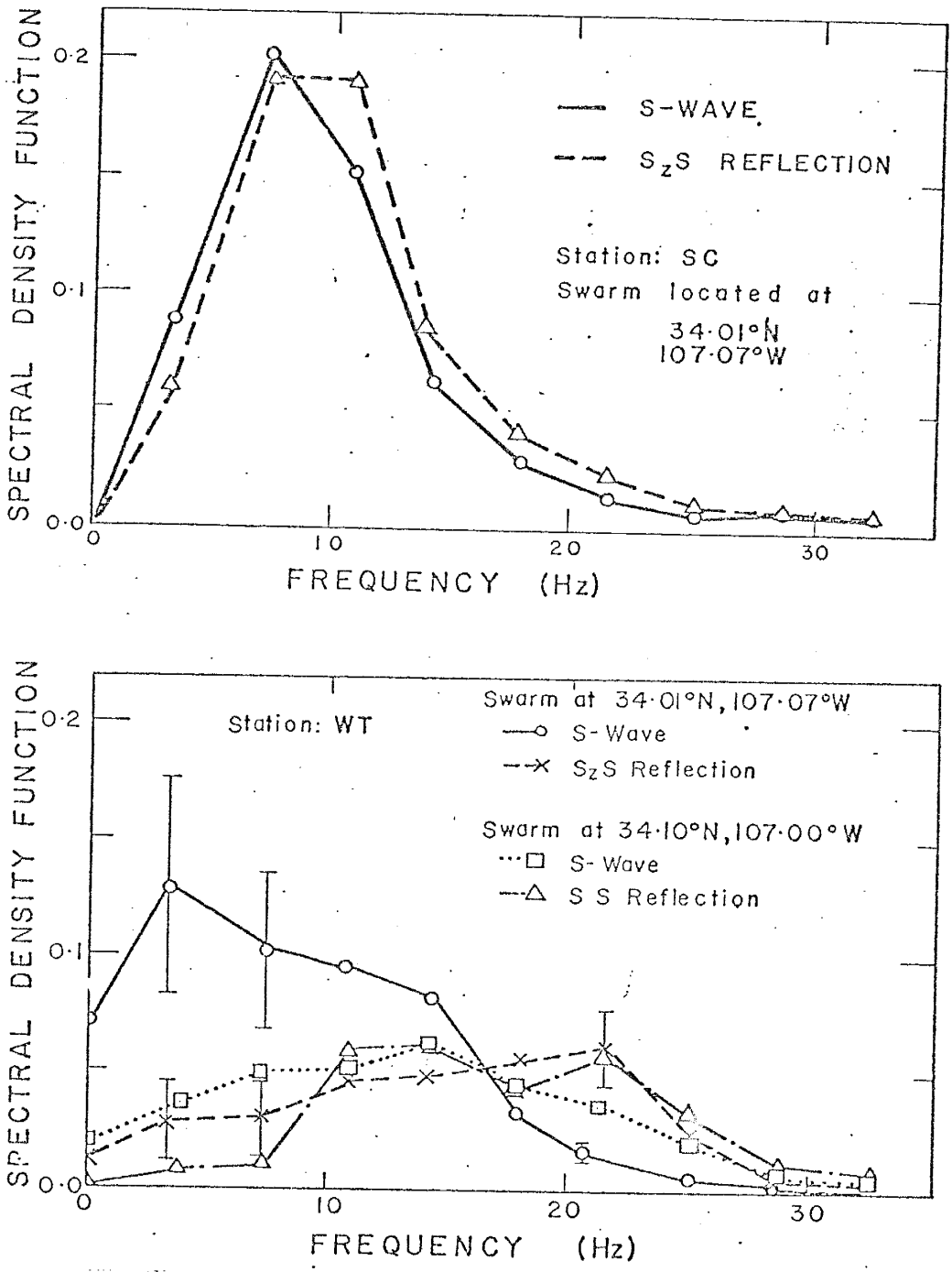

Figure 6. Spectral density functions obtained for direct S-waves and S_zS reflections recorded at stations SC and WT. The spectrums are averages of as many as 14 shocks recorded during individual microearthquake swarms.

at all frequencies. Individual station differences are seen and are believed to be caused by near surface heterogeneities. This is implied by the similar spectrums obtained at station WT for S_zS reflections derived from different source regions.

In addition to the spectral analysis of the two microearthquake swarms, seismograms appearing in Figure 5 and in Appendix 4 have been qualitatively analyzed for frequency content by counting zero crossings. The data, origin times, instrument used and predominate frequencies are given in Table 2. Predominate frequencies as high as 18.7 Hz and as low as 3 Hz are present in the reflected signals.

The simple form of the S_zP, the similarity of the station dependent spectral density functions of the direct S-waves and the S_zS reflections, and the broad frequency content of other S_zS reflections indicate that the discontinuity is singular to S-wave energy.

One unusual feature of the reflections is the large amplitudes relative to the direct S-wave. For nearly 150 vertical component seismograms recorded at SNM, the measured S_zS to direct S-wave amplitude ratios average around 1.3 (Sanford et al., 1973). The large ratios, particularly those above the average, cannot be explained even if one assumes (1) ten times more SV energy radiated downward from the focus along the S_zS raypath than outward along the direct S raypath, and (2) a large reflection coefficient for a solid to solid velocity discontinuity. On the other hand, a solid to non-rigid (magma or partial melt) interface can account for the observations.

Further evidence for a solid to liquid interface comes from an analysis of the S_zP to S_zS amplitude ratios. S_zP and S_zS reflections are generated by S-wave energy traveling only slightly separated ray

TABLE 2. Qualitatively Analysed Frequency Content of the S_zS Reflection.

Date	Time (UST)	Station	Instrument	Predominate Frequency (Hz)
Aug. 24, 1975	03:44	CC	MEQ-800	11.0
		WT	MEQ-800	15.0
Nov. 5, 1975	22:28	WT	MEQ-800	13.0
		CC	MEQ-800	>15.0
Aug. 12, 1976	00:51	SC	MEQ-800	15.4
		WT	MEQ-800	18.0
Aug. 12, 1976	01:45	SNM	LRSM	4.3
Aug. 12, 1976	07:52	SNM	LRSM	4.3
Aug. 23, 1976	00:53	WT	MEQ-800	13.2
Aug. 26, 1977	10:32	SC	MEQ-800	12.0
		CC	MEQ-800	18.7
Aug. 26, 1978	22:53	SNM	LRSM	4.3
		WM	MEQ-800	14.0
Dec. 27, 1978	09:29	SNM	LRSM	3

paths and thus their amplitude ratios are relatively unaffected by differences in the S-energy radiation pattern. These ratios can be used to estimate the general magnitude of the reflection coefficients which are functions of the velocity and density contrasts across the discontinuity. All measured S_zP and S_zS ratios were corrected to take into account the angle of incidence of the emerging waves as calculated using a homogeneous half-space with an S-wave velocity of 3.4 km/sec. The measured ratios were corrected by multiplying by the sine of the theoretical angle of incidence for the S_zS wave and dividing by the cosine of the angle of incidence for the S_zP wave. Figure 7 shows the observed data from both Class A reflections and, where feasible, Class B reflections. Actual values of the corrected amplitude ratios are given in Appendix 1. To find possible station related effects, each station is shown with a different symbol. It is apparent that station differences do exist and are probably related to differences in near surface structure and rocks. Also included in Figure 7 are three theoretical amplitude ratio curves assuming plane wave theory. Curve A is calculated for a solid to solid interface across which the P-wave velocity increases from 5.8 to 6.5 km/sec and the rock density increases from 2.8 to 2.9 g/cm^3. This model of an intercrustal discontinuity is taken from an interpretation of a north to south refraction profile through central New Mexico (Toppozada and Sanford, 1976). Curves B and C are for interfaces separating rigid and non-rigid crustal rock, i.e. interfaces across which the S-wave velocity abruptly drops to zero. Curve B is for a discontinuity separating rigid crustal rock and a full melt. P-wave velocities and densities change from 5.8 km/sec and 2.8 g/cm^3 above the discontinuity to 3.0 km/sec and 2.5 g/cm^3 below the discontinuity.

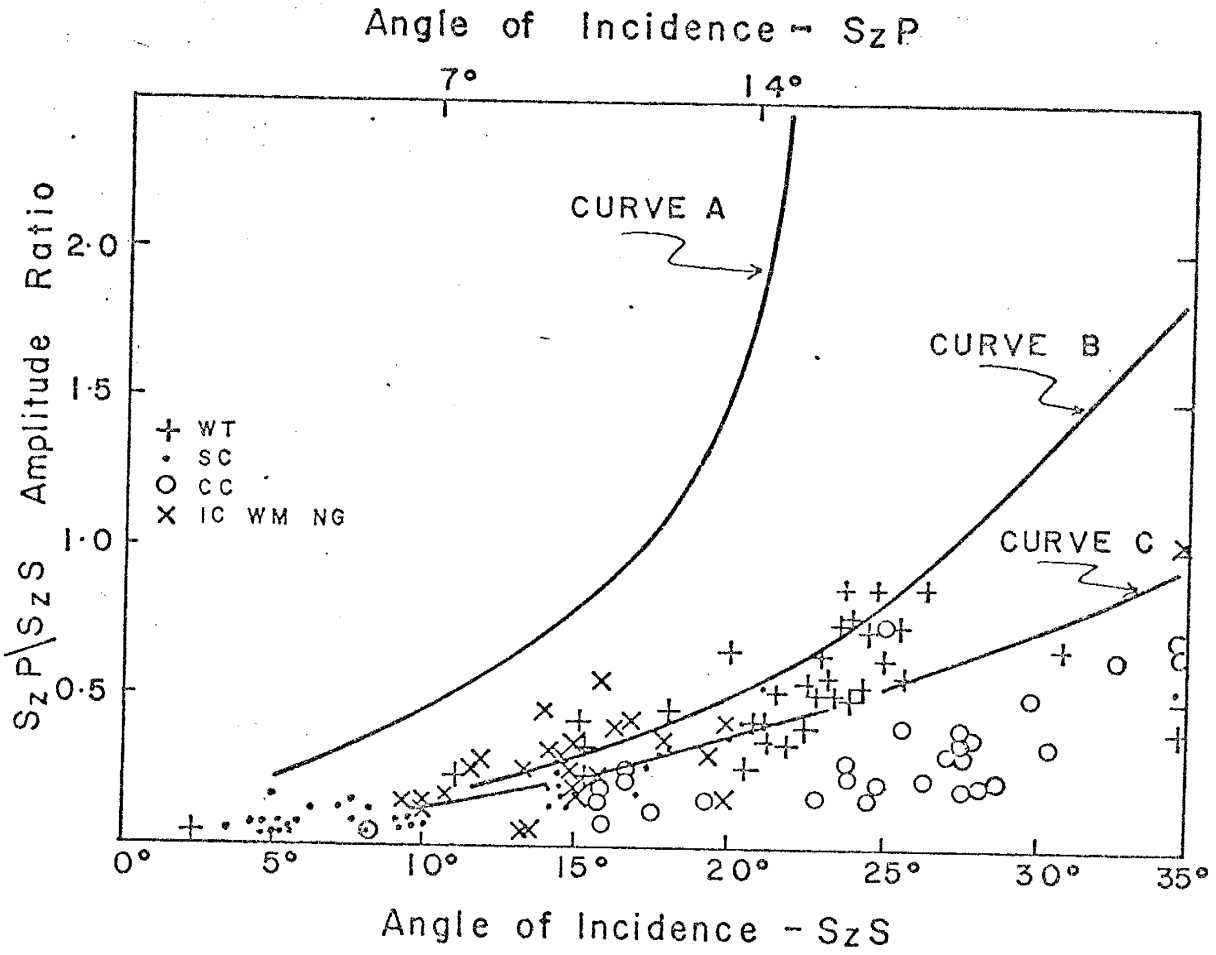

Figure 7. Observed S_zP/S_zS amplitude ratios versus angles of incidence. Curves A, B and C are theoretical ratios for three different types of discontinuities described in the text. Observed data are discriminated by recording station.

These velocity and density contrasts approximate the experimental reductions measured by Murase and McBirney (Fig. 13, 1973) for a transition from solidus to full melt of two types of basalts. Curve C is for a discontinuity across which no rock density contrast exists; however, the P-wave velocity drops from 5.8 km/sec to 4.5 km/sec. This velocity reduction accounts for the complete loss of rigidity while keeping the bulk modulus of the material constant. This model was chosen to represent an initial partial melt wherein the solid rock grains are completely surrounded by a thin film of liquid. This type of initial melting has been proposed as "My preferred description of the initial melt, in contrast to an array of isolated droplets of variable aspect ratio." (Yoder, p. 164, 1976) and was supported by several experimental and real observations. Although complete loss of S-waves in either a full or partial melt is not entirely valid (Aki et al., 1978), almost complete S-wave reflection is required. Theoretical Curves B and C are believed to represent the extremes possible for an interface separating rigid and non-rigid crustal rock.

The measured ratios cannot be related to the theoretical curve A, especially at the higher angles of incidence. They are, however, scattered around curves B and C. Appreciable differences in these two curves do not appear until the angle of incidence for the S_zS exceeds approximately 25°. Unfortunately, this is also the same region where the S_zP and S_zS energies arrive in the coda of the direct S-wave and accurate amplitude measurements become difficult. Because of this, data for angles of incidence greater than 25°, although quite select, may be subject to some error. In addition to this problem, calculated angles of incidence could be in error by as much as 8° for the larger angles of incidence if both the P and S wave velocities were to decrease by 20% just above the discontinuity. Such a velocity decrease might be expected because the temperatures of the crustal

rock above the magma should be elevated. The decrease would make angles of incidence for the observed data actually less than those calculated from straight ray paths. Moreover, calculated angles of incidence could also be less than actual angles of incidence because of near surface velocity decreases, implied by the positive station corrections found for many stations and the apparent station differences observed in the amplitude ratios. Because of these problems in addition to the scatter in the data, differentiation between types of melt or rock types is not warranted; however, it is clear that the discontinuity is one between rigid and non-rigid rock.

Lateral Extent of the Magma Body

Figure 8 shows the basic ray path configuration used for calculating reflection points employing equations

$$(2Z - D)^2 = (T_{S_zS} \cdot V_s)^2 - \Delta^2 \quad (1)$$

and $A = \text{Tan}(r) \cdot (Z - D)$. (2)

Figure 9 shows the lateral extent of the magma body as defined by both Class A and B data. Reflection points have been calculated assuming a depth to the reflector of 19.2 km and an average S-wave velocity of 3.405 km/sec. Justification for use of these values is given in the next section of this paper. A solid boundary line in Figure 9 indicates the boundary has been closely defined by calculated reflection points and/or COCORP P-wave reflection data. Beyond the solid boundaries to the south, no clear reflections have been observed, although there have been many opportunities for such reflections to occur. This was determined by calculating hypothetical reflection points for microearthquakes that did not actually contain reflection phases. Very weak S_zS reflections from points outside the boundaries are occasionally observed. These are interpreted as being from a solid to solid discontinuity at approximately the same depth as the magma layer. Dashed boundaries

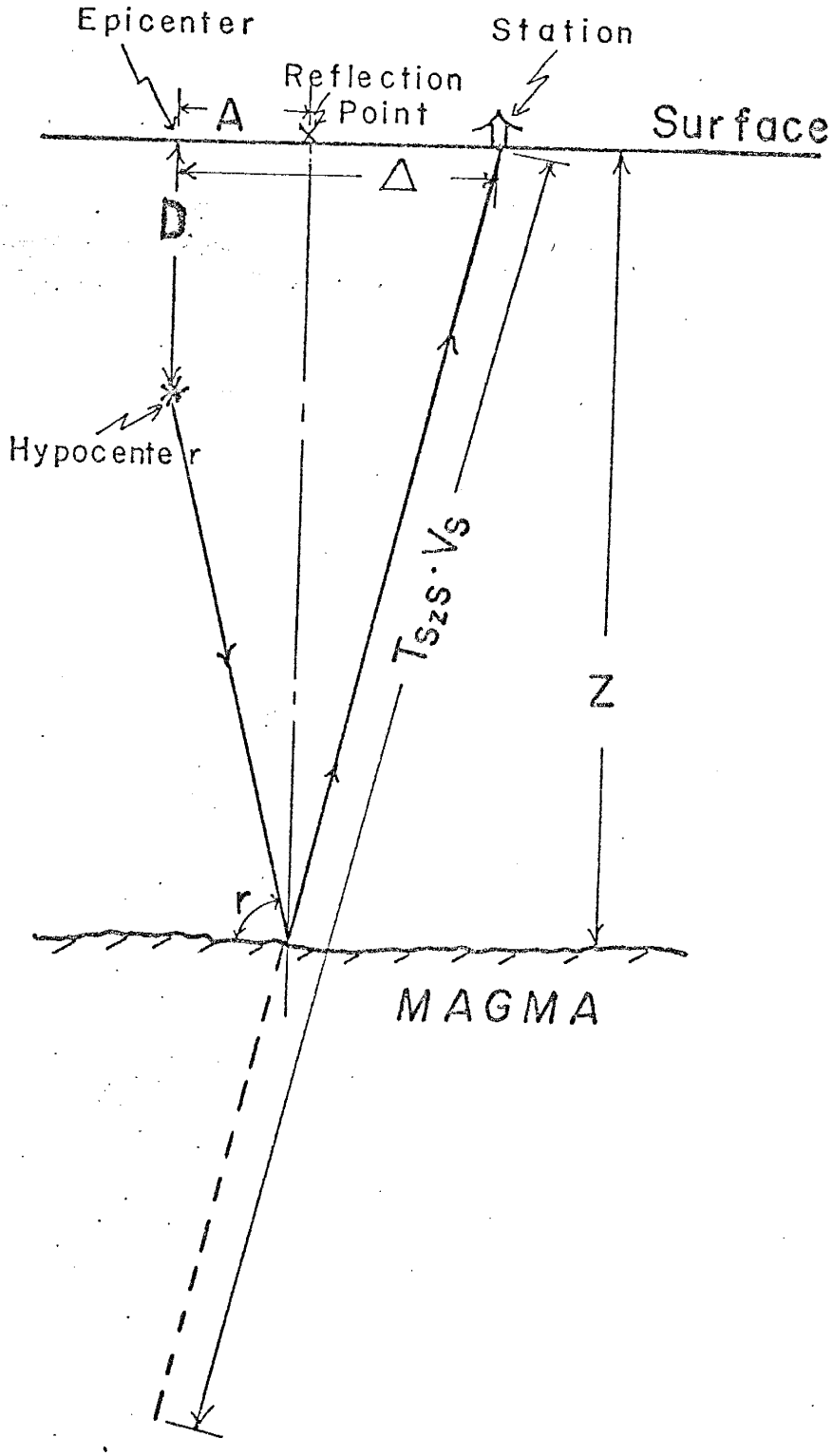

Figure 8. Cross section of the crust showing ray paths and distances. Either the depth to the magma layer or the depth of focus for the microearthquake can be calculated from the S_zS travel times.

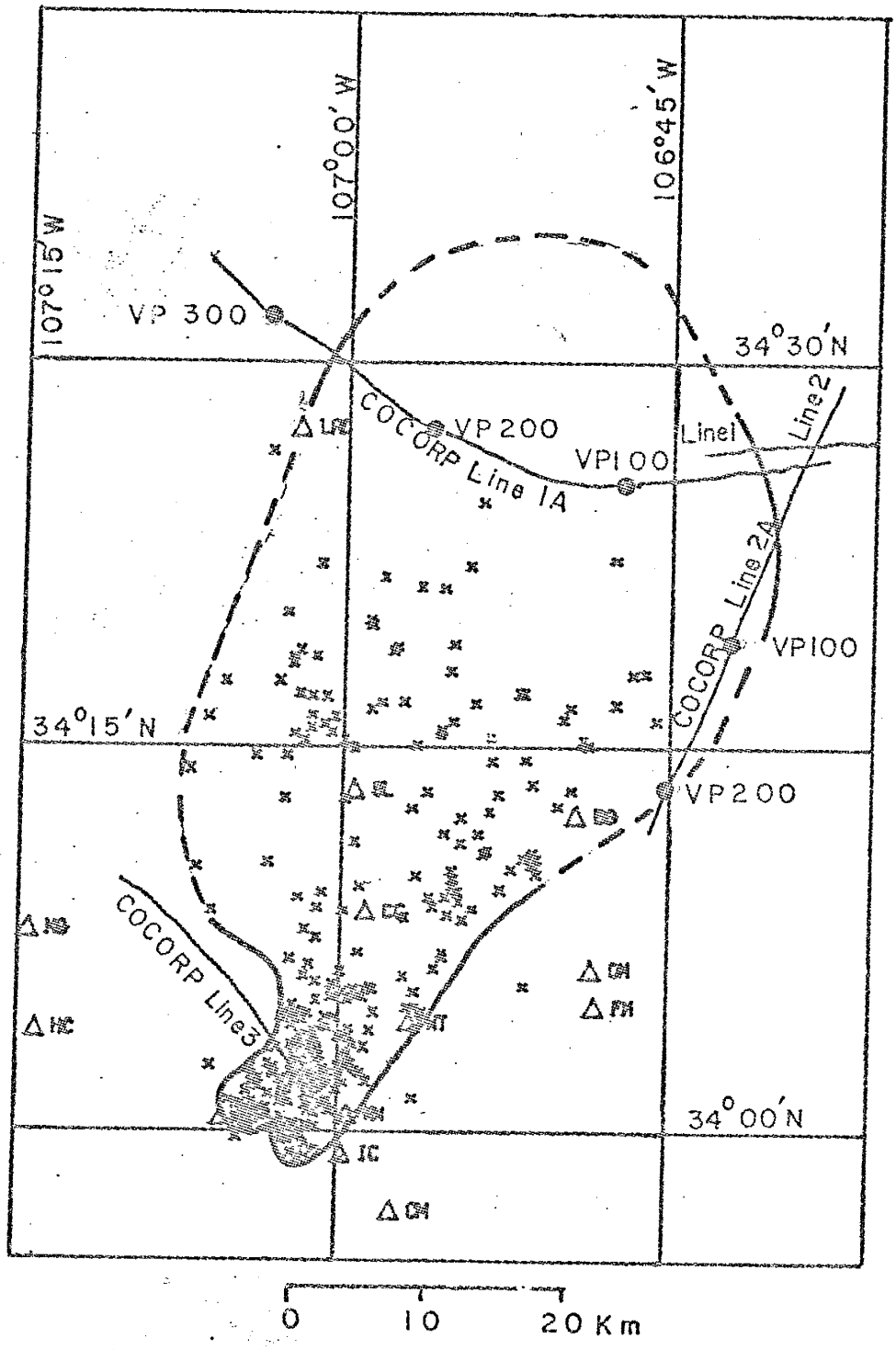

Figure 9. A map of Class A and B reflection points and the outline of the magma body. Reflection points were calculated using reflection travel times and crustal model M2. Also shown is the lateral extent of the body. Solid lines indicate the actual boundary of the body while dashed lines indicate a minimum outward extent of the body. Outliers are caused by poor Class B epicenter locations

indicate only a minimum extent of the magma body due to lack of data.

Errors in the lateral position of reflection points in Figure 9 are dependent mostly upon both epicentral errors and S_zS travel time errors. Depths of focus errors are eliminated by calculating the reflection points using a known S-wave velocity and reflector depth. Errors due to epicentral uncertainties are less than one half the epicentral errors themselves. For well constrained epicenters, reflection point errors are less than 0.2 km; however, for the poorly constrained epicenters for Class B events errors may be nearly 1.0 km. Errors due to the S_zS travel time uncertainties are more complicated to determine. For near vertical ray paths (e.g. reflection points in the southern portion of the area) errors due to travel times are negligible. For an epicentral distance of 30 km, travel time errors of the S_zS reflection of 1.0 second will produce a 1.5 km lateral error in the reflection point. Both the epicentral error and travel time error are additive. For events to the south, then, reflection points probably have errors of less than 0.2 km. Reflection points with epicentral distances greater than 30 km may have errors greater than 2 to 3 km.

North of approximately 34.3°N, the S-wave reflection data do not closely define the boundaries of the magma body. In these regions, the control comes primarily from a strong P-wave reflector seen on COCORP profiles and identified as being the same as the magma body (Brown et al., 1979). On the basis of S_zS reflections observed on seismograms recorded at Albuquerque, the magma body is believed to extend as far north as 34.5°N (Sanford et al., 1973). Considering all available data, the minimum geographical extent of the magma body is on the order of 1700 km^2. The reflecting surface appears to be continuous over this entire

areal extent.

Surface Relief on the Magma Body

A major question in all studies of the magma body has been the amount of surface relief on its upper surface. Mott (1976) was the first to propose some relief on the body. Rinehart (1976) mapped an apparent relief of up to 2 km on the upper surface of the southern portion of the body. The reflection points used to determine this apparent relief were calculated on the assumption that the S-wave energy was reflected from a horizontal surface, i.e., actual dip was not taken into account when determining the reflection points. With this assumption, the shallowest point on the reflecting surface was beneath station WT; from this point the surface dipped in all directions, except the north. A difficulty with this interpretation became apparent when the reflection points were migrated to take into account the effect of their being reflected from a dipping surface (Telford et al., 1976 and Michaels, 1977). The migrated surface became at best, a line source; that is, the reflections were merely a diffraction pattern. That this cannot be the case is clearly shown by time-distance graphs for microearthquake reflection phases in Sanford and Long (1965) and Sanford et al. (1973).

In the earlier interpretations of surface relief, no corrections for travel through low velocity material beneath the stations were applied to the S_zS travel times. When station corrections were applied, any systematic departure from a horizontal discontinuity was lost in the statistical uncertainties of the depth calculations which were on the order of ±3.0 km.

Other observations were used to demonstrate that the reflecting surface has very low relief. First, a study was made of reflector

depths for individual shocks producing reflection phases at two or more stations. If one portion of the reflector is truly deeper than the rest, reflection points falling in this deeper area will always appear differentially deeper. Data thus far analyzed do not indicate any correlatable differential depths over the surface of the magma body.

A second important observation indicating low relief on the upper surface of the magma body is illustrated in Figure 10. Let microearthquakes located at E2 and E3 be recorded at stations CM and WT, respectively. If the dip on the upper surface of the magma body was comparable to that shown in cross section 2, then reflected phases should be recorded at these two stations. Several seismograms of microearthquakes with a ray path geometry similar to Figure 10 were found to have no reflection phases.

Seismograms for microearthquakes with ray paths similar to E1-FM in Figure 10 were also found to have no reflection phases. Cross section 1 indicates reflections would be observed at station FM if the body had 10° or more of dip. Therefore, the approximately eastward dip must be 10° or less which allows no more than about 0.8 km of east to west relief on the upper surface of the magma body.

The last observation indicating low relief on the magma body was an analysis of P-wave reflection data from COCORP profile 1A (Brown et al., 1979). Figure 11 is a simplified drawing of the time-section for line 1A which shows the two major continuous reflectors. The interpretation applied to this section is that the early reflection is from a boundary between low-velocity rock and underlying rock with a velocity of 5.8 km/sec, the average P-wave velocity of the upper crust. The second reflection is the P-wave discontinuity that Brown et al. (1979)

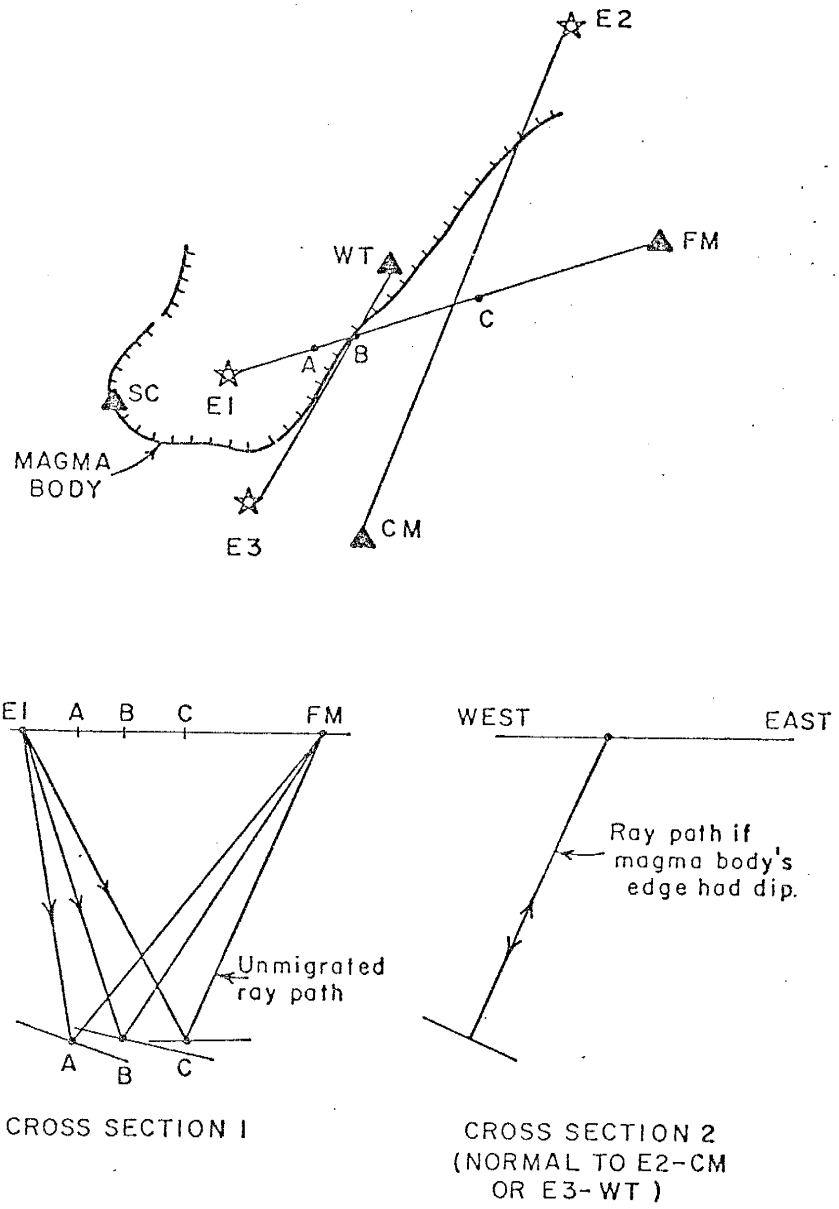

Figure 10. Raypaths for microearthquakes which helped define the relief on the upper surface of the magma body. See text for explanation.

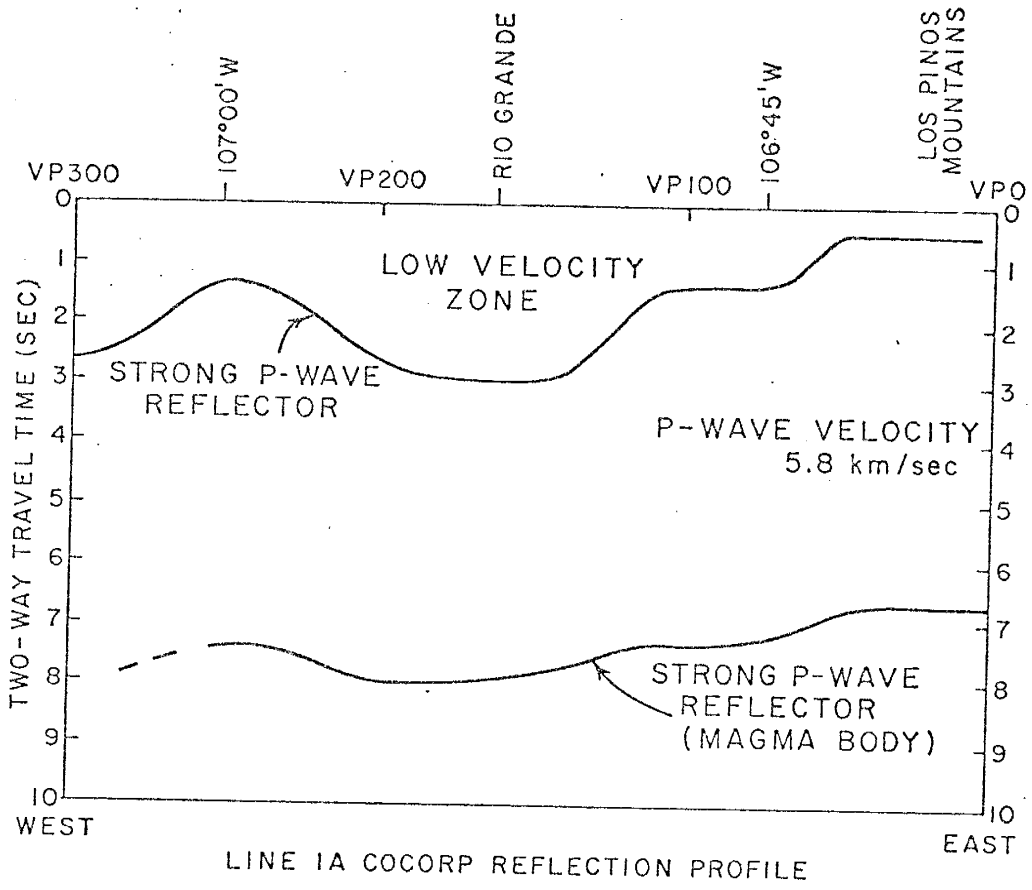

Figure 11. Simplified diagram of COCORP Line 1A showing the two major P-wave reflectors.

associate with the upper surface of the magma body. The apparent relief of the upper surface of the magma body can be explained by time delays associated with the low velocity rock. Consider the two-way travel times to the magma body at VP240, VP175 and VP90. If the low velocity rock has an average velocity of 3.4 km/sec, these travel times indicate a horizontal discontinuity at 19.8 km beneath the surface. Sonic logs from Shell Oil Company Well Shell 2, Santa Fe, located approximately 50 km north of COCORP Line 1A in the Albuquerque-Belen basin given an average velocity for the upper 3.24 km of low velocity material near 3.3 km/sec. (R. W. Foster, personal communication, 1979). Application of a velocity of 3.3 km/sec to the reflection travel times on Line 1A only decreases the depth to the reflector by 0.1 km and the resulting relief is undetectable.

The three observations described above, indicate that to a first approximation the upper surface of the magma body is planar. However, statistical uncertainties in the relief calculated from the above observations still permit a maximum relief of 0.8 km from the extreme edges to the center of the body.

Depth to the Magma Body

The major problem associated with determining depth to any reflector, in this case the magma body, is deciding on the appropriate velocity model to be used. In addition, when using microearthquakes, any error in the hypocentral locations, especially the depths of focus, will affect calculated depths to the reflector. Table 3 gives a comparison between different crustal models, average depths of focus and resulting depths to the magma body for all of the past and present studies. S-wave crustal velocities for the earlier studies were based on P-wave

TABLE 3. S-wave Velocities, Average Depth of Focus, and Depth to Reflector for Four Studies.

Study	S-wave Velocity (km/sec)	Average Depth of Focus (km)	Method of Depth Calculation	Depth Beneath Station WT (km)
Sanford and Long (1965)	3.46	4.8	S-P vs. reflection times	18.0
Sanford et al. (1973)	3.35	8.0	Statistical	17.8
Sanford et al. (1977)	3.35	8.0	Calculation of reflection points	18.0
This Paper	3.40 ± 0.05	7.8 ± 2.2	Crustal inversion	19.2 ± 0.6

velocities and a Poisson's ratio of 0.25. For this study, microearthquake locations, recording station locations and corrected S_zS reflection travel times were used in a least squares, iterative inversion program to determine the average S-wave velocity of the upper crust as well as depth to the magma layer. This inversion will be discussed in the next section.

Thickness of the Magma Body

The available observational data indicate that the magma body is very thin relative to its extent. Analysis of the Gasbuggy refraction data (Toppozada and Sanford, 1976) does not support delays in the refracted Pn arrivals through the magma layer much greater than 0.1 seconds (Sanford, personal communication, 1979). P-wave residuals for teleseisms (Fischer, 1977), with station corrections applied, show delays for stations located above the magma layer which cannot be greater than 0.1 to 0.2 seconds. Tang (1978), inverting teleseismic delay times and Pn delay times obtained from regional mining explosions, found no substantial P-wave velocity reductions due to a magma body located at 19 km. The lack of substantial delay times limits the thickness of the magma layer to 0.6 to 1.2 km if the magma is a full melt. Brocher (1979) using P-wave reflection coefficients estimated from spectral ratios obtained from only COCORP Line 1, estimates thicknesses are between 23-35 m thick.

INVERSION OF S_zS REFLECTION DATA

Introduction

This section presents the inversion schemes, forward models and results of three generalized linear (least squares) inversion models that were applied to the S_zS reflection travel times. These analytical procedures resulted in an average S-wave velocity structure for the Rio Grande rift in the Socorro area and a depth to the extensive magma body.

The three models used for the inversion of the reflection data had different degrees of complexity and goals. The first model, M1, calculated the average S-wave velocity for the entire area and the depths to 36 separate, horizontal rectangular surfaces representing the upper surface of the magma body. The other two models, M2 and M3, assumed a horizontal reflection surface as a first approximation. Model M2 had as its unknown parameter the overall average S-wave velocity of the crust or an average reflector depth. M3 initially permitted three unknown parameters, velocities of a two-layered crustal model and the thickness of the deeper layer; however, only the lower layer velocity could accurately be solved for in the final analysis. The upper layer velocity was constrained to 3.35 km/sec and the depth to the magma body was constrained to 19.2 km. Model M3 was also used with spatially varying data to determine possible lateral velocity inhomogeneities and velocity anisotropies. Data for model M1 and M2 included all Class A reflection data. Model M3 used a restricted data set which only allowed Class A microearthquakes producing three or more reflections.

Inversion Technique

The least squares inversion technique used in this paper is based on one outlined by Braile (1973) and explained in detail by Jackson (1972) and Wiggins (1972). A description of the method used in this study is presented below.

The notation used in this discussion is as follows. Lower case letters represent scalers. Underlined or doubly subscripted capital letters represent entire matrixes or single matrix elements, respectively. Overlined or singly subscripted capital letters represent multi-dimensional vectors. The superscripts "o" and "t" designate observed and theoretically calculated data. The superscript "T" indicates the transpose of a matrix.

The basic purpose of this generalized inversion technique is to minimize, in a least squares sense, the differences between the observed S_zS reflection travel times and the theoretically determined S_zS travel times by calculating and applying appropriate changes to parameters in assumed crustal models. Theoretical travel times are calculated using a forward model whose equation is the parametric functional

$$\bar{T}^t = F(\bar{X}) \tag{3}$$

where $\bar{X}$ is a vector containing all of the model parameters. An expression for the difference between the observed and theoretical travel times is obtained by applying Taylor's expansion about the theoretical travel times obtaining

$$T_i^o \simeq T_i^t + \sum_{k=1}^{m} \frac{\partial T_i^t}{\partial X_k} \Delta X_k + \ldots, \quad i = I, \ldots n, \tag{4}$$

where T_i^o = i^{th} observed travel time,

T_i^t = i^{th} theoretical travel time,

$\frac{\partial T_i^t}{\partial X_k}$ = change of the theoretical travel time with respect to the k^{th} parameter,

ΔX_k = change to be applied to the k^{th} parameter,

n = total number of data,

and m = total number of parameters.

By assuming that second and higher order terms are small, putting the theoretical travel time on the left hand side of equation (4), and calculating the partial derivatives using the functional $F(\bar{X})$, a set of first order, but in these models, non-linear equations can be calculated:

$$\overline{\Delta T} = \underline{A}\,\Delta\bar{X}\,, \tag{5}$$

where $$A_{ki} = \left(\frac{\partial F(\bar{X}_k)}{\partial X_i}\right)_k . \tag{6}$$

We can now solve equation (5) for $\Delta\bar{X}$ such that $\sum_{k=1}^{n}(T_k^{\,o} - T_k^{\,t})^2$ becomes a minimum. The resulting $\Delta\bar{X}$, when added to the starting model parameters, produces new parameters that should best fit the data. If, however, the higher order terms in equation (4) cannot be neglected, or equation (5) is nonlinear in $\bar{X}$, iteration of the inversion becomes necessary until resulting $\Delta\bar{X}$ converges to zero. Physical insight to the problem is also necessary to determine if the least squares results are indeed realistic.

The solution of equation (5) requires an operator $\underline{H}$, the "natural inverse of $\underline{A}$", such that $\underline{H}$ produces the following results (Jackson, 1972):

1. $\underline{R} = \underline{HA} \approx I$, where I is an identity matrix. R measures the uniqueness of the solution.
2. The variances of $\bar{X}$, given by

$$\text{var}\,(\Delta X_k) = \sum_{i=1}^{n} H_{ki}^{\,2}\ \text{var}\,(\Delta T_i) \tag{7}$$

   are not too large .
3. $\underline{S} = \underline{AH}$, where, in this overdetermined problem, $\underline{S}$ measures how the model uses the data.

To obtain the desired inverse, the $\underline{A}$ matrix is decomposed into its eigenvectors ($\bar{U}$ and $\bar{V}$) and eigenvalues ($\underline{\Lambda}$) by (Lanczos, 1961)

$$\underline{A}\,\bar{V}_j = \Lambda_{jj}\,\bar{U}_j \quad , j = 1 \ldots m \tag{8}$$

$$\text{and} \quad \underline{A}^T\,\bar{U}_i = \Lambda_{ii}\,\bar{V}_i \quad , i = 1 \ldots n \tag{9}$$

$$\text{or} \quad \underline{A} = \underline{U}\,\underline{\Lambda}\,V^T \quad , \tag{10}$$

where $\bar{U}$ and $\bar{V}$ are the columns of $\underline{U}$ and $\underline{V}$, respectively. The columns of $\underline{U}$ are the eigenvectors associated with the unknowns or crustal parameters and the columns of $\underline{V}$ are the eigenvectors associated with the data. $\underline{\Lambda}$ is a diagonal (m x m) matrix containing the eigenvalues of $\underline{A}$ representing all of the m unknowns. $\underline{\Lambda}$ and the corresponding eigenvectors are ordered such that the largest eigenvalue appears first, with remaining values in decreasing order. If the original number of parameters in the starting model is greater than the given data can resolve, unresolvable or poorly defined parameters are identified by their zero or near zero eigenvalues. Elimination of these parameters is accomplished merely by reducing the rank or the degrees of freedom of $\underline{\Lambda}$ to p instead of m, where p is now the number of solvable degrees of freedom. It is usually helpful to have in mind some maximum ratio between the highest and lowest usable eigenvalues. Using only p degrees of freedom the "inverse of $\underline{A}$" becomes

$$\underset{(n \times m)}{\underline{H}} = \underset{(n \times p)}{\underline{V}} \quad \underset{(p \times p)}{\underline{\Lambda}^{-1}} \quad \underset{(p \times m)}{\underline{U}} \quad , \tag{11}$$

where the matrixes' orders are given. The solution to the original equation is

$$\underset{(m)}{\overline{\Delta X}} = \underset{(m \times n)}{H} \underset{(n)}{\overline{\Delta T}} \quad . \tag{12}$$

Notice that all of the parameters are solved for; however, poorly defined or unresolved unknowns will have

$$\Delta X_k \simeq 0 \tag{13}$$

with a very small variance and a near null resolution vector (see below).

This method of parameter solution is identical to a classical least squares method only if all of the parameters are resolvable and p = m. One advantage with eigenvector/value decomposition is that if certain unknowns cannot be resolved they are identified and the inversion can still continue by merely changing the number of degrees of freedom from m to p. When $p \neq m$, the classical least squares method fails because the $\underline{A}$ matrix is singular or at best ill conditioned and cannot be inverted unless an entirely new model is calculated. Also, using the eigenvalue elimination method, parameters can be eliminated according to one's wishes by eliminating the respective eigenvalues.

The variances for the changes to the parameters and thus the variances of the parameters are found by equation (7). This may be done by normalizing equation (7) so that the variance of ΔT_i is 1. This is done by dividing $(\overline{\Delta X}\underline{A})$ by the variance $\overline{\Delta T}$ so that equation (7) becomes

$$\text{var}\ (\Delta X_k) = \sum_{i=1}^{n} H_{ki}^2 \quad , \tag{14}$$

which, for statistically independent parameters, becomes

$$\text{var}\ (\Delta X_k) = \text{diag}_k[\underline{H}\underline{H}^T] \tag{15}$$

or the square of the diagonal terms of the $\underline{H}$ matrix (Jackson, 1972).

A useful constant in the inversion routine is the weighting factor τ, which is an estimate of the variance of an unknown parameter. For this study, if any model parameter was assumed known, its τ (or estimate of the variance of the parameter) was set to 0.01. Other than this, no other value different than 1 was given to τ. To use τ, the particular column of the $\underline{A}$ matrix corresponding to the parameter is multiplied by τ which in turn requires that the resulting parameter change also be multiplied by τ. Weighting by very small values produces small eigenvalues which then can be eliminated. This method allows certain parameters to be made constant without rewriting the computer program.

Resolution of the changes to the model parameters is a measure of independence from the starting model a particular unknown retains after the inversion. This should not be confused with variances or uncertainties. The resolution is determined by looking at the k^{th} row of the $\underline{R}$ matrix

$$\underline{R} = \underline{V}\underline{V}^T = \underline{H}\underline{A} \tag{16}$$

for the k^{th} unknown. For complete model independence, a Dirac delta function centered about the k^{th} element is necessary. A zero or null vector results for the k^{th} row of $\underline{R}$ if the k^{th} unknown is completely model dependent. In general, as model independence is lost the resolution decreases, as also does the variance of the parameter.

A most useful tool used in the inversions is the goodness of fit factor

$$r = \left\{ \frac{1}{n} \sum_{i=1}^{n} \frac{(T_i^o - T_i^t)^2}{\text{var}\,(\Delta T_i^o)} \right\}^{1/2} , \tag{17}$$

which is a normalized estimate of the average standard deviation of the entire model with respect to observed travel time errors. If the average is near 1, the resulting standard deviation derived from the model is approximately the same as that observed and the model has provided a satisfactory fit with respect to the data. If the average is much greater than 1, the standard deviation resulting from the model is too large indicating another model should be tried (assuming that the estimates of the variances of the travel times are reliable). On the other hand, if the average is much less than 1, the resulting model has more detail than is reasonable for the expected errors in the data (again assuming the estimates of the variances of the travel times are accurate). The amounts greater than or less than 1 that are permissible are arbitrary.

The ability of generalized inversion to be able to identify which parameters cannot be resolved and how many degrees of freedom a particular data set has, makes it a very powerful tool. On the other hand, it is up to the investigator to decide what eigenvalue range (i.e. the number of degrees of freedom) should be used. It is also up to the investigator to decide what goodness of fit factors are acceptable and when another model should be used. Finally, although answers are always provided, this method still does not eliminate nonuniqueness inherent in many geophysical problems. The validity of the model is still very much dependent upon the investigator.

Inversion Models

For all of the inversion models the following will be given: a figure of the model, theoretical travel time equations, the A matrix equation, the data used and the results. For each model, the observed reflection travel times were calculated by subtracting the associated

microearthquake origin time, as determined by methods outlined previously, from the reflection arrival time. Theoretical reflection travel times were calculated from ray path tracing techniques using hypocentral locations, station locations, crustal model velocities and model depths to the reflector. In all of the models, the resulting inversion was nonlinear and iteration was necessary. All theoretical travel times and the $\underline{A}$ matrix were recalculated before each iteration.

In order to find the standard deviations of the model parameters using equation (16), an estimate of the standard deviation of the observed travel times of the S_zS reflections was necessary. The most important contribution to the travel time error was associated with the origin time of the microearthquake producing the reflection. Although no direct measurement of this error was possible an estimate can be calculated by assuming the average error associated with the hypocentral locations of the microearthquakes is related to the average travel time error. By applying a Taylor expansion to the S_zS reflection travel time equation (1) and taking the proper expected values (see Meyer, 1965, p. 128), the standard deviation of the reflection travel time due to hypocentral errors is

$$\sigma_L = \left\{ \left(\frac{\partial T_{S_zS}}{\partial \Delta} \right)^2 \sigma_\Delta^2 + \left(\frac{\partial T_{S_zS}}{\partial D} \right)^2 \sigma_D^2 \right\}^{1/2}, \qquad (18)$$

where σ_L^2 = variance of the reflection travel times,

σ_Δ^2 = variance of the epicenters (0.16 km^2),

σ_D^2 = variance of the depths of focus (0.81 km^2),

$\frac{\partial T_{S_zS}}{\partial \Delta}$ = the change of reflection travel time with respect to a change in epicenters,

and $\frac{\partial T_{S_zS}}{\partial D}$ = the change of reflection travel time with respect to a change in depths of focus.

Estimates of the variances of epicenters and depths of focus for Class A data are, from Section II, 0.16 km^2 and 0.81 km^2 respectively. The errors in epicenters are probably accurate. The errors in depths of focus are too low when using depths of focus calculated by the iterative location program; but are probably accurate when using the very restricted data set used for model M3. Although a low estimate when using M1 and M2, the error in the depths of focus was kept constant for comparative purposes. Using an hypocentral to station distance of 16.5 km, an S-wave velocity of 3.4 km/sec and a depth to reflector of 18 km, the estimate of the standard deviation due to hypocentral location errors is 0.45 seconds.

The other important error in the travel times was the ability to pick the first arrival of the S_zS properly. This standard deviation was estimated to be ±0.15 second. Since both major errors are additive, the standard deviation of the observed reflection travel time is, by assuming statistical independence of the parameters and adding variances

$$\sigma T_{S_zS} = \left\{\sigma_L^2 + \sigma_{S_zS}^2\right\}^{1/2} , \qquad (19)$$

where $\sigma_{S_zS}^2$ is the variance of the first arrival of the S_zS. The estimate of σT_{S_zS}, which was used in all of the inversion models, was 0.5 seconds. The S-wave velocity and depth to reflector are also in equation

(1) and could contribute some error to the estimate.

Model 1. Model M1 was used to calculate an average S-wave velocity and depth to 36 horizontal reflectors representing the surface of the magma body. Figure 12 shows both a cross section and a plan view of the model. The unequal areal subdivision is an attempt to make the total number of reflection points per horizontal reflecting surface approximately equal. Note that 27 reflectors are contained in the single southwestern most rectangle of Figure 12. Using only Class A data, the theoretical travel time for the i^{th} ray reflecting from the k^{th} surface was calculated using

$$T_i^t = \frac{\left\{(2Z_k - D_i)^2 + \Delta_i^2\right\}^{1/2}}{V_s} \tag{20}$$

where Z_k = depth to the k^{th} reflector,

D_i = depth of focus for the i^{th} event,

Δ_i = i^{th} epicentral distance,

V_s = average S-wave velocity.

The equations defining the sparse $\underline{A}$ matrix were

$$\Delta T_i = \frac{\partial T_i^t}{\partial V_s} \Delta V_s + \sum_{k=1}^{36} \frac{\partial T_i^t}{\partial Z_k} \Delta Z_k \tag{21}$$

where ΔT_i^t = change in theoretical time for the i^{th} ray,

ΔV_s = change in the average S-wave velocity,

ΔZ_k = change in the k^{th} depth to reflector,

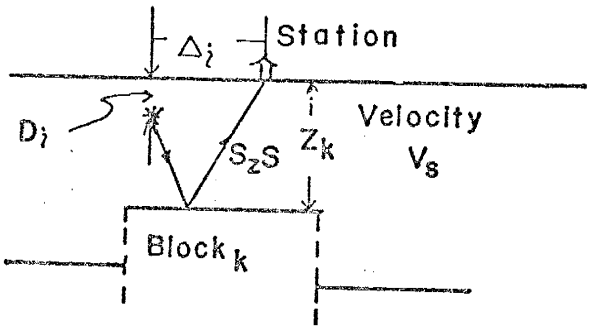

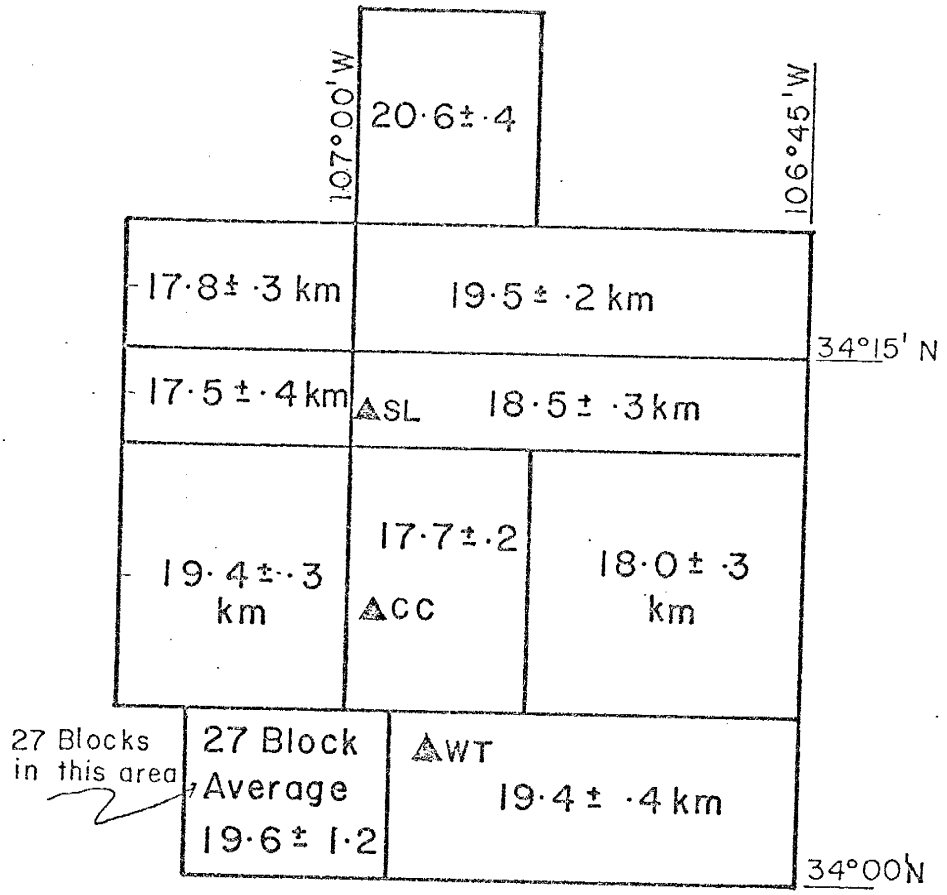

Figure 12. Cross section and areal view of inversion model M1. Included are the means and standard deviations obtained for the depths to reflecting rectangles. Note that there are 27 rectangles contained in the southwestern most area.

$\frac{\partial T_i^t}{\partial V_s}$ = change in the theoretical travel time with respect to change in the velocity

$\frac{\partial T_i^t}{\partial Z_k}$ = changes in the theoretical travel time with respect to a change in the k^{th} depth to reflector.

Figure 13 shows the convergence of the average S-wave velocity and the goodness of fit factor for the entire model. Both the average velocity and goodness of fit factor appear to have approached their best values by iteration number four. All but three of the 36 reflector depths also reached, to within ±0.3 km, their final value by the fourth iteration.

The depths to reflectors (given in Figure 12) are physically unreasonable. Differential depths of up to 2.8 km are present between several adjacent rectangles. This apparent relief is in contradiction to observations, discussed in Section III, which only allow relief on the order of 0.8 km. When the depths obtained from the inversion were plotted against actual values for individual reflection points, it was seen that the inversion values were, indeed, the best average of the data for any particular rectangle. This suggested that the rectangles were too small to adequately model a realistic overall average. Degrees of freedom were eliminated in the model inversion in an attempt to produce one, data dependent, reflecting layer. This resulted in complete model dependence of affected depths of the reflecting rectangles.

The most important result from model M1 is the overall S-wave velocity of 3.405±0.2 km/sec (95% C.I.) obtained from iteration number four. Throughout the remaining analysis, it is this velocity that essentially determines the crustal S-wave velocity structure and depth to

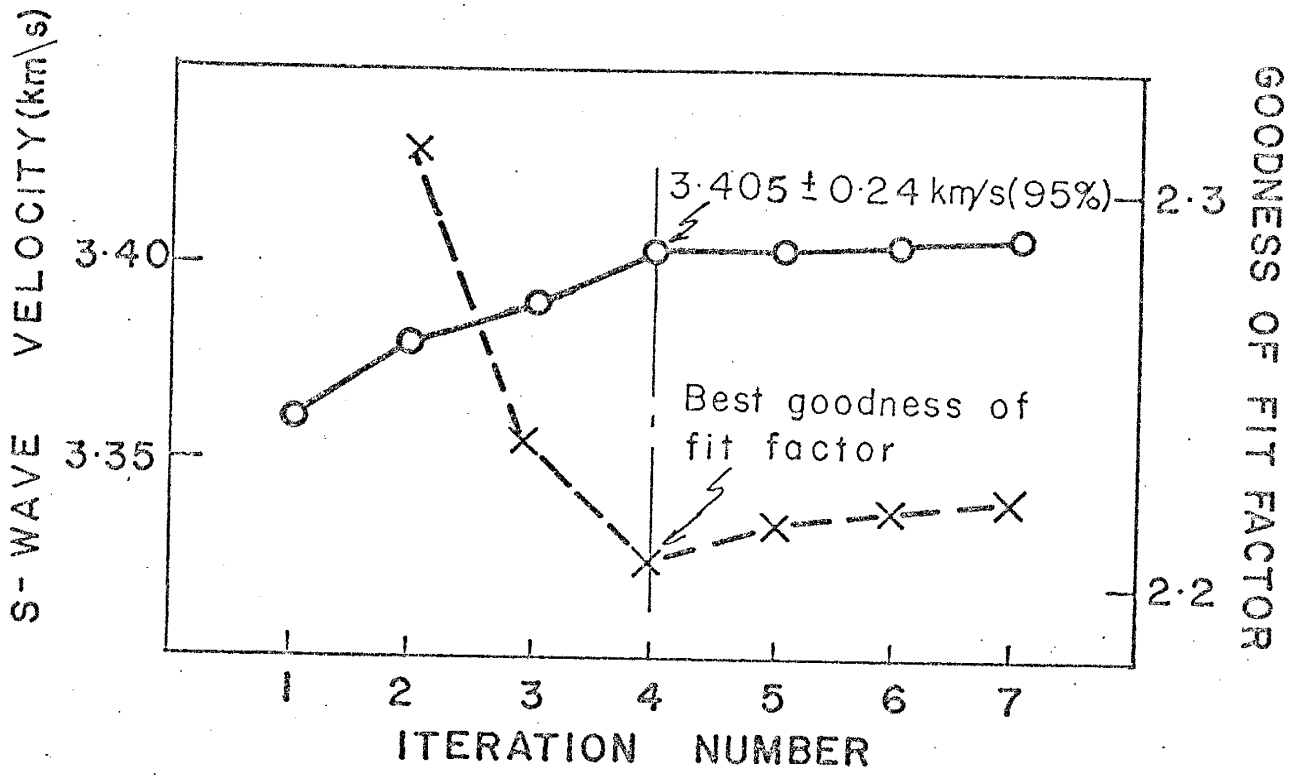

Figure 13. Simultaneous plot of the calculated average S-wave velocity of model M1 (solid line) and the goodness of fit factor (dashed line) versus the iteration step.

the magma body. Three observations lead me to believe that this is a good estimate. First, the velocity obtained was completely data dependent. Second, the velocity converged in a stable manner to a particular solution. Finally, the large range in depths to the rectangles, although physically unrealistic, have, I believe, helped to compensate for errors in depths of focus. Statistically speaking, the average S-wave velocity was found after accounting for errors in the depths of focus.

Two independent observations confirm this S-wave velocity. Using surface wave dispersion data, the first 18 km of the crust in the Rio Grande rift was found to have an average S-wave velocity of 3.4 km/sec (Keller et al., 1979). Sanford et al. (1973) found that an S-wave velocity of 3.38 km/sec produced the smoothest transition of the S_zS reflector depths as they extended it northward from station SNM.

Model 2. M2 was constructed to provide the simpler crustal model required to obtain a physically reasonable depth to the reflector. Model M2, assuming a horizontal, flat reflector, had as a parameter the average crustal S-wave velocity or the average depth to the reflector. It would have been desirable to simultaneously solve for both depth to the reflector and an average S-wave velocity; however, when this was tried with a specialized, more accurate data set (as explained in the discussion of model M3), a continuous trade off between the two occurred. In addition to the tradeoff, the variances of both parameters became too large (on the order of the parameter itself); thus violating condition ? (as set forth by equation (7)), which is required for the "proper inverse of A".

Figure 14a shows the crustal cross section for model M2. Using Class A data, theoretical travel times were calculated by

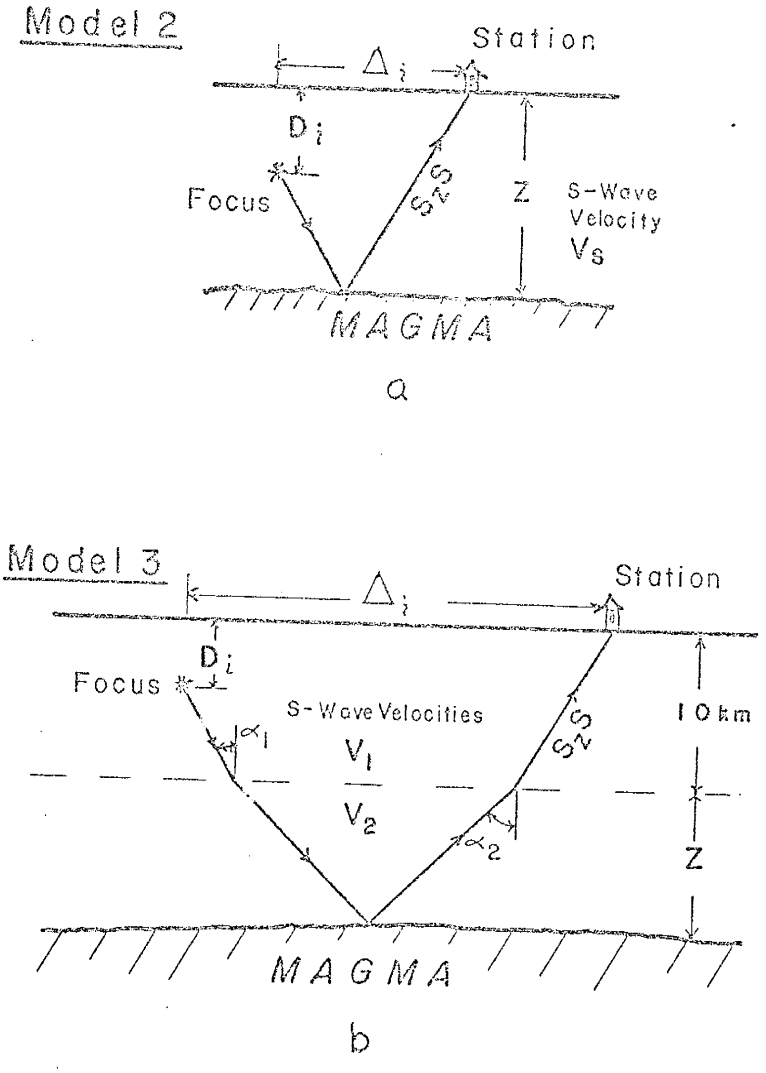

Figure 14. A comparison of inversion model M2 with model M3.

$$T_i^t = \frac{\left\{(2Z - D_i)^2 + \Delta_i^2\right\}^{1/2}}{V_s} , \qquad (22)$$

where Z = depth to the reflector

Δ_i = epicentral distance of the i^{th} event,

D_i = depth of focus for the i^{th} event,

and V_s = average S-wave velocity.

The equations that were solved when the average depth to reflector was the unknown were

$$\Delta T_i^t = \frac{\partial T_i^t}{\partial Z} \Delta Z , \qquad (23)$$

where $\frac{\partial T_i^t}{\partial Z}$ = change in travel time with respect to the depth to the reflector,

and ΔZ = change in the average depth.

The equations that were solved when the average velocity was the unknown parameter were

$$\Delta T_i^t = \frac{\partial T_i^t}{\partial V_s} \Delta V_s \qquad (24)$$

where $\frac{\partial T_i^t}{\partial V_s}$ = the change in travel time with respect to the velocity,

and ΔV_s = change in the average velocity.

In all calculations, convergence to a solution that was completely independent of the starting model, as determined by the resolution matrix

and equation (16), was obtained by the fourth iteration.

Using the S-wave velocity of 3.405 km/sec, found in M1, the average depth to the reflector is 19.3±0.6 km (s.d.), with a goodness of fit factor of 2.0. On the other hand, when a depth to reflector of 19.3 km was used to find the best S-wave velocity, a value of 3.436±0.02 km/sec (s.d.) resulted, also yielding a goodness of fit value of 2.0. The disparity between the two results, although both are within each other's 95 percent confidence intervals, is a result of which parameter (i.e. depth or velocity) was changed to minimize the travel time residuals in the least squares sense. To obtain a best least squares velocity of 3.405 km/sec using model M2, the required depth to the reflector was of 19.1 km.

Once an average S-wave velocity and depth to reflector are known, depths of focus for every Class A and Class B microearthquake producing a reflection can be calculated from equation (22) using S_zS reflection travel times. Assuming that the microearthquakes are independent and randomly distributed both in time and space, a Central Limit Theorem of Probability (Meyer, 1965, p. 233) can be applied to differences found subtracting depths of focus calculated using the iterative location program from the depths of focus calculated using the reflection travel times. If the depths of focus calculated by the iterative program are considered to be, on the average, accurate, the average differences between the two types of depths should be zero if a proper depth to reflector is used. Using all Class A data and 41 additional Class B hypocenters, a depth to reflector of 19.1 km resulted in a zero average difference using a S-wave velocity of 3.405 km/sec. The S_zS reflection time from the closest recording station was used to calculate the depths of focus to minimize any errors arising from a poor estimate of the assumed S-wave velocity. In addition, the histograms of both types of depths of focus should be the same. Figure 15

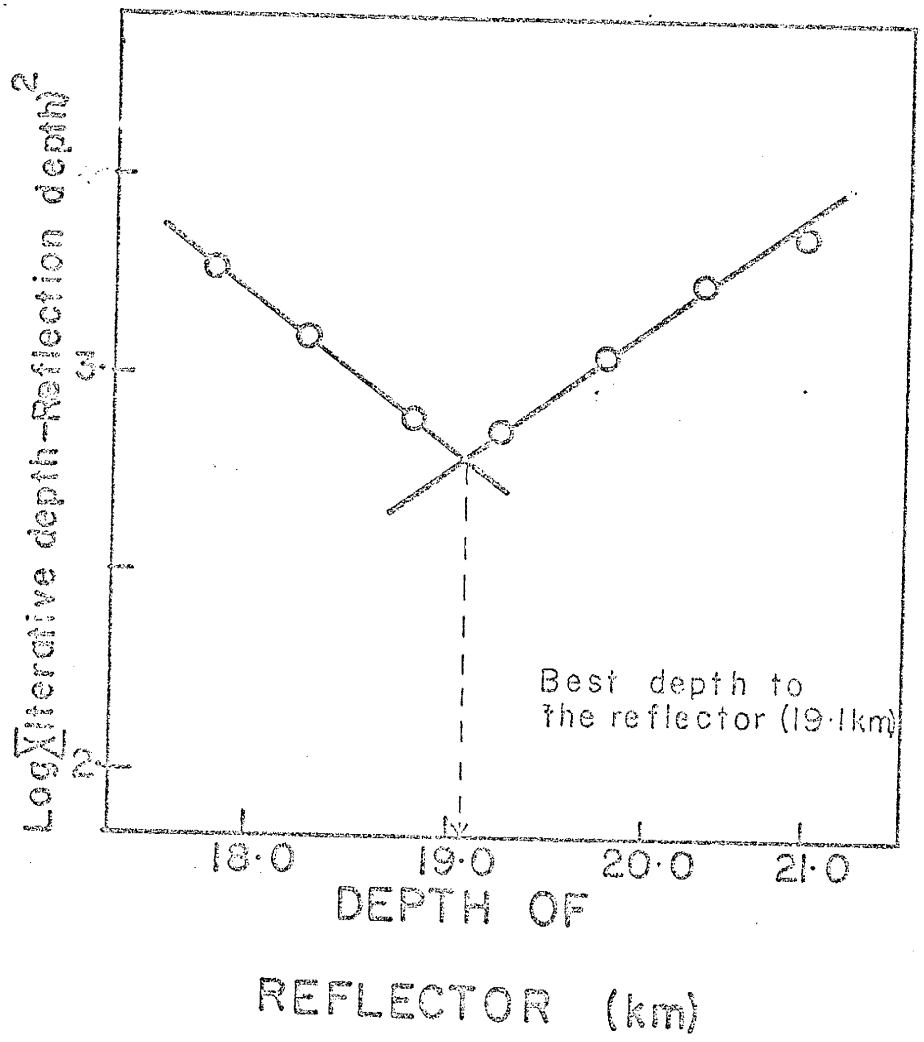

Figure 15. Logarithmic sum of the squared residuals of microearthquake depths of focus obtained in two ways. The residuals are the differences between depths calculated using the iterative location program and the depths calculated using $S_z S$ travel times. Model M2 was used with 158 microearthquakes. The average minimum residual is 2.0 km.

shows the sum of the squares of the differences between the histogram for iterative depths of focus and several histograms calculated using S_zS travel times and assuming different depths to reflector. A depth to reflector of 19.1 km gave the best fit. The advantage in using the histogram matching method is that different data sets can be used.

The final results from model M2 are (1) an average S-wave velocity of 3.405±0.025 km/sec (s.d.) and (2) a best reflector depth between 19.1 km and 19.3 km or 19.2 km with standard deviation of ±0.6 km. This depth is based upon a best velocity of 3.405 km/sec.

Iterative depths of focus and depths of focus calculated using S_zS reflection travel times for both Class A and Class B events are listed in Appendix 2. Differences of up to 5 km exist between them. These larger than expected differences help explain the large goodness of fit factors obtained in the very detailed M1 inversion model because the estimate of var (ΔT_i^o) in equation (17) was too low. Because of the large discrepancies between the two depths of focus, it was decided that if any detailed information was to be determined using reflection data, depths of focus based on S_zS reflection travel times must be used. Using a standard deviation of 0.3 seconds in the S_zS reflection travel times and a standard deviation of 0.6 km in the depth to the reflector, a standard deviation of approximately 1.4 km is obtained for the new depths of focus calculated using the reflection data. This standard deviation is now a closer agreement with the value used in equation (18).

Model 3. To obtain a more detailed velocity structure from the S_zS travel time data, model M3, containing two horizontal crustal layers, was constructed (see Figure 14b). The velocities of each layer and the thickness of the deeper layer were parameters in the model. Changes in angles of incidence of the ray path within the different layers was incorporated. As

explained later, all depths of focus used were calculated using model M2 and S_zS travel times. Theoretical travel times were

$$T_i^t = \frac{(20 - D_i)}{V_1 \cos(\alpha_1)} + \frac{2Z}{V_2 \cos(\alpha_2)} \tag{25}$$

for events with depths of focus less than 10 km and

$$T_i^t = \frac{10}{V_1 \cos(\alpha_1)} + \frac{2z - D_i}{V_2 \cos(\alpha_2)} \tag{26}$$

for events with depths of focus greater than 10 km, where T_i^t and D_i are as previously defined and,

z = thickness of the lower layer,

V_1 = S-phase velocity of the first layer,

V_2 = S-phase velocity of the second layer,

α_1 = angle of incidence of the ray in the first layer,

α_2 = angle of incidence of the ray in the second layer.

α_1 and α_2 are related by Snell's law. The equations to be solved were

$$\Delta T_i^t = \frac{\partial T_i^t}{\partial Z} \Delta Z + \frac{\partial T_i^t}{\partial V_1} \Delta V_1 + \frac{\partial T_i^t}{\partial V_2} \Delta V_2 \ , \tag{27}$$

where ΔZ, ΔV_1 and ΔV_2 are changes in the unknown parameters and

$\frac{\partial T_i^t}{\partial Z}$ = change in theoretical travel time with respect to the lower layer thickness,

$\frac{\partial T_i^t}{\partial V_1}$ = change in theoretical travel time with respect to the upper layer velocity

and $\frac{\partial T_i^t}{\partial V_2}$ = change in theoretical travel time with respect to the lower layer velocity.

The upper layer thickness was fixed at 10 km because it is at this depth in the crust where microearthquakes start to be scarce, possibly implying a crustal change.

Application of perfect travel time data for the two-layered model showed that the inversion could produce correct results. However, when the test data contained random errors of up to ±0.2 seconds, accurate results were elusive. Individual layer velocities, although apparently completely independent, produced overall average velocities and not the individual layer velocities used for calculating the perfect data. Variances, depending upon ray path orientations and estimates of observed travel time errors remained approximately the same for both data sets as did the depth to the reflector. It is easy to show that many velocity and depth combinations produce essentially the same theoretical travel time curves, especially for small angles of incidences. For example, a 19.3 km layer having a constant velocity of 3.4 km/sec produces to within ±0.1 sec the same travel time reflection curve up to a distance of 100 km as a two-layered case having a 10 km thick upper layer with rock having an S-wave velocity of 3.223 km/sec and a lower, 9.3 km thick layer of 3.6 km/sec velocity rock. It is only at much greater distances or with the introduction of refraction data that these two different structures can be properly distinguished. Similar problems with inverting reflection data to find both velocities and depths of layers have been noted by Gibson et al. (1979).

Because of the inherent lack of parameter resolution, model M3 was reduced to one degree of freedom from the start. The S-wave velocity selected for the upper layer was 3.35 km/sec. This velocity was obtained by multiplying the upper crustal P-wave velocity of 5.8 km/sec

by $\sqrt{3}$ corresponding to a Poisson's ratio of 0.25. This estimate of Poisson's ratio was established as the best local average by Fender (1978) using measured S-P intervals for local microearthquakes in conjunction with locations found from the iterative location program. Total depth to the reflecting interface was set at 19.2 km as determined in model M2.

The epicentral locations and S_zS reflection travel times used in model M3 were taken directly from the Class A data set; however, depths of focus were calculated using the average S-wave velocity of 3.405 km/sec and the depth to an horizontal reflector of 19.2 km. To be used in model M3, the microearthquakes must have produced S_zS reflections at three or more stations. From the 106 resulting restricted travel times, the S_zS reflection travel times from seismograms obtained at the closest recording stations were used to calculate the individual depths of focus. Only the remaining 77 reflection travel times were used in the inversion with the newly calculated depths of focus. Because the depths of focus were calculated using reflection travel times, the estimate of 0.5 seconds for the standard deviation of the reflection travel times is approximately correct.

The restricted data set was further broken down to determine if any lateral inhomogeneities and/or anisotropies are present in the Socorro area. To check for anisotropy, two data sets were used; one having horizontally projected ray path azimuths within ±30° of north or south, and the other having projected ray path azimuths within ±30° of east or west. The data were also separated into three geographic areas; one north of 34.125°N, one between stations SC and WM and one located in the south-central part of La Jencia basin (See Figure 3). The inversions converged quickly and the results are shown in Table 4.

TABLE 4. Velocities Calculated Using Model M3 and a Restricted Data Set

Data Set	Velocity of Lower Layer (95% C.I.)	Goodness of Fit Factor
Basic data	3.44 ± 0.05 km/sec	0.8
North-South Ray Paths	3.43 ± 0.07 km/sec	1.1
East-West Ray Paths	3.49 ± 0.08 km/sec	1.0
North of 34.125°N	3.50 ± 0.07 km/sec	1.3
East of SC	3.57 ± 0.14 km/sec	0.8
Central La Jencia Basin	3.25 ± 0.11 km/sec	0.7

The one degree of freedom system indicated that at the 95% confidence level, the lower layer has a three percent higher velocity than the upper layer. On the average there are no differences between east-west or north-south S-wave velocities. S_zS travel paths originating near station SC and being recorded at stations WT and CC have, however, produced travel times that required a six percent decrease in the S-wave velocity. This indicated either a low velocity area in the south-central part of La Jencia basin or time delays near the recording stations. It must also be remembered that all of these results are based on depths of focus and depth to the reflector that were calculated using the average S-wave velocity of 3.405 km/sec.

Discussion of the Inversion Results. Figure 16 is a time versus epicentral distance plot for Class A reflection travel times. All observed data have time and distance corrections to take into account the different depths of focus of each separate shock. These corrections were calculated using hypocenters, calculated by the iterative location program, in conjunction with the results of model M3 and equations (25) and (26). The corrections essentially raise the foci of the events to the surface. The data plotted include all Class A reflection travel times; that is, there was no segregation of data based on azimuth or spatial position of the reflection ray paths. Reflection travel times for small epicentral distances include data from events located in the northern area that were recorded by northern stations as well as southern events that were recorded by southern stations. The reflection travel times for large distances include both northern event-southern station and southern event-northern station combinations. That is, the data shown contain both reversed and unreversed profile data.

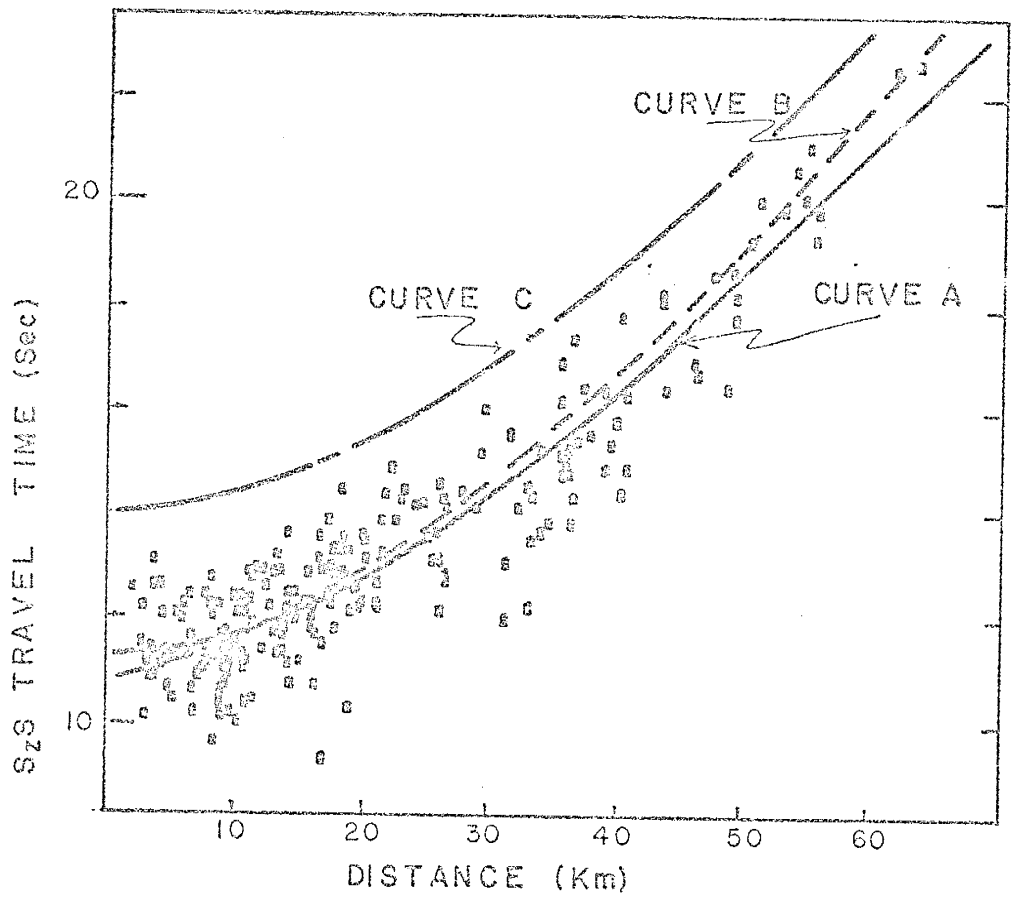

Figure 16. Travel time of Class A S_zS reflections versus epicentral distance. Times and distances have been corrected to account for different depths of focus of individual shocks. Curve A is the theoretical travel time curve for either final model M2 or M3. Curves B and C are the northward (dashed) and southward (dot-dashed) travel times for the crustal model proposed by Sanford et al. (1973).

The solid line (Curve A) in Figure 16 is the theoretical travel time curve calculated using the best final least squares result from model M3. The upper 10 km thick layer contains crustal material with an S-wave velocity of 3.35 km/sec and the deeper, 9.2 km layer, has material with a 3.44 km/sec S-wave velocity. The solid line is quite close to (within the line thickness) another theoretical travel time curve for a 19.2 km thick layer having an average crustal velocity of 3.405 km/sec which is the best least squares result obtained for model M2. The fit between both theoretical curves and the data is good. Most of the scatter in the data is due to erroneous depths of focus.

Curve B, the dashed line in Figure 16, is a theoretical travel time curve assuming the crustal model proposed by Sanford et al. (1973). This model assumes a depth to reflector of 17.8 km beneath station SNM, a crustal S-wave velocity of 3.35 km/sec and a northward dip of the reflector of 6 degrees. At first glance this model also appears to fit the data quite well; unfortunately, this good fit is only for the south to north (unreversed) travel time curve. Curve C is a theoretical curve calculated for a north to south (reversed) travel path starting 50 km north of station WT (near station LAD) using the 1973 crustal model. This curve lies above all of the actual reflection travel times, including shocks located near station LAD which produced reflections at station LAD. If the 1973 model were valid, there should be at least some occasional reflection data near Curve C. The data are not consistent with an interface dipping to the north by 6 degrees.

Figure 17 is a similar type of time versus epicentral distance plot showing the restricted data set used in model M3. Again, times and epicentral distances for the data are corrected for their different depths

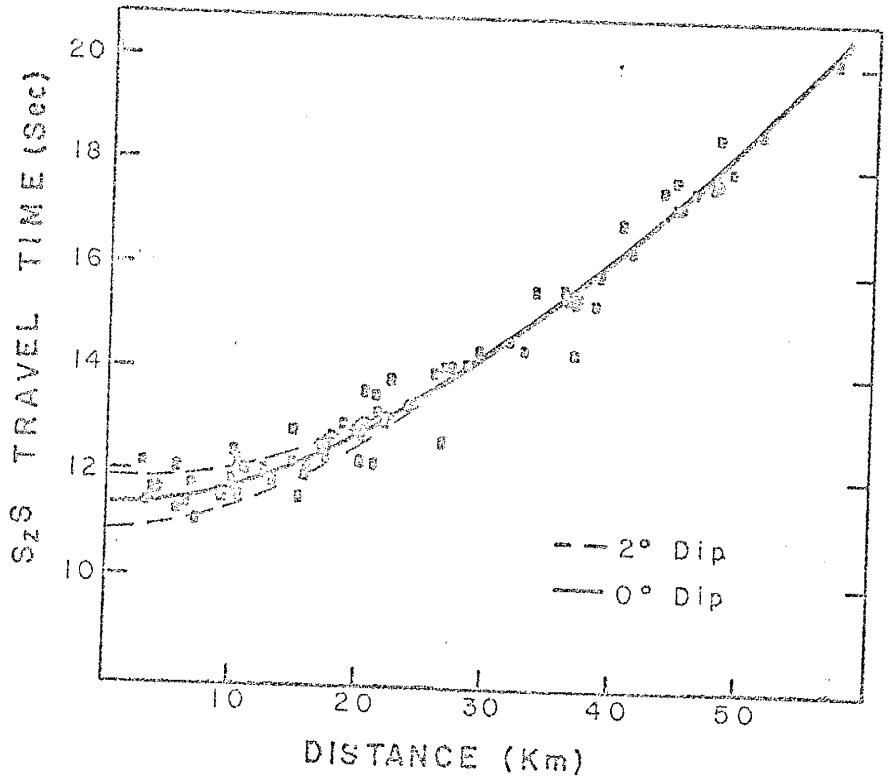

Figure 17. Travel time of S_2S reflections versus epicentral distance using a restricted data set. Times and distances have been corrected to account for different depths of focus. The solid line is the theoretical travel time curve for final model M3. The dashed curves are calculated for a discontinuity with a northward dip of two degrees.

of focus by mathematically bringing the foci to the surface. The depths of focus used for Figure 17 were calculated using S_zS reflection times. Again the solid line is the theoretical travel time curve for the two-layered model obtained from model M3. Also included in Figure 17 are two dashed lines representing both the reversed (upper curve) and unreversed (lower curve) theoretical travel times for a simple one-layered model with an interface dipping 2 degrees northward. Depth to the interface is 18.6 km beneath station WT and the average crustal velocity is 3.405 km/sec. It is seen that the data also fit this model to sufficient closeness.

Three models apparently fit the data equally well; (1) a two-layer horizontal interface crustal model found from model M3, (2) a one-layer crustal model with an horizontal interface found from model M2 and (3) a one-layer model having an interface dipping 2 degrees toward the north. Each of these crustal models was found using a different mathematical approach. It is clear that no absolutely unique solution can ever be found. On the other hand, various models can be eliminated. Perhaps a more useful approach to the inversion of travel times would be to calculate all possible crustal models that fit the data rather than to solve for one particular "correct" model, in other words, to use the Monto Carlo inversion technique (see Parker, 1977). Included in this Monto Carlo technique could be more than just the reflection travel times. For example, the upper crustal P-wave velocity, Poisson's ratio, density restrictions placed on the model by gravity studies and refraction travel time data could also be included. Rather than one particular crustal model being made to fit the data, a range of acceptable models would be produced which might give more realistic physical insight to the inversion.

DISCUSSION

Distribution of Hypocenters

Two important byproducts of this study have been the accurate areal location of 99 microearthquake epicenters and the calculation of depths of focus for more than 135 microearthquake hypocenters to within ±1.0 km (s.d.). The distribution of these locations is now discussed.

Epicenters. Figure 18 shows the epicenters of all Class A and Class B microearthquakes. Errors in epicentral locations, discussed in Section 2, are less than ±0.4 km (s.d.) for Class A data and are believed to be less than 1 km for Class B data (Sanford et al., 1979). Superimposed on this figure are the major Quaternary rift faults that are exposed at the surface, major physiographic features of the area (R. Chamberlin, personal communications, 1979; and Sanford et al., 1979) and the extensive magma body described in Section 3. There may be some bias in the location of epicenters on the map because only events with reflections appearing on at least one recorded seismogram are shown; however, when compared with Sanford's et al. (1979, Fig. 2) Rio Grande rift seismicity map the only major discrepancies appear in the southeastern and the northern areas. Sanford et al. (1979) show much more activity beneath and to the south of stations DM and FM as well as more activity near station LAD than is indicated in Figure 18. Nevertheless, two dominant observations remain: (1) diffuse activity with no overall integral relationship with tectonic rift faults and (2) centering of epicenters over the magma body.

The correlation of the diffuse pattern of epicenters in the Socorro area with the magma body and not tectonic features was expected and is noted by Sanford et al. (1977) and Sanford et al. (1979). Aki et al.

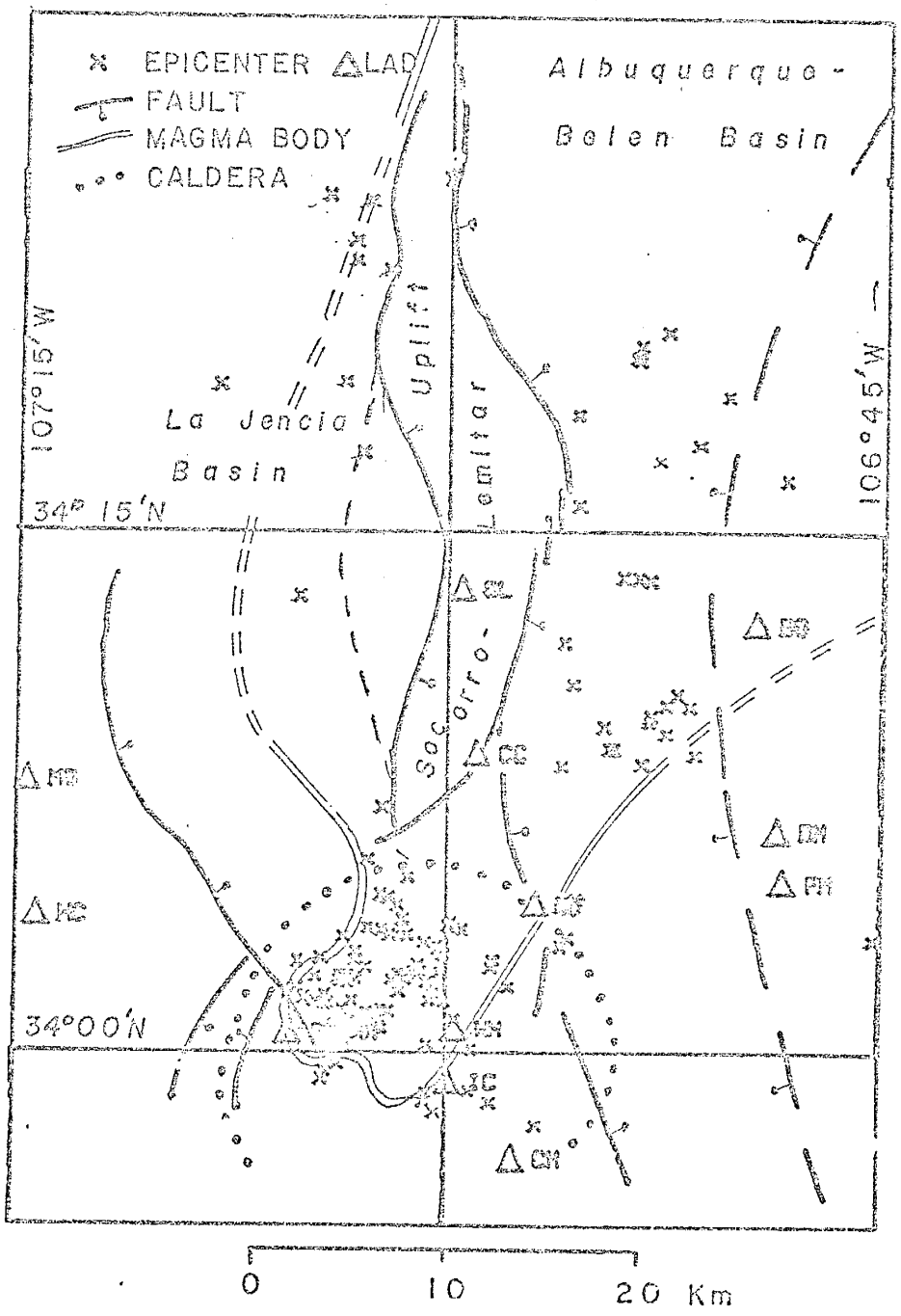

Figure 18. Map of Class A and B epicenters of microearthquakes in relation to major faults, the margin of the extensive magma layer and the intra-rift Socorro-Lemitar uplift. The geology is from R. Chamberlin (1979, personal communication) and Sanford et al. (1979).

(1978), in a passive seismic recording experiment designed to locate a known, shallow, basaltic sill magma body in Kilauea Iki, found that the spatial distribution of seismic events originating from the crust above the magma body best defined it. The present study suggests the same thing; however, there is a lack of defining epicenters near the western boundary of the extensive magma body and there is also very limited activity within the Socorro-Lemitar intra-rift uplift. The lack of activity in both areas could be because of poor temporal sampling. On the other hand, it may represent, on the western edge, a lack of contemporaneous magmatic activity. The lack of contemporaneous activity in the intra-rift uplift may possibly reflect the lifting of the intra-rift uplift block en masse. The abundance of activity southwest of station WT has been attributed to the possible intrusion of small magma bodies into the upper crust (Sanford et al., 1979).

Depths of Focus. Figure 19 shows four west to east cross sections, with no vertical exaggeration, of both Class A and Class B hypocentral locations between 34.00°N and 34.08°N latitudes. Figure 20 shows four west to east cross sections of wider dimensions, with a 2.5 to 1 horizontal exaggeration. All depths of focus were calculated using reflection travel times from the closest recording station, a reflector at 19.2 km and an S-wave crustal velocity of 3.405 km/sec. All southern (below approximately 34.10°N latitude) and the northern events with small recording station to hypocenter distances, have depths of focus that are accurate to within ±1.4 km (s.d.). Northern events with large hypocentral distances have depths of focus believed to be accurate to within ±3.0 km. For convenience, appropriate stations, the Socorro-Lemitar intra-rift uplift and two identifiable, large surficial

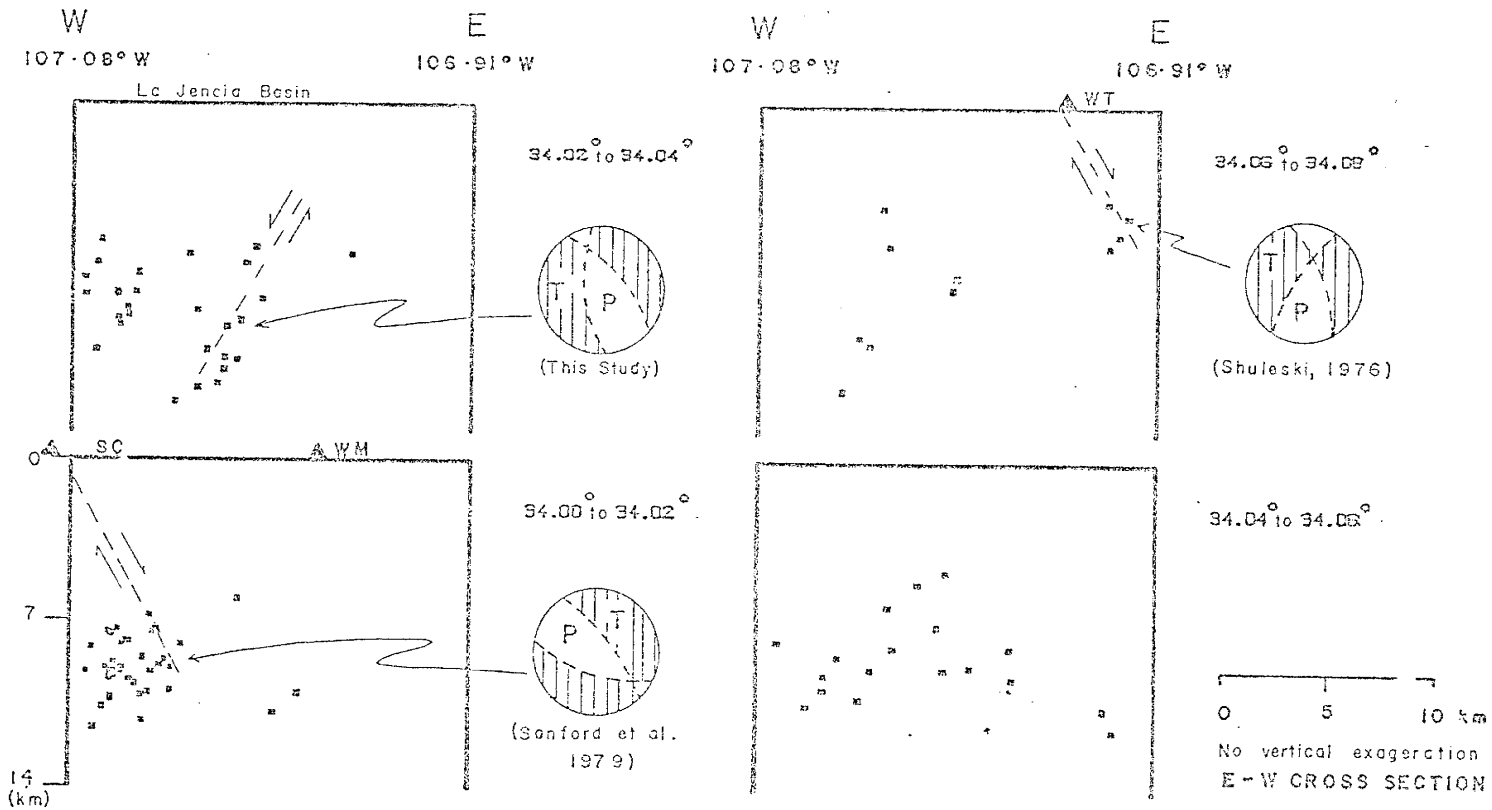

Figure 19. Four west to east cross sections of microearthquake hypocenters located in the local Socorro area. Dashed fault zones are inferred from the indicated fault plane solutions and where possible from surface features.

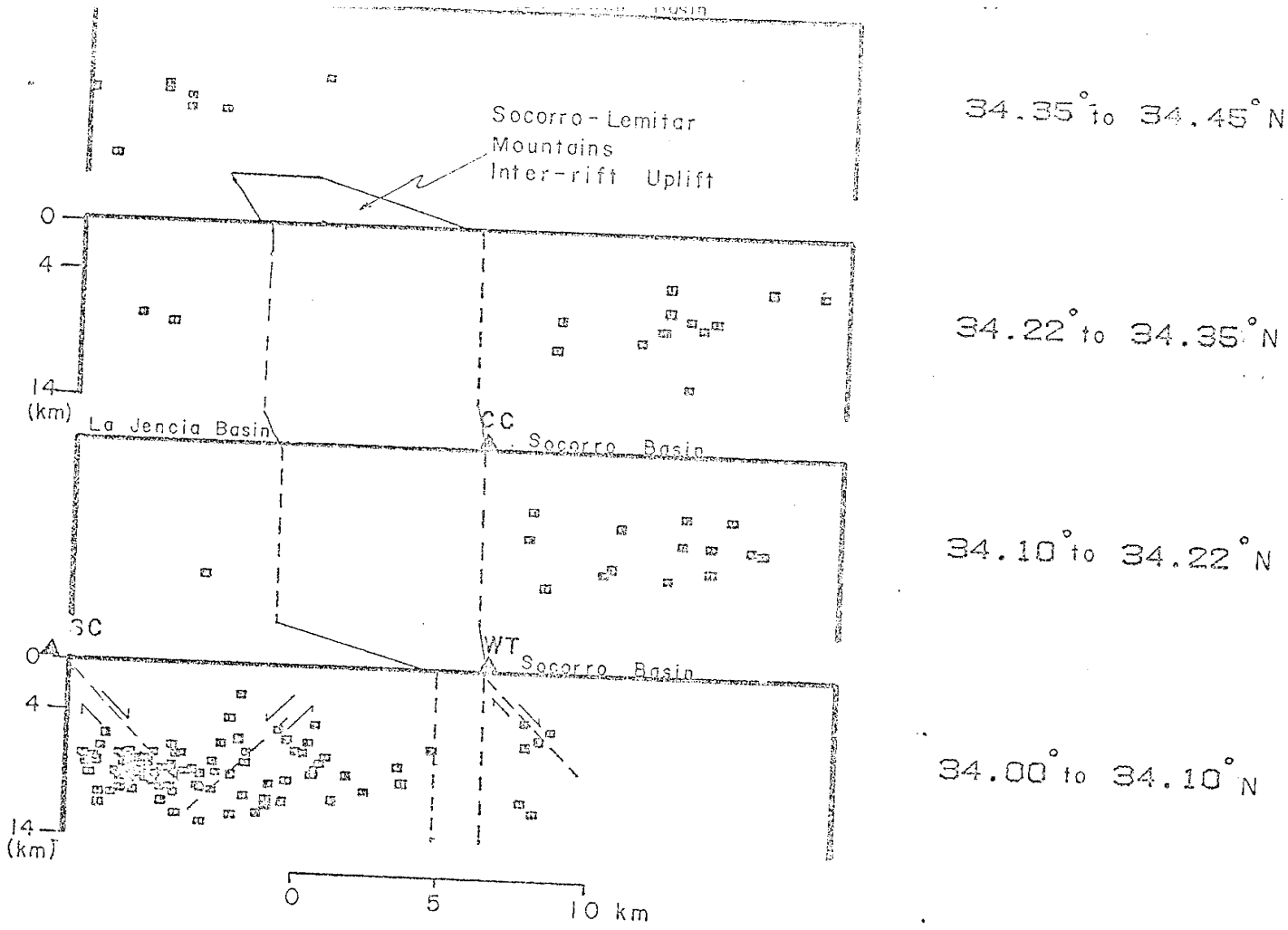

Figure 20. Four west to east cross sections of microearthquake hypocenters determined for a crustal volume extending from just south of Socorro to approximately 50 km to the north. The Socorro-Lemitar uplift (R. Chamberlin, personal communication, 1979) is also shown.

Quaternary faults are shown in Figures 19 and 20. The two surficial faults near stations SC and WT have been extended into the cross sections using the 60 degree fault zone dip angle obtained from first motion fault plane solutions. The implied fault in the cross section between 34.02°N and 34.04°N was drawn only as a result of a first motion P-wave composite fault solution obtained by using seven well located events that occurred in the fault zone. No definite surface feature has yet been identified in the area because of a Pliocene lava extrusion.

Five substantial observations are made from the two figures. (1) Hypocenters generally occur randomly in the crust. (2) If major surficial faults are located, hypocenters are not restricted to individual major fault planes but rather are contained in broad fault zones. This has also been observed in other regions of normal faulting such as the Basin and Range province (Stauder and Ryall, 1967) and in the Intermountain Seismic belt to the west of Socorro (Smith, 1978). (3) Hypocenters are limited in depth to between 3 and 13 km. (4) There is no difference in the hypocentral depths from one intra-rift basin to another, i.e. activity in the Socorro basin is distributed about the same as it is in La Jencia basin. (5) There is, as previously observed, a lack of activity in the intra-rift uplift.

Figure 21 shows the histogram of both Class A and Class B events. The activity is almost normally distributed between 3 and 13 km. Occasional surface shocks have been observed that are not apparent in this survey (Sanford et al., Fig. 9, 1973). The lack of activity above 3 km is expected because the accumulation of stresses is released either by slow frictional sliding along preexisting surface fractures or by stable sliding in limestone, alluvial fill or ash flow tuff surficial sections

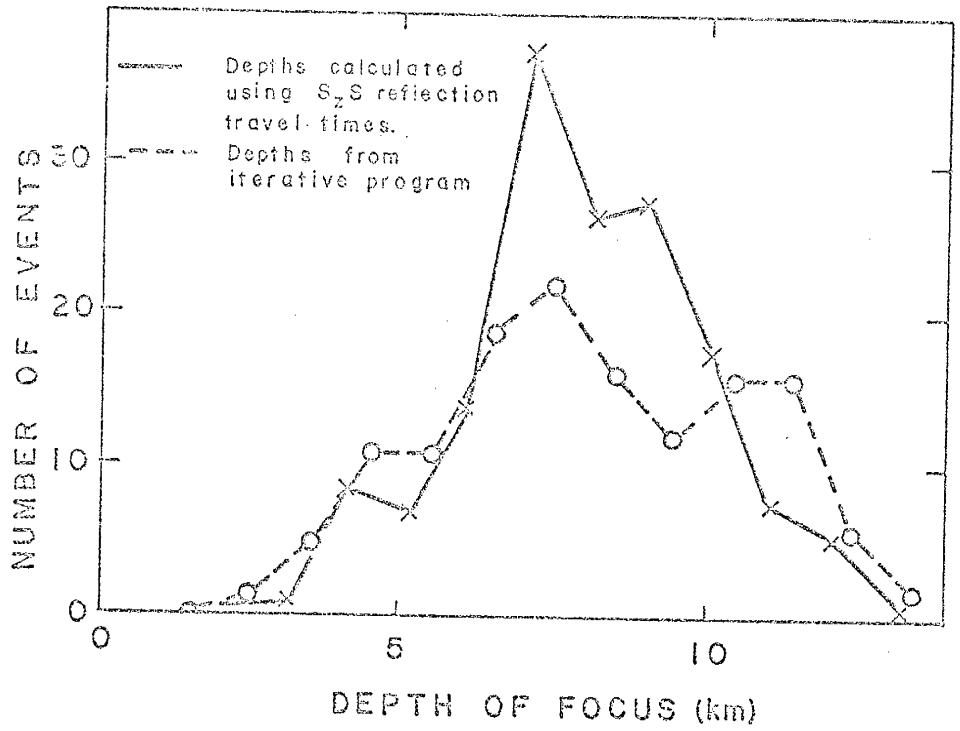

Figure 21. Histogram of microearthquake depths of focus. The solid line is for depths calculated using S_zS travel times and the final crustal model M3. The dashed line is for iterative depths of focus.

overlying the zones of failure (Byerlee and Brace, 1968). Both surface fractures and the specified overlying surface sequences are present in the Socorro area. The beginning of microearthquake activity at 3 km in depth is the result of increased forces normal to the fracture that prevent further slow frictional sliding and result in the beginning of the stick slip release mechanism. The very few surface events that do occur in the area could possibly be caused by compressive stresses released in exposed, nonfractured basement rock, well indurated sandstones or basaltic lava flows, again all of which exist in the Socorro area and all of which fail by stick slip at low temperatures and pressures (Byerlee and Brace, 1968).

The lower limit of the stick slip zone (or microearthquake zone) is dependent upon the type of basement rock and the pressure-temperature regime of the crust. Increasing pressure should enhance the strength of the crustal material and stress release should be by stick slip; on the other hand, increasing temperature should decrease the yield strength of the asperities on the fault surface producing stable sliding and perhaps plastic or ductile flow. Comparisons of depths of focus for microearthquakes recorded in other normally faulted areas may indicate that the Socorro area is not seismically abnormal especially when considering the higher than normal heat flows measured in the area (Reiter et al., 1975; Reiter and Smith, 1977; and Sanford, 1977). Smith (Fig. 6-7, 1978) indicates that for four known hotter than normal crustal zones (Marysville, MT: Yellowstone Nat'l. Park; Pocatello Valley, ID-UT; and Roosevelt Hot Springs, UT) microearthquake activity is above 15 km and that the activity peaks between 5 to 10 km; almost identical in nature to the depths of focus measured in the Socorro area. Normal faulting activity in

cooler crustal zones (Central Nev.) has been independently measured to be mostly between 10 and 15 km in depth (Stauder and Ryall, 1967 and Westphal and Lange, 1967), which is substantially deeper than the 7.8±2.0 km obtained in the Socorro area depths of focus. Nonetheless, it is possible that there exists in the Socorro area, below approximately 10 to 13 km, a crustal zone that allows long term strains to be released via stable sliding, i.e. plastic or ductile flow.

The Magma Body

Upper Surface. This study has shown that the upper surface of the extensive magma body is located approximately at 19 km beneath the Socorro area and is a sharp, flat, nearly horizontal discontinuity. The data are also consistent with a northward dip of the interface of less than two degrees. Study of COCORP data, especially Figure 11 of this report and Figure 3 of Brown et al. (1979) uphold these conclusions.

Perhaps the most unusual feature of the magma layer is the absence of any resolvable relief even though it lies beneath surface rift structures which have vertical displacements that are quite large (see Figure 18). Near Socorro, differential movements between horsts and grabens of up to 3.8 km have been interpreted from gravity observations (Sanford, 1968) and movements of up to 5 km have been postulated on the basis of geologic mapping (Chapin et al., 1978). The lack of substantial relief on the magma body indicates detachment of the brittle uppermost crust from a more ductile zone at lower levels of the upper crust.

The limitation of northward dip on the upper magma surface to less than two degrees allows the upper surface to be concordant with gross crustal layering inferred from seismic refraction data including both the upper surface of the crust and/or the Moho.

The upper surface of the extensive magma body appears to blend directly into a solid to solid interface. COCORP Line 1A (Brown et al., Figure 3, 1979; and Figure 11 of this study) indicates that beneath VP250, the strong P-wave reflector identified by Brown et al. (1979) to be the magma body appears to abruptly transform, as one goes west, into a less definite, although prominent reflector at the same depth. Because of the reduced P-wave reflection coefficient it is probable that this is a solid to solid interface. The lateral transformation zone between the magma and solid crust may be as little as a few hundreds of meters as indicated by Line 1A. A similar transition zone is seen in COCORP Line 1 beneath VP30 (see Brown et al., Figure 3, 1979) as one goes to the east. The inferred solid to solid P-wave reflector has also produced several very weak S_zS reflections that bring about calculated reflection points that lie outside of, but at the same approximate depth as, the southern boundary of the extensive magma body. For example, during the entire microearthquake study, approximately five to 10 percent of the microearthquakes originating near station SC and producing seismograms at station GL had a hint of an apparent S_zS reflection. On the other hand, many coincidental hypothetical reflection points and the lack of any unmistakable reflections in the same area resulted in the interpretation that no magma layer existed in this area. The absence of the magma body in this area has been substantiated by COCORP Line 3. Similar observations are applicable for an area just to the east of station WT.

Two independent seismic refraction studies indicate that there exists, at approximately the same depth as the magma body, a solid to solid interface (Conrad) over an extensive area both within and to the

west of the rift (Toppozada and Sanford, 1976) and to the east of the rift (Olsen et al., 1979). The proximity of the magma layer and the Conrad suggest that the material above the Conrad has sufficient strength to resist further upward movement of the magma; it provides a magma cap rock.

Type of Magmatic Material. A basic question often asked is what type of material is contained in the extensive magma body. Although direct geophysical measurement is almost impossible, indirect lines of evidence suggest that the material is mafic. Intermediate magmatic material is eliminated as a possibility in this discussion because (1) it is usually associated, not with the rifting process, but with subduction zones and (2) the rapid decline of observed intermediate extrusions beginning around 12 to 14 m.y. ago (Chapin and Seager, 1975). The possibility of silicic or acidic material will be greatly reduced by the following discussion.

The most recently extruded material within the central Rio Grande rift including the Socorro area is basalt. Starting approximately 20 km north of the mapped northern limit of the magma body as shown in Figure 8 and proceeding southward, dates of the most recent extrusions are: (1) Cat Hills dated to be 0.14 m.y. old by Kudo (1976), (2) Los Lunas basaltic flows dated to be 3.4 and 1.3 m.y. old, (3) Black Mesa at San Acacia dated to be 4.5 m.y. old, (4) Black Mesa 30 km east of Socorro dated to be 3.5 m.y. old, (5) Black Mesa 15 km southwest of Socorro dated to be 4.0 m.y. old and (6) the extensive San Marcial basalt flow 40 km south of Socorro dated to be 3.5 m.y. old. ((2) through (6) are from Backmen and Mehnert, 1978.) The youngest silicic extrusion to be dated in the entire local Socorro area is at least 6 m.y. old (Chapin, personal

communication, 1979).

Several arguments can be made for an actively intruded magma body rather than in place partial melting. The best argument in favor of intrusion is made by considering heat and mass requirements. For in place melting to be a viable option Lachenbruch et al. (1976) suggest that both extensive amounts of heat and some additional amounts of H_2O must be brought into the crustal zone. H_2O is necessary to affectively reduce the melting temperature of the crust to a value near 700 to 800°C which is perhaps more compatible with the measured heat flow values of the area. Any preexisting H_2O was probably used up by earlier generation partial melts; these partial melts are implied by the numerous observed silicic extrusions in the area. Lachenbruch and Sass (1977) suggest that the only practical method of bringing sufficient heat close enough to the surface to cause crustal melting, even at a relatively low 700°C if the H_2O is somehow supplied, is by crustal intrusion of lower crustal/upper mantle material. In addition Lachenbruch et al. (1976) indicate that the injected material must have (1) low viscosity, (2) high temperature and (3) high heat capacity or enthalpy; that is be a mafic magma. In other words, to have a partial melt, intruded mafic material is almost a prerequisite.

The geometrical shape and estimated maximum thickness of the magma body indicate that it is a sill. Two arguments, assuming an intruded sill shaped magma body, can be made for mafic material. The first is that the material is derived from lower crustal/upper mantle material. The high velocity, lower crustal material (Vp $\cong$ 6.5 km/sec) is characteristic of denser (more mafic) materials as is the high velocity (Vp $\cong$ 7.9 km/sec; Toppozada and Sanford (1976)) upper mantle material

postulated for the area. The second argument is the fact that the only material with low enough viscosity to be intruded as a sill is mafic. Experimental data from Murase and McBirney (1973) indicate that there exists at least a four order magnitude viscosity difference between basalts ($\approx 10^2$ p) and rhyolites ($\gtrsim 10^6$ p) which have been fully melted. Because the intrusion is into cold country rock further restraints are placed on the amount of enthalpy and viscosity. Lachenbruch and Sass (1978) indicated that the only material to meet these requirements is again mafic.

Actively intruding lower crustal or upper mantle mafic magma would very easily explain the amounts and distribution of the local seismicity observed by Sanford et al. (1979), the microearthquake swarming (Sanford et al., 1977) and the rapid surface uplift observed by Reilinger et al. (1979). An intruded, fully melted material might also be expected to have both the observed sharp upper and lateral boundaries observed in this paper. In place melting would probably produce gradational changes from the solidus to partial melt.

There are supporting hypotheses and observations from other workers to support a basalt layer. Conservation of the mass required to obtain the higher than normal heat flows observed in the area necessitates mafic intrusions (Lachenbruch and Sass, 1978; and Cook et al., 1978). Basaltic intrusions have been predicted also on petrologic grounds. Baldridge (1979) suggested that "the importance of olivine and plagioclase as fractionating phases [of basaltic extrusions occurring in the rift] indicates that this fractionation occurs at depths . . . compatible with the [extensive] magma body." If indeed, crystal fractionating is taking place in the intruded basalt, the crystal settlings on the

lower surface of the magma body would probably not form a singular, sharp lower boundary thus causing no reflections to be generated. Ramberg et al. (1978), after "stripping" gravity anomalies caused from all lower density Cenozoic sediments, found a broad +30 mgal gravity anomaly which they interpreted to be a shallow slab of basalt or a deep upwarp of the mantle that results in crustal attenuation. This last observation is from the Southern Rio Grande rift; similar "stripping" procedures have not as yet been applied to gravity data for the Socorro area.

Confirmation of the ability of basalt to form thin (2.1 to 0.5 km) extensive (100's to 1000's km^2) magma sheets or sills comes from Hunter (1978). In the Bushveld Complex in Africa several thin basaltic sills crop out and have been geologically and geophysically mapped over extensive areas.

Crustal Model

The geophysical and geologic evidence presented in this study allows an upper crustal rift model to be postulated for the zone above the Conrad and/or magma body in the Socorro area. Figure 22 is a diagram of the model which shows two zones above a crustal depth of 19 km. The first zone extends from the surface to approximately 10 km. The second zone begins at approximately 10 km in depth and extends to the magma body. The transition between the two layers is not sharp and may be on the order of 2 to 3 km. Also, the entire upper crust beneath the Precambrian upper surface is quite transparent to S-wave seismic energy, except for the shallow magma bodies postulated by Sanford et al. (1979).

The three basic substantiating observations for an uppermost brittle layer are (1) the stick slip mechanism for stress release (i.e. microearthquakes), (2) observed vertical offsets of up to 3 to 5 km and (3) the substantially lower than normal P-wave and S-wave velocities indicating

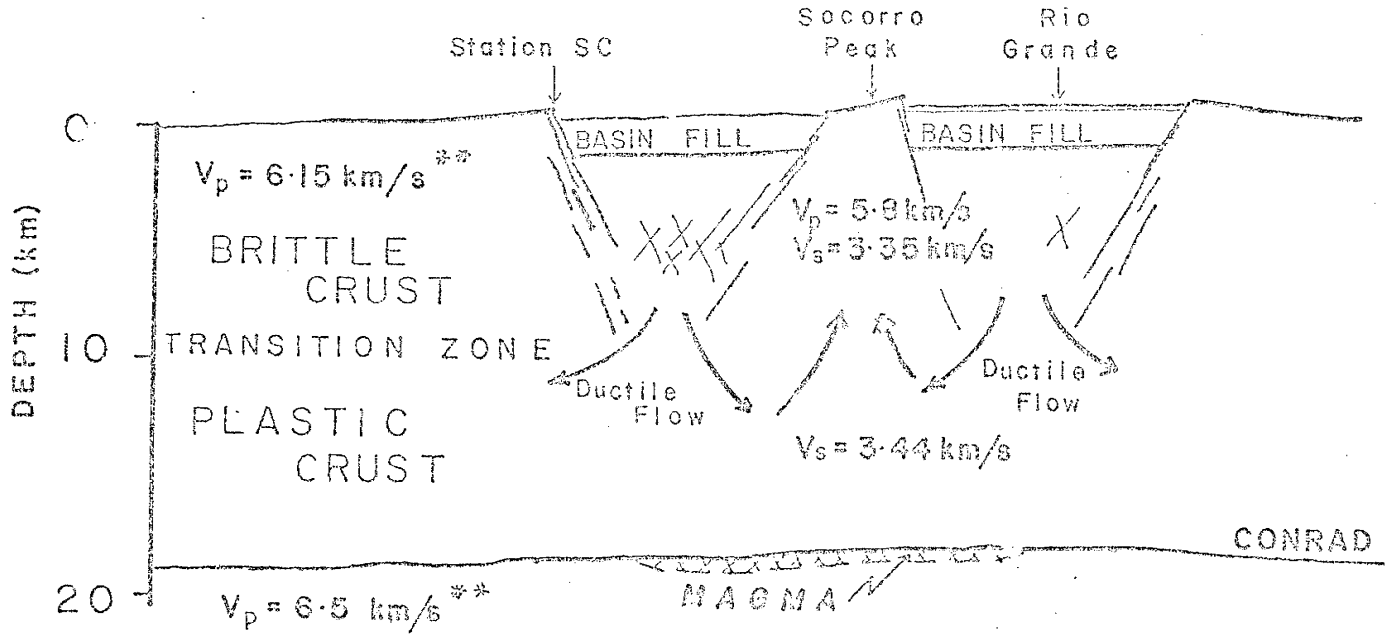

** Toppazada & Sanford (1976)

Figure 22. A diagram of the postulated model of the upper crust near Socorro, New Mexico. Verticle scale exaggerated approximately two times.

preservation of many crustal fractures sustained in the brittle crust.

The brittle failure, or microearthquake activity observed appears to be confined to the region of the crust directly above the extensive magma body. This suggests that the magma body, most likely through active inflation, is the cause of the activity. As a result, the need for general extension of the entire crust as a means for present day stress and strain accumulation as perhaps expected by the recent normal fault scarps severing Pleistocene surfaces (Chapin and Seager, 1975) is minimized. Indeed, it has been observed that the Socorro area is not now undergoing active extension (Prescott and Savage, 1979).

The lower layer in the crustal model is interpreted to be a ductile or plastic layer beginning around 10 km. The two primary observations to support this interpretation are (1) lack of any microearthquakes within this lower zone and (2) detachment of the flat, horizontal magma layer from an extremely brittle upper crust supporting vertical displacements of up to 5 km.

The importance of a ductile layer in the upper crust is twofold. It allows easy flow of crustal material away from crustal zones that have an overabundance of material such as down dropped structural basins and it allows for substantial lower crustal flow into voids caused by any crustal extension or crustal compression. The zone also allows detachment from the basement of any preexisting or contemporaneous stress regime existing at the surface (Jaeger and Cook, p. 398, 1976). This would in turn allow the shape of the extensive magma body to be structurally controlled. This, of course, lends more support to the idea of an extensive crustal discontinuity (the Conrad) controlling the placement of magma at depth.

It is interesting to note that from a detailed seismic refraction study a crustal low-velocity layer located between 10 and 15 km in depth has been suggested to be continuous from the Basin and Range province into the Middle Rocky Mountains by Braile et al. (1974). This low-velocity layer was implied using time delays associated with retracted Pn arrivals. They also indicate that Poisson's ratios as high as 0.32 may be interpreted suggesting a zone of low rigidity in the physiographic provinces to the west and northwest of Socorro. The low rigidity zone in the Socorro area may perhaps be an extension of the same layer into the Rio Grande rift.

The transition zone between the two different physical states of the upper crust, beginning at approximately 10 km is supported by the rapid decline of brittle or stick slip rock failure. This transition zone appears to coincide rather well with a major electrical discontinuity. Jiracek et al. (1979) using magnetotelluric sounding techniques near COCORP Line 1A detected a decrease in resistivity by two orders of magnitude from a 2000 or 200 ohm-m upper layer to a 20 or 2 ohm-m lower layer maintaining the two orders of magnitude drop. This decrease, interpreted to be a decrease in rigidity, occurred between 8 and 10 km in depth. The transition zone produces no reflections nor refractions of seismic waves and is thought to be on the order of a few kilometers thick.

Aki, K., B. Chouet, M. Fehler and G. Zandt: Seismic properties of a shallow magma reservoir in Kilauea Iki by active and passive experiments, J. Geophys. Res., 83, 2273, 1978.

Bachman, G. O. and H. H. Mehnert: New K-Ar dates and late Pliocene to Holocene geomorphic history of the central Rio Grande region, New Mexico, Geol. Soc. Amer. Bull., 89, 283-292, 1978.

Baldridge, W. S.: Petrology and petrogenesis of Plio-Pleistocene basaltic rocks from the Central Rio Grande rift, New Mexico, and their relation to rift structure, in Riecker, R. E., ed., Rio Grande Rift: Tectonics and Magmatism, A. G. U. Wash., D. C., 323-353, 1979.

Braile, L. W.: Inversion of crustal seismic refraction and reflection data, J. Geophysics. Res., 78, 7738-7744., 1973.

Braile, L. W., R. B. Smith, G. R. Keller and R. M. Welch: Crustal structure across the Wasatch Front from detailed seismic refraction studies, J. Geophys. Res., 79, 2669-2677, 1974.

Brocher, T. M.: Geometry and physical properties of a magma body in the Rio Grande rift from COCORP data, Transactions, (E@S), A. G. U., 60, p. 396, 1979.

Brown, L. D., P. A. Krumhansl, C. E. Chapin, A. R. Sanford, R. A. Cook, S. Kaufman, J. E. Oliver and F. S. Schilt: COCORP seismic reflection studies of the Rio Grande rift, in Riecker, R. E., ed., Rio Grande Rift: Tectonics and Magmatism, A. G. U., Wash., D. C., 169-184, 1979.

Byerlee, J. D. and W. F. Brace: Stick slip, stable sliding, and earthquakes--effect of rock type, pressure, strain rate, and stiffness, J. Geophys. Res., 73, 6031-6038, 1968.

Chamberlin, R. M.: Structural development of the Lemitar Mountains, an intrarift tilted fault-block uplift, Central New Mexico, 1978, International Sym. on the Rio Grande rift, Prog. and Abstracts, 22-24, 1978.

Chapin, C. E.: The Rio Grande rift, Part I: Modifications and additions, N. Mex. Geol. Soc. Field Conf. Guideb., 21, 191-201, 1971.

Chapin, C. E.: Evolution of the Rio Grande rift--a summary, in Riecker, R. E., ed., Rio Grande Rift: Tectonics and Magmatism, A. G. U. Wash., D. C., 1-5, 1979.

Chapin, C. E., R. M. Chamberlin and J. W. Hawley: Socorro to Rio Salad[illegible], in Hawley, J. W., ed., Cir. 163, N. Mex. Bur. of Mines and Resour., Socorro, NM, 121-134, 1978.

Chapin, C. E., R. M. Chamberlin, G. R. Osburn, D. W. White and A. R. Sanford: Exploration framework of the Socorro Geothermal Area, New Mexico, Field Guide to Selected Cauldrons and Mining Districts of the Datil-Mogollon Volcanic Field New Mexico, New Mexico Geol. Soc. Special Pub. 7, 114-129, 1978.

Chapin, C. E. and W. R. Seager: Evolution of the Rio Grande rift in the Socorro and Las Cruces area, N. Mex. Geol. Soc. Field Conf. Guideb., 26, 297-321, 1975.

Cook, F. A., E. R. Decker and S. B. Smithson: Preliminary transient heat flow model of the Rio Grande rift in Southern New Mexico, Earth Planetary Sci. Let., 40, 316-326, 1978.

Eaton, G. P.: A plate-tectonic model for late Cenozoic crustal spreading in the Western United States, in Riecker, R. E., ed., Rio Grande Rift: Tectonics and Magmatism, A. G. U. Wash., D. C., 7-32, 1979.

Fender, J. J.: A study of Poisson's ratio in the upper crust in the Socorro, New Mexico area, N.M.I.M.T. M.S. Independent Study (Geophysics Open-File Report No. 25, Geoscience Dept., N.M.I.M.T.), 1978.

Fischer, J. A.: The use of relative travel time residuals of P phases from teleseismic events to study the crust in the Socorro, New Mexico area, N.M.I.M.T. M.S. Independent Study (Geophysics Open-File Report No. 14, Geoscience Dept., N.M.I.M.T.), 1977.

Gibson, B. S., M. E. Odegard and C. H. Sutton: Nonlinear least-squares inversion of travel time data for a linear velocity-depth relationship, Geophysics, 44, 185-194, 1979.

Hawley, J. W., ed.: Guidebook to the Rio Grande rift in New Mexico and Colorado, Cir. 163, N. Mex. Bur. Mines and Miner. Resourc., Socorro, NM, 1978.

Hunter, D.: The Bushveld Complex and its remarkable rocks, Am. Scientist, 66, 551-559, 1978.

Jackson, D. D.: Interpretation of inaccurate, insufficient and inconsistent data, Geophy. Jour. Royal astr. Soc., 28, 97-109, 1972.

Jaeger, J. C. and N. G. W. Cook: Fundamentals of Rock Mechanics, Chapman and Hall, London, 1976.

Jenkins, G. M. and D. G. Watts: Spectral Analysis and its Applications, Holden-Day, Sydney, 1968.

Jiracek, G. R., M. E. Ander and H. T. Holcombe: Magnetotelluric soundings of crustal conductive zones in major continental rifts, in Riecker, R. E., ed., Rio Grande Rift: Tectonics and Magmatism, A. G. U. Wash., D. C., 209-222, 1979.

Johnston, J. A.: Microearthquake frequency attenuation of S phases in the Rio Grande rift near Socorro, New Mexico, N.M.I.M.T. M.S. Independent Study (Geophysics Open-File Report No. 24, Geoscience Dept., N.M.I.M.T.), 1978.

Keller, G. R., L. W. Braile and J. W. Schlue: Regional crustal structure of the Rio Grande rift from surface wave dispersion measurements, in Riecker, R. E., ed., Rio Grande Rift: Tectonics and Magmatism, A. G. U. Wash., D. C., 115-126, 1979.

Kudo, A. M.: Volcanism within the Rio Grande rift (abstract), Abstracts with Program, Geol. Soc. Amer. Rocky Mtn. Sec. Ann. Mtg., 8, 597, 1976.

Lachenbruch, A. H., J. H. Sass, R. J. Munroe and T. H. Moses, Jr.: Geothermal setting and simple heat conduction models for Long Valley Caldera, Jour. Geophys. Res, 81, p. 769-784, 1976.

Lachenbruch, A. H. and J. H. Sass: Heat flow in the United States and the thermal regime of the Crust, in J. G. Heacock, ed., The Earth's Crust, Amer. Geophys. Union Monograph 20, 626-675, 1977.

Lachenbruch, A. H. and J. H. Sass: Models of an extending lithosphere and heat flow in the Basin and Range province, in Smith, R. B. and G. Eaton, eds., Cenozoic Tectonics and Regional Geophysics of the Western Cordillera, Geol. Soc. Amer. Mem., 152, 209-250, 1978.

Meyer, P. L.: Introductory Probability and Statistical Applications, Addison-Wesley, Inc., Reading, Mass., 1965.

Michaels, P.: Seismic ray path migration with the pocket calculator, Geophysics 42, 1056-1063, 1977.

Mott, R. P.: The relationship of microearthquake activity to structural geology for the region around Socorro, New Mexico, N.M.I.M.T. M.S. Independent Study (Geophysics Open-File Report No. 7a, Geoscience Dept., N.M.I.M.T.), 1976.

Murase, T. and A. R. McBirney: Properties of some common igneous rocks and their melts at higher temperatures, Geol. Soc. Amer. Bull., 84, 3563-3592, 1973.

O'Connell, R. J. and B. Budiansky: Seismic velocities in dry and saturated cracked solids, J. Geophys. Res., 79, 5412-5426, 1974.

Olsen, K. H., G. R. Keller and J. N. Stewart: Crustal structure along the Rio Grande rift from seismic refraction profiles, in Riecker, R. E., ed., Rio Grande Rift: Tectonics and Magmatism, A. G. U., Wash., D. C., 87-106, 1979.

Parker, R. L.: Understanding inverse theory, Ann. Rev. Earth Plan. Sci., 1977, 5, 35-74, 1977.

Prescott, W. H., J. C. Savage and W. T. Kinoshita: Strain accumulation rates in the western United States between 1970 and 1977, submitted to Jour. Geophys. Res., 1979.

Ramberg, I. B., F. A. Cook and S. B. Smithson: Structure of the Rio Grande rift in southern New Mexico and West Texas based on gravity interpretation, Geol. Soc. Amer. Bull., 89, 107-123, 1978.

Reilinger, R. E., L. D. Brown and J. E. Oliver: Recent vertical crustal movements from leveling observations in the vicinity of the Rio Grande rift, in Riecker, R. E., ed., Rio Grande Rift: Tectonics and Magmatism, A. G. U., Wash., D. C., 223-236, 1979.

Reiter, M., C. L. Edwards, J. Hartman and C. Weidman: Terrestrial heat flow along the Rio Grande rift, New Mexico and Southern Colorado, Geol. Soc. Ameri. Bull., 86, 811-818, 1975.

Reiter, M. and R. Smith: Subsurface temperature data in the Socorro Peak KGRA, New Mexico, Geothermal En. Mag., 5, 37-41, 1977.

Richter, C. F.: Elementary Seismology, W. H. Freeman and Co., San Francisco, 1958.

Riecker, R. E., ed., Rio Grande Rift: Tectonics and Magmatism, American Geophys. Union, Washington, D. C., 1979.

Rinehart, E. J.: The use of microearthquakes to map an extensive magma body in the Socorro, New Mexico area, N.M.I.M.T. M.S. Independent Study, (Geophysics Open-File Report No. 10, Geoscience Dept., N.M.I.M.T., Socorro, NM), 1976.

Robinson, E. A.: Predictive decomposition of time series with application to seismic exploration, Geophysics, 32, 418-484, 1967.

Sanford, A. R.: Gravity survey in central Socorro County, New Mexico, Circ. 91, N. Mex. Bur. of Mines and Miner. Resour., Socorro, 1968.

Sanford, A. R.: Temperature gradient, heat-flow measurements in the vicinity of Socorro, N. M., 1965-1968, (Geophysics Open-File Report No. 15, Geoscience Dept., N.M.I.M.T., Socorro, NM), 1977.

Sanford, A. R. and L. T. Long: Microearthquake crustal reflections, Socorro, New Mexico, Bull. Seismol. Soc. Amer., 55, 579-586, 1965.

Sanford, A. R., A. J. Budding, J. P. Hoffman, O. S. Alptekin, C. A. Rush, and T. R. Toppozada: Seismicity of the Rio Grande rift in New Mexico, Circ. 120, N. Mex. Bur. of Mines and Miner. Resour., Socorro, 1972.

Sanford, A. R., O. S. Alptekin, and T. R. Toppozada: Use of reflection phases on microearthquake seismograms to map an unusual discontinuity beneath the Rio Grande rift, Bull. Seismol. Soc. Amer., 63, 2021-2034, 1973.

Sanford, A. R., R. P. Mott, Jr., P. J. Shuleski, E. J. Rinehart, F. J. Caravella, R. M. Ward and T. C. Wallace: Geophysical evidence for a magma body in the crust in the vicinity of Socorro, N.M., in Heacock, J. G., ed., The Earth's Crust, Amer. Geophys. Union Monograph 20, 385-403, 1977.

Sanford, A. R., K. H. Olsen and L. H. Jaksha: Seismicity of the Rio Grande rift, in Riecker, R. E., ed., Rio Grande Rift: Tectonics and Magmatism, A. G. U., Wash., D. C., 145-168, 1979.

Seager, W. R. and P. Morgan: Rio Grande rift in Southern New Mexico, West Texas, and Northern Chihuahua, in Riecker, R. E., ed., Rio Grande Rift: Tectonics and Magmatism, A. G. U., Wash., D. C., 87-106, 1979.

Shuleski, P. J.: Seismic fault motion and SV wave screening by shallow magma bodies in the vicinity of Socorro, New Mexico, N.M.I.M.T. M.S. Independent Study (Geophysics Open-File Report No. 8, Geoscience Dept., N.M.I.M.T.), 1976.

Smith, R. B.: Seismicity, crustal structure and intraplate tectonics of the interior of the Western Cordillera, in Smith, R. B. and G. Eaton, eds., Cenozoic Tectonics and Regional Geophysics of the Western Cordillera, Geol. Soc. Amer. Mem., 152, 111-144, 1978.

Stauder, W. and A. Ryall: Spatial distribution and source mechanism of microearthquakes in central Nevada, Bull. Seismol. Soc. Amer., 57, 1317-1345, 1967.

Tang, S.: Three dimensional crustal velocity model beneath the Socorro, New Mexico area from inversion of relative travel-time residuals, N.M.I.M.T. M.S. Independent Study (Geophysics Open-File Report No. 23, Geoscience Dept., N.M.I.M.T.), 1978.

Telford, W. M., L. P. Geldart, R. E. Sheriff and D. A. Keys: Applied Geophysics, Cambridge U. Press, London, 1976.

Toppozada, T. R. and A. R. Sanford; Crustal structure in Central New Mexico interpreted from the Gasbuggy explosion, Bull. Seismol. Soc. Amer., 66, 877-886, 1976.

Westphal, W. H. and A. L. Lange: Local seismic monitoring-Fairview Peak area, Nevada, Bull. Seismol. Soc. Amer., 57, 1279-1298.

Wiggins, R. A.: The general linear inverse problem: implications of surface waves and free oscillations for earth structure, Rev. Geophys. Space Phys., 10, 251-285, 1972.

Yoder, H. S.: Generation of Basaltic Magma, Nat. Acad. Sci., Washington, D. C., 1976.

Appendix 1

Appendix 1 contains data for all Class A and Class B reflections. Class A reflections are indicated by an "*" before each data line. Refined data that was used in model M3 are indicated by an "R" before each data line. Included are the data, origin time, latitude, longitude, depth of focus calculated using the least squares iterative location program, P-arrival times, S_zS minus P-arrival times (listed as SZS-P), recording stations and the S_zP/S_zS amplitude ratios corrected for geophone orientation.

	DATE	ORIGIN TIME	LATITUDE	LONGITUDE	DEPTH	P-ARRIVAL	SZS-P	STATION	RATIO
	60375	40301.00	34.0245	106.9988	0.00	3.88	6.65	CC	
*	60375	151015.50	34.0155	107.0452	9.00	18.45	7.00	SC	
**	61675	234320.76	34.0184	107.0439	10.00	22.99	7.30	SC	
*	61675	234320.76	34.0184	107.0439	10.00	23.80	7.00	CC	
*	62675	25644.81	34.0559	107.0576	8.10	46.90	7.03	SC	
*	62675	25644.81	34.0559	107.0576	8.10	46.94	6.55	CT	
R *	70275	10020.49	34.2272	106.8817	9.00	21.43	7.55	CC	
R *	70275	10020.49	34.2272	106.8817	9.00	24.38	7.56	CM	
*	70275	23422.05	34.2272	106.8817	9.00	24.42	7.55	CC	
*	70275	23422.05	34.2272	106.8817	9.00	25.13	7.80	FM	
*	70275	23422.05	34.2272	106.8817	9.00	27.33	7.56	CM	
	70975	21224.49	34.0511	106.9315	0.00	26.98	6.38	CC	
	70975	91648.07	34.0554	106.9275	0.00	50.23	6.31	CC	
	72375	145642.06	34.0119	107.0387	0.00	44.86	6.97	CC	.40
	72375	145642.06	34.0119	107.0387	0.00	43.81	7.33	SC	.10
	72475	42313.95	34.0505	107.0025	0.00	16.11	7.47	CC	
	72475	42313.95	34.0505	107.0025	0.00	16.44	8.63	SC	
	72475	171014.32	34.0094	107.0409	0.00	16.21	7.87	SC	.03
	72475	171014.32	34.0094	107.0409	0.00	17.26	6.82	CC	.23
	80175	112620.93	34.0710	107.0266	0.00	23.05	8.74	SC	
R *	80575	41720.31	34.0159	106.9927	11.60	22.51	6.05	WT	.35
R *	80575	41720.31	34.0159	106.9927	11.60	23.20	6.27	SC	
R *	80575	41720.31	34.0159	106.9927	11.60	23.56	6.11	CC	
R *	80575	141921.94	34.0127	107.0625	11.70	24.38	7.24	SC	
R *	80575	141921.94	34.0127	107.0625	11.70	24.71	6.46	WT	.58
R *	80575	141921.94	34.0127	107.0625	11.70	25.31	6.96	CC	.33
	80875	105722.23	34.0689	106.9263	0.00	25.75	7.82	SC	
*	81375	73918.14	34.0703	106.9312	11.00	21.78	8.02	SC	
*	81375	112226.40	34.0017	106.9824	11.60	29.44	6.34	SC	
	81375	201825.49	34.0763	107.0367	0.00	27.28	6.89	CC	
	81375	201825.49	34.0763	107.0367	0.00	27.30	7.08	WT	1.4
*	81975	81146.46	34.0445	106.9703	11.60	49.09	6.45	CC	
*	81975	81146.46	34.0445	106.9703	11.60	49.69	6.72	SC	.55
*	81975	100007.00	33.9766	107.0105	10.80	9.67	6.45	SC	.44
*	81975	100007.00	33.9766	107.0101	10.80	10.59	6.10	CC	
	82075	52219.47	34.0741	106.9225	0.00	21.38	7.74	WT	
*	82075	152836.20	34.0726	106.9303	9.80	37.78	7.79	WT	.04
*	82075	152836.20	34.0726	106.9303	9.80	38.46	7.53	CC	.19
*	82175	34448.20	34.0129	107.0587	11.70	50.65	7.26	SC	.09
*	82175	34448.20	34.0129	107.0587	11.70	51.00	6.05	WT	.35
*	82175	34448.20	34.0129	107.0587	11.70	51.53	6.81	CC	.33
*	82175	190405.66	34.0409	106.9714	13.30	9.08	6.69	SC	.42
	102975	72135.16	34.0532	107.0108	0.00	37.25	8.54	SC	
	102975	72135.16	34.0532	107.0108	0.00	37.10	8.17	CC	.12

	DATE	ORIGIN TIME	LATITUDE	LONGITUDE	DEPTH	P-ARRIVAL	SZS-P	STATION	RATIO
	102975	73437.02	34.0249	107.0077	0.00	39.28	7.37	SC	.20
	102975	73437.02	34.0248	107.0077	0.00	38.58	7.00	WT	.42
	103075	70938.40	34.0196	107.0443	0.00	40.78	6.79	SC	.23
	103075	70938.40	34.0196	107.0443	0.00	40.84	6.49	WT	.69
R	* 110475	163011.38	34.0315	107.0845	10.60	14.14	7.00	WT	.52
R	* 110475	163011.38	34.0315	107.0845	10.60	14.50	7.06	CC	
	110575	143504.61	34.0129	107.0844	0.00	7.77	6.76	WT	
	* 110575	222826.14	34.0339	107.0550	7.90	28.29	6.73	WT	.42
	* 110575	222826.14	34.0339	107.0550	7.90	28.86	6.88	CC	.74
	110675	93358.27	34.0199	107.0317	0.00	0.98	6.42	WT	.49
	110675	93358.27	34.0199	107.0317	0.00	1.22	7.28	SC	.10
R	* 110775	82735.65	34.0343	107.0594	9.20	38.56	6.84	CC	
	12276	160510.75	34.0144	107.0542	0.00	13.56	6.54	WT	.35
	12276	160510.75	34.0149	107.0542	0.00	13.29	7.50	SC	.06
	* 12376	25332.79	34.0154	107.0426	10.10	35.04	7.53	SC	.07
	* 12376	25332.79	34.0154	107.0426	10.10	35.15	6.64	WT	.29
	* 12976	150640.20	33.9816	106.9838	6.00	42.61	7.67	SC	
	* 12976	150640.20	33.9816	106.9838	6.00	43.25	7.04	CC	
	13076	135623.78	34.0611	106.9971	0.00	25.70	7.40	CC	
	13076	135623.78	34.0611	106.9971	0.00	26.15	8.03	SC	
	* 20676	92157.40	34.3763	107.0348	0.00	1.79	7.65	CC	
	* 20676	92157.40	34.3763	107.0348	0.00	3.51	7.61	DM	
	* 20676	92157.40	34.3763	107.0348	0.00	3.30	7.64	WT	
	* 21776	61749.51	34.0203	107.0586	6.20	51.61	6.79	WT	.56
	* 21776	173405.00	34.0382	107.0260	10.80	7.35	7.00	IC	.31
	* 21776	173405.00	34.0382	107.0260	10.80	7.71	6.59	CC	.17
	* 21876	54455.59	34.0056	107.0694	11.10	57.91	7.15	SC	.05
	* 21876	54455.59	34.0056	107.0694	11.10	58.07	6.95	IC	.27
	* 21876	54455.59	34.0056	107.0694	11.10	57.95	6.90	WM	.04
	* 21876	54455.59	34.0056	107.0694	11.10	58.48	6.45	WT	.88
	* 21876	54455.59	34.0056	107.0694	11.10	59.02	6.75	CC	
	21876	232535.19	34.0261	107.0806	0.00	37.15	7.35	SC	.04
	* 21976	836.65	34.0103	107.0685	9.60	38.74	7.12	SC	
	* 21976	836.65	34.0103	107.0685	9.60	38.85	6.89	WM	.05
	* 21976	836.65	34.0103	107.0685	9.60	38.87	6.31	IC	.19
	* 22076	125145.06	34.0027	107.0568	10.50	47.29	7.25	SC	.08
	* 22076	125145.06	34.0027	107.0568	10.50	47.28	6.91	WM	
	* 22076	125145.06	34.0027	107.0568	10.50	47.69	6.66	WT	.76
	* 32376	125219.80	34.2924	106.8548	11.50	23.80	7.60	DM	
	* 32376	125219.80	34.2924	106.8548	11.50	24.77	7.41	WT	.40
	* 32376	125219.80	34.2924	106.8548	11.50	26.34	8.20	IC	
	* 32376	125219.80	34.2924	106.8548	11.50	27.03	8.35	CM	
	* 41376	94540.40	34.0640	107.0239	10.50	43.05	7.60	SC	.18
	* 41376	94540.40	34.0640	107.0239	10.50	42.79	7.43	CC	.08

		DATE	ORIGIN TIME	LATITUDE	LONGITUDE	DEPTH	P-ARRIVAL	SZS-P	STATION	RATIO
	*	41376	114125.16	34.0248	107.0739	10.60	27.50	7.10	WM	.49
	*	41376	114125.16	34.0248	107.0739	10.60	27.93	6.78	WT	.64
	*	41376	115834.55	33.9760	106.9713	6.60	37.16	7.68	SC	
		41376	231514.92	34.0209	107.0354	0.00	17.37	6.10	CC	
	*	41476	131221.10	34.0601	107.0435	5.50	22.83	6.50	WM	.33
	*	41576	84552.24	34.0598	107.0236	9.90	54.35	7.93	WM	
	*	41576	84552.24	34.0598	107.0236	9.90	54.08	8.54	SC	
	*	41576	84552.24	34.0598	107.0236	9.90	54.58	7.36	CC	
R	*	41676	93342.74	34.0564	107.0212	7.70	44.48	7.15	WM	.18
R	*	41676	93342.74	34.0564	107.0212	7.70	44.45	7.34	WT	
R	*	41676	93342.74	34.0564	107.0212	7.70	44.89	7.42	IC	.28
R	*	41676	93342.74	34.0564	107.0212	7.70	45.06	7.96	SC	.14
R	*	41676	93342.74	34.0564	107.0212	7.70	44.86	7.09	CC	.19
	*	41676	140733.01	34.0624	106.9953	10.20	34.76	7.33	WT	
	*	41676	140733.01	34.0624	106.9953	10.20	35.09	7.55	WM	.18
	*	41676	140733.01	34.0624	106.9953	10.20	35.50	7.50	IC	.18
	*	41676	140733.01	34.0624	106.9953	10.20	35.26	7.09	CC	.22
	*	41676	140733.01	34.0624	106.9953	10.20	35.87	8.08	SC	.28
	*	42076	25219.50	34.0456	107.0705	9.10	21.81	6.81	WT	.34
	*	42076	25219.50	34.0456	107.0705	9.10	22.21	7.06	CC	
	*	42176	111619.50	34.3159	106.8381	5.10	21.79	8.35	BG	.17
R	*	42176	111619.50	34.3159	106.8381	5.10	22.65	7.39	SL	.40
R	*	42176	111619.50	34.3159	106.8381	5.10	22.73	7.34	CU	
R	*	42176	111619.50	34.3159	106.8381	5.10	23.33	6.96	CC	.64
R	*	42176	111619.50	34.3159	106.8381	5.10	23.61	8.10	DM	
R	*	42176	111619.50	34.3159	106.8381	5.10	24.42	7.33	WT	
	*	42376	55859.35	34.0364	107.0732	8.50	1.80	6.85	WT	.40
	*	42376	55859.35	34.0364	107.0732	8.50	2.16	7.05	CC	.44
	*	52576	30816.03	34.0441	107.0841	4.40	18.24	8.08	WT	.52
		60176	83848.01	34.0094	107.0486	0.00	50.20	6.53	WT	.55
		60376	153113.12	34.0340	107.0093	0.00	14.80	6.35	WT	.31
		60876	52454.37	34.0516	106.9991	0.00	57.02	8.19	SC	.25
R	*	71576	105834.53	34.0229	107.0685	6.40	36.11	7.16	SC	.17
R	*	71576	105834.53	34.0229	107.0685	6.40	36.62	6.68	NG	.32
R	*	71576	105834.53	34.0229	107.0685	6.40	36.87	6.50	WT	.71
R	*	71576	164306.88	34.0242	107.0665	10.20	9.68	7.31	SC	.09
R	*	71576	164306.88	34.0242	107.0665	10.20	10.10	7.38	RM	
R	*	71576	164306.88	34.0242	107.0665	10.20	10.33	6.53	WT	.41
		80376	71016.54	34.4272	107.0022	10.60	23.40	8.08	WT	
		80376	71016.54	34.4272	107.0022	10.60	25.69	9.40	NG	
		80376	71016.54	34.4272	107.0022	10.60	24.74	8.76	HC	
		80376	71016.54	34.4272	107.0022	10.60	25.11	8.66	SC	
		81076	43825.63	34.0103	107.0718	0.00	27.32	7.84	SC	
		81076	43825.63	34.0103	107.0718	0.00	28.10	6.73	WT	.62

		DATE	ORIGIN TIME	LATITUDE	LONGITUDE	DEPTH	P-ARRIVAL	SZS-P	STATION	RATIO
	*	81076	122841.70	34.0473	106.9997	11.30	43.77	6.49	WT	.23
	*	81076	122841.70	34.0473	106.9997	11.30	44.46	7.13	SC	.18
R	*	81176	31519.20	34.1457	106.9016	7.00	23.56	8.06	SC	.54
R	*	81176	31519.20	34.1457	106.9016	7.00	20.97	8.14	WT	
R	*	81176	31519.20	34.1457	106.9016	7.00	23.32	7.97	NG	
R	*	81176	31519.20	34.1457	106.9016	7.00	25.06	7.84	HC	
	*	81276	5908.36	34.0383	107.0144	8.40	10.08	6.36	WT	.20
	*	81276	5908.36	34.0383	107.0144	8.40	10.66	7.08	SC	.19
	*	81276	45605.52	34.0392	107.0147	7.70	7.16	6.45	WT	.20
	*	81276	45605.52	34.0392	107.0147	7.70	7.65	6.85	NG	.58
	*	81276	45605.52	34.0392	107.0147	7.70	7.75	7.09	SC	.13
	*	81276	230712.90	34.0421	107.0139	7.20	14.46	6.34	WT	.21
	*	81276	230712.90	34.0421	107.0139	7.20	15.00	6.35	NG	
	*	82476	13113.96	34.0349	107.0295	4.50	15.65	8.40	SC	.06
	*	82576	223223.53	34.0390	107.0136	0.00	25.88	7.20	SC	.28
	*	82576	223223.53	34.0390	107.0136	0.00	25.76	6.90	NG	.41
R	*	82776	14440.12	34.0396	107.0174	6.00	42.10	6.88	SC	.13
R	*	82776	14440.12	34.0396	107.0174	6.00	42.09	6.50	NG	.38
		82776	81528.49	34.0091	107.0647	0.00	30.14	7.30	SC	
		82776	81528.49	34.0091	107.0647	0.00	30.50	6.80	NG	.13
	*	90276	125137.40	34.1436	106.8552	10.50	43.70	7.29	GM	
	*	90276	125137.40	34.1436	106.8552	10.50	43.99	7.34	HC	
	*	90376	64629.73	33.9717	107.0037	6.20	31.85	6.90	SC	.35
	*	90376	64629.73	33.9717	107.0037	6.20	34.80	7.62	GM	
		90376	152927.10	34.0842	107.0210	0.00	29.41	7.91	SC	
		100576	192608.47	34.0320	106.9610	0.00	10.84	7.55	IC	.13
R	*	100776	232109.56	34.0128	107.0366	9.80	11.57	6.72	IC	.19
R	*	100776	232109.56	34.0128	107.0367	9.80	11.78	7.03	SC	.09
R	*	100776	232109.56	34.0128	107.0367	9.80	11.81	6.55	WT	
		12177	616.33	33.9950	107.0607	0.00	18.55	7.60	SC	
	*	12177	164228.18	33.9913	107.0680	11.10	31.20	6.59	WT	.57
	*	12177	164228.18	33.9913	107.0680	11.10	31.44	7.25	CC	.35
	*	12277	42405.17	34.0151	107.0540	7.50	6.99	7.58	SC	.13
	*	12277	42405.17	34.0151	107.0540	7.50	8.01	7.18	CC	.34
		20977	13616.79	34.0293	107.0257	0.00	18.43	6.65	NG	
		20977	13616.79	34.0293	107.0257	0.00	18.26	7.00	SC	
		20977	110713.59	34.0038	107.0082	0.00	16.62	7.50	CC	
		20977	110713.59	34.0038	107.0082	0.00	16.06	7.80	SC	
		21077	73328.10	34.1379	106.9314	0.00	29.55	7.80	CC	.05
		21177	115445.23	34.2753	106.8043	0.00	52.07	7.49	CM	
R	*	21677	144449.69	34.0127	107.0481	6.70	51.42	7.48	SC	.14
R	*	21677	144449.69	34.0127	107.0481	6.70	51.42	6.80	IC	.29
R	*	21677	144449.69	34.0127	107.0481	6.70	52.52	6.99	CC	.18
		22577	708.38	34.0144	107.0482	0.00	11.18	7.00	CC	

	DATE	ORIGIN TIME	LATITUDE	LONGITUDE	DEPTH	P-ARRIVAL	SZS-P	STATION	RATIO
	22577	708.38	34.0144	107.0482	0.00	10.50	6.55	WT	
	22577	708.38	34.0144	107.0482	0.00	10.07	7.40	SC	
*	30877	45506.17	34.0035	107.0588	7.50	7.92	7.45	SC	.07
*	30877	45506.17	34.0035	107.0588	7.50	8.54	6.74	WT	.64
*	30977	115016.01	34.0030	107.0620	7.50	17.71	7.46	SC	
*	30977	115016.01	34.0030	107.0620	7.50	18.40	6.59	WT	.77
	30977	114902.53	34.0084	107.0607	0.00	4.27	7.75	SC	
	30977	114902.53	34.0084	107.0607	0.00	4.94	6.70	WT	
	30977	112544.52	34.0036	107.0603	0.00	46.98	7.30	CM	
	30977	112544.52	34.0036	107.0603	0.00	46.29	7.66	SC	
	30977	112544.52	34.0036	107.0603	0.00	46.95	6.69	WT	
	31077	132733.31	33.9877	107.0699	0.00	36.18	6.71	WT	.89
	31077	132733.31	33.9877	107.0699	0.00	35.43	7.75	SC	
	40577	193431.13	34.0116	107.0356	0.00	33.10	7.34	SC	.08
	40577	193431.13	34.0116	107.0356	0.00	34.15	7.87	CC	.18
	41277	32503.26	34.0591	107.0357	0.00	5.06	6.99	CC	
	41377	123952.13	34.0350	107.0218	0.00	54.05	7.00	SC	
	41377	123952.13	34.0350	107.0218	0.00	54.50	6.50	CC	
	41377	201531.79	34.1987	106.8503	0.00	34.17	6.62	CC	
	41377	201531.79	34.1987	106.8503	0.00	34.17	6.35	CC	
	42677	20820.67	34.0569	107.0308	0.00	22.30	7.10	WT	
*	42677	165608.00	34.0369	107.0554	7.20	9.97	7.32	WT	
	42677	165608.23	34.0437	107.0544	0.00	9.97	7.20	WT	
	42677	165608.23	34.0437	107.0544	0.00	10.33	6.75	CC	
	42777	121556.32	34.0107	107.0592	0.00	58.08	7.50	SC	
	42777	121556.32	34.0107	107.0592	0.00	58.78	6.60	WT	
*	42877	105910.81	34.0489	107.0505	5.40	12.49	7.87	SC	
*	42877	105910.81	34.0489	107.0505	5.40	13.01	6.74	CC	.99
	42877	105910.74	34.0469	107.0538	0.00	12.49	7.77	SC	
	42877	105910.74	34.0469	107.0538	0.00	12.74	6.85	WT	
	42877	110331.25	34.0445	107.0509	0.00	33.15	6.75	WT	
	42877	110331.25	34.0445	107.0509	0.00	32.19	7.35	SC	
	50677	104318.52	34.1766	106.9256	0.00	19.73	7.00	CC	
	51277	61914.45	34.0747	107.0318	0.00	16.37	6.38	WT	
	51277	61914.45	34.0747	107.0318	0.00	18.43	7.59	FM	
	60177	64045.08	34.0043	107.0575	0.00	46.66	7.64	SC	
	60177	64045.08	34.0043	107.0575	0.00	47.37	6.80	WT	.77
*	60277	65024.36	34.0118	107.0635	8.00	26.09	7.58	SC	
*	60277	65024.36	34.0118	107.0635	8.00	26.87	6.64	WT	.50
	60277	173008.27	34.0027	107.0612	0.00	10.66	6.45	WT	
	60377	34901.59	34.0097	107.0602	0.00	3.30	7.66	SC	
	60377	34901.59	34.0097	107.0602	0.00	4.00	6.60	WT	
*	60377	193829.82	34.2280	106.8883	0.00	33.21	7.50	DM	
*	60377	204502.97	34.2284	106.8973	11.00	6.23	7.28	DM	

	DATE	ORIGIN TIME	LATITUDE	LONGITUDE	DEPTH	P-ARRIVAL	SZS-P	STATION	RATIO
R *	60377	204502.97	34.2284	106.8973	11.00	6.34	6.68	WT	.69
R *	60377	204502.97	34.2284	106.8973	11.00	8.90	7.67	CM	
	60377	230119.24	33.9809	107.0094	0.00	21.45	6.75	WT	
	60377	230119.24	33.9809	107.0094	0.00	23.29	6.70	DM	
	60777	122528.61	34.0119	107.0534	0.00	30.27	7.45	SC	
	60877	33223.37	34.1967	106.9304	0.00	26.58	7.59	DM	
	60877	33223.37	34.1967	106.9304	0.00	28.57	7.52	GM	
	60877	33223.37	34.1967	106.9304	0.00	26.58	7.50	DM	
	60877	53029.67	34.0251	107.0524	0.00	31.93	7.27	SC	
	61077	40444.94	34.0141	107.0620	0.00	46.73	7.70	SC	.05
	61077	40444.94	34.0141	107.0620	0.00	47.38	6.60	WT	.88
	71177	235234.88	34.1179	107.0364	0.00	36.21	6.95	CC	
*	71477	23402.03	34.1590	106.8814	5.30	3.62	8.19	BG	.24
*	71477	23402.03	34.1590	106.8814	5.30	3.81	7.70	CC	.23
*	71577	122625.73	34.0064	107.0611	8.50	27.62	7.55	SC	.04
*	71577	122625.73	34.0064	107.0611	8.50	28.96	7.03	CC	.40
	71977	61654.87	34.1535	106.8721	0.00	56.64	7.18	CC	
	71977	61654.87	34.1535	106.8721	0.00	56.33	8.05	BG	
	72177	31227.43	34.0412	107.0448	0.00	29.48	7.48	SC	
	72777	120730.54	33.9656	106.9443	0.00	33.29	7.66	SC	
	72777	120730.54	33.9656	106.9443	0.00	36.21	8.07	GM	
	72777	155315.12	34.0056	107.0568	0.00	17.14	7.52	SC	
	72777	155315.12	34.0056	107.0568	0.00	18.35	6.92	CC	
	72777	171729.49	34.1571	106.9072	0.00	30.89	7.19	CC	
	727.7	171729.49	34.1571	106.9072	0.00	34.69	7.46	GM	
	72977	120722.72	34.1457	106.9045	0.00	24.74	8.26	BG	
	72977	120722.72	34.1457	106.9045	0.00	27.01	7.51	SC	
	72977	120722.72	34.1457	106.9045	0.00	27.99	7.05	GM	
*	81777	22020.68	34.2882	107.0497	7.80	24.83	6.97	GM	
*	81777	22020.68	34.2882	107.0497	7.80	25.68	8.10	DM	
*	81777	60319.97	34.1671	106.8721	6.00	21.50	7.90	BG	.27
*	81777	60319.97	34.1671	106.8721	6.00	25.78	6.90	GM	
	81777	153722.00	34.2628	106.9233	5.70	27.45	7.52	GM	
	81777	153722.00	34.2628	106.9233	5.70	24.13	7.50	BG	.43
	81977	92822.91	34.0105	107.0613	0.00	24.80	6.95	SC	
*	82477	112235.90	34.0123	107.0512	7.80	37.82	7.65	SC	.15
*	82477	112235.90	34.0123	107.0512	7.80	37.94	6.92	NG	
*	82477	112235.90	34.0123	107.0512	7.80	38.93	6.55	CC	.24
R *	82677	103258.00	34.0093	107.0599	8.50	59.88	7.50	SC	.06
R *	82677	103258.00	34.0093	107.0599	8.50	0.19	6.80	NG	.23
R *	82677	103258.00	34.0093	107.0599	8.50	0.58	6.63	WT	
R *	82677	103258.00	34.0093	107.0599	8.50	1.04	6.67	CC	.55
*	83077	183728.97	34.0391	107.0013	2.40	30.73	8.46	NG	.35
*	83077	183728.97	34.0391	107.0013	2.40	33.30	7.72	BG	

	DATE	ORIGIN TIME	LATITUDE	LONGITUDE	DEPTH	P-ARRIVAL	SZS-P	STATION	RATIO
	*90177	182002.11	34.0548	106.7526	3.00	6.30	8.19	CC	
	* 90177	182002.11	34.0548	106.7526	3.00	10.12	8.19	GM	
R	*90177	215848.71	34.0139	107.0456	7.50	50.50	6.96	SC	.12
R	* 90177	215848.71	34.0139	107.0456	7.50	50.81	6.96	NG	.30
R	*90177	215848.71	34.0139	107.0456	7.50	51.66	7.02	CC	
R	* 91577	5335.40	34.0371	107.0595	7.70	37.24	7.65	SC	.13
R	*91577	5335.40	34.0371	107.0595	7.70	38.11	7.18	CC	.25
R	* 91577	5335.40	34.0371	107.0595	7.70	40.53	6.90	BG	
R	*91577	5335.40	34.0371	107.0595	7.70	43.38	7.69	RI	
R	* 91577	64517.00	34.3401	106.8883	0.50	22.41	6.75	RI	
R	*91577	64517.00	34.3401	106.8883	0.50	19.66	8.00	BG	
R	*91577	64517.00	34.3401	106.8883	0.50	22.20	7.74	TD	
R	* 91577	64517.00	34.3401	106.8883	0.00	23.61	7.95	GM	
R	*91577	114334.47	34.3068	106.9246	0.40	37.56	6.95	CC	.69
R	* 91577	114334.47	34.3068	106.9246	0.40	41.02	8.15	SC	
R	*91577	114334.47	34.3068	106.9246	0.40	40.00	7.85	TD	
R	* 91577	114334.47	34.3068	106.9246	0.40	40.23	7.63	GM	
	*91677	80408.23	34.0593	106.9885	0.00	9.89	7.40	CC	
	91677	80408.23	34.0593	106.9885	0.00	10.51	8.18	SC	
	*92077	12008.81	34.0352	107.0511	10.10	11.66	7.03	CC	.29
	* 92077	81923.32	34.1615	106.8804	3.80	24.78	8.75	BG	
	*92077	81923.32	34.1615	106.8804	3.80	28.98	7.48	GM	
	* 92077	81923.32	34.1615	106.8804	3.80	30.62	8.02	RI	
	*92277	52127.96	34.3340	106.8907	5.30	30.84	7.30	BG	
	* 92277	52127.96	34.3340	106.8907	5.30	31.80	7.29	CC	.69
	*92277	52127.96	34.3340	106.8907	5.30	33.01	7.30	FM	.79
	* 92277	52127.96	34.3340	106.8907	5.30	33.19	7.45	TD	.65
	*92277	52127.96	34.3340	106.8907	5.30	34.64	7.25	GM	
	* 92277	191916.59	34.3329	106.8897	11.30	20.90	6.79	CC	.70
	*92277	191916.59	34.3329	106.8897	11.30	21.98	7.64	FM	
	* 92277	191916.59	34.3329	106.8897	11.30	22.47	7.66	RI	
	*92277	191916.59	34.3329	106.8897	11.30	23.30	7.40	GM	
R	*101877	81632.86	34.0353	107.0603	7.70	35.65	6.94	CC	.24
R	*101877	81632.86	34.0353	107.0603	7.70	38.09	6.99	BG	
R	*101877	81632.86	34.0353	107.0603	7.70	40.82	8.24	RI	
	*111577	190241.73	34.1391	106.8857	0.00	43.34	7.06	CC	
	111777	25417.59	34.3807	107.0541	0.00	22.50	7.39	CC	
	111777	25417.59	34.3807	107.0542	0.00	22.96	7.25	BG	
	*111877	65812.49	34.4121	107.0703	0.90	17.90	6.53	BG	
	*111877	65812.49	34.4121	107.0703	0.90	20.70	8.15	IC	
	*111877	65812.49	34.4121	107.0703	0.90	19.22	6.98	WT	
	111877	65812.29	34.4125	107.0806	0.00	17.55	8.77	CC	
	111877	65812.29	34.4125	107.0806	0.00	17.94	7.79	BG	
	111877	65812.29	34.4125	107.0806	0.00	19.18	7.94	WT	

	DATE	ORIGIN TIME	LATITUDE	LONGITUDE	DEPTH	P-ARRIVAL	SZS-P	STATION	RATIO
	111877	65812.29	34.4125	107.0807	0.00	19.18	7.00	WT	
*	111877	124249.40	34.3902	107.0540	3.30	54.43	7.90	BG	
*	111877	124249.40	34.3902	107.0540	3.30	55.81	7.67	WT	
*	111877	124249.40	34.3902	107.0540	3.30	57.18	8.15	SC	
*	120577	205719.47	34.4084	107.0783	5.50	23.41	7.13	SL	1.1
*	120577	205719.47	34.4084	107.0783	5.50	24.70	7.59	CC	
*	120577	205719.47	34.4084	107.0783	5.50	25.08	7.72	BG	
*	120577	205719.47	34.4084	107.0783	5.50	26.71	8.36	LP	
	121377	195007.98	34.4633	107.0795	0.00	13.96	6.59	BG	
	121477	174833.18	34.0949	107.0234	0.00	37.08	8.63	BG	
*	121477	205727.46	34.2846	106.8770	12.50	30.46	7.29	SL	
*	121477	205727.46	34.2846	106.8770	12.50	32.01	7.36	LA	
	121477	205728.32	34.2915	106.8924	0.00	31.27	8.97	CC	
*	121577	171540.41	34.3225	107.0596	11.20	43.24	6.76	SL	.32
*	121577	171540.41	34.3225	107.0596	11.20	44.45	6.86	CC	
*	121577	171540.41	34.3225	107.0596	11.20	45.21	6.96	BG	
*	121577	171540.41	34.3225	107.0596	11.20	46.97	7.29	BB	
*	121577	171540.41	34.3225	107.0596	11.20	47.16	7.65	LP	
	122077	122118.72	34.0121	107.0556	0.00	22.78	7.92	SL	
	122077	122118.72	34.0121	107.0556	0.00	21.71	7.08	CC	
*	122377	13739.40	34.0927	107.0444	8.90	41.41	6.48	CC	.18
*	122377	13739.40	34.0927	107.0444	8.90	42.31	6.24	SL	
*	122377	35144.35	34.3202	107.1322	0.00	47.13	6.43	SL	
	10678	151237.02	34.4097	107.0465	0.00	41.94	7.61	CC	
	10678	151237.02	34.4097	107.0465	0.00	43.03	7.85	BB	
	11178	72247.55	34.0281	107.0682	0.00	50.24	7.07	CC	.24
	11178	103919.18	34.0284	107.0054	0.00	22.87	7.45	SL	
	11778	50501.02	34.3102	106.7201	0.00	6.40	6.95	CC	
	11778	50501.02	34.3102	106.7201	0.00	4.26	7.26	BG	
	11778	50501.02	34.3102	106.7201	0.00	6.40	6.64	SL	
	11778	231421.22	34.3463	106.8731	0.00	25.63	7.20	CC	
	11778	231421.22	34.3463	106.8731	0.00	24.46	7.01	SL	
	11778	231421.22	34.3463	106.8731	0.00	24.73	7.70	BB	
	11878	122432.84	34.1661	106.8587	0.00	34.85	8.22	CC	
	11878	122432.84	34.1661	106.8587	0.00	35.20	7.50	SL	
	11878	124942.99	34.1721	106.8656	0.00	44.91	8.29	CC	

Appendix 2

Appendix 2 contains a comparison between depths of focus calculated using both the S_zS travel times using model M3 (Reflection Depths) and the depths of focus calculated by the iterative location program (Iterative Depths). For convenience, the date, origin time of the event and its epicentral location are also given.

DATE	ORIGIN TIME	LATITUDE	LONGITUDE	REFLECTION DEPTH	ITERATIVE DEPTH
60375	40301.00	34.0245	106.9988	8.40	0.00
60375	151015.50	34.0155	107.0452	6.70	9.00
61675	234320.76	34.0184	107.0439	7.40	10.00
62675	25644.81	34.0559	107.0576	10.40	8.10
70275	10020.49	34.2272	106.8817	12.20	9.00
70275	23422.05	34.2272	106.8817	6.90	9.00
70975	21224.49	34.0511	106.9315	10.50	6.10
70975	91648.07	34.0554	106.9275	11.40	8.70
72375	145642.06	34.0119	107.0387	8.00	0.00
72475	42313.95	34.0505	107.0025	7.00	5.20
72475	171014.32	34.0094	107.0409	8.80	0.00
80175	112620.93	34.0710	107.0266	4.40	0.00
80575	41720.31	34.0159	106.9927	10.80	11.60
80575	141921.94	34.0127	107.0625	7.40	11.70
80875	105722.23	34.0689	106.9263	5.50	8.80
81375	52949.08	34.2194	107.0852	13.00	9.40
81375	73918.14	34.0703	106.9312	4.10	11.00
81375	112226.40	34.0017	106.9824	10.00	11.60
81375	201825.49	34.0763	107.0367	9.90	0.00
81975	81146.46	34.0445	106.9703	9.20	11.60
81975	100007.00	33.9766	107.0105	10.80	10.80
82075	52219.47	34.0741	106.9225	4.70	12.10
82075	152836.20	34.0726	106.9303	6.00	9.80
82175	34448.20	34.0129	107.0587	7.30	11.70
82175	190405.66	34.0409	106.9714	7.90	13.30
102975	72135.16	34.0532	107.0108	5.20	4.00
102975	73437.02	34.0249	107.0077	9.30	0.00
103075	70938.40	34.0196	107.0443	9.10	0.00
110475	163011.38	34.0315	107.0845	7.50	10.60
110575	143504.61	34.0129	107.0844	6.70	12.50
110575	222826.14	34.0339	107.0550	9.10	7.80
110675	93358.27	34.0199	107.0317	7.90	14.10

DATE	ORIGIN TIME	LATITUDE	LONGITUDE	REFLECTION DEPTH	ITERATIVE DEPTH
110775	82735.65	34.0343	107.0594	9.20	9.20
12276	160510.75	34.0144	107.0542	7.80	12.40
12376	25332.79	34.0154	107.0426	7.30	10.10
12976	150640.20	33.9816	106.9838	8.70	6.00
13075	135623.78	34.0611	106.9971	7.80	6.40
20676	92157.40	34.3763	107.0348	8.60	0.00
21776	61749.51	34.0203	107.0586	9.50	6.20
21776	173405.00	34.0382	107.0260	8.90	10.80
21876	54455.59	34.0056	107.0694	8.10	11.10
21876	232535.19	34.0261	107.0806	8.60	8.88
21976	836.65	34.0103	107.0685	11.50	9.60
22076	125145.06	34.0027	107.0568	8.90	10.50
32376	125219.80	34.2924	106.8548	4.50	11.50
41376	94540.40	34.0640	107.0239	6.00	10.50
41376	114125.16	34.0248	107.0739	7.50	10.60
41376	115834.55	33.9760	106.9713	7.30	6.60
41376	231514.92	34.0209	107.0354	12.80	4.50
41476	131221.10	34.0601	107.0435	12.20	5.50
41576	84552.24	34.0598	107.0236	6.20	9.90
41676	93342.74	34.0564	107.0212	7.90	7.70
41676	140733.01	34.0624	106.9953	7.30	10.20
42076	25219.50	34.0456	107.0705	7.70	9.10
42176	111619.50	34.3159	106.8381	4.70	5.10
42376	55859.35	34.0364	107.0732	8.20	8.50
52576	30816.03	34.0441	107.0841	4.90	4.40
60176	83848.01	34.0094	107.0486	10.10	6.00
60376	153113.12	34.0340	107.0093	11.00	7.70
60876	52454.37	34.0516	106.9991	4.70	9.20
71576	105834.53	34.0229	107.0685	10.60	6.40
71576	164306.88	34.0242	107.0665	5.90	10.20
80376	71016.54	34.4272	107.0022	5.90	10.60
81076	43825.63	34.0103	107.0718	9.10	7.50
81076	122841.70	34.0473	106.9997	8.80	11.30

DATE	ORIGIN TIME	LATITUDE	LONGITUDE	REFLECTION DEPTH	ITERATIVE DEPTH
81176	31519.20	34.1457	106.9016	5.90	7.00
81276	5908.36	34.0383	107.0144	10.90	8.40
81276	45605.52	34.0392	107.0147	11.40	7.70
81276	230712.90	34.0421	107.0139	11.40	7.20
82476	13113.96	34.0349	107.0295	6.50	4.50
82576	223223.53	34.0390	107.0136	9.60	8.20
82776	14440.12	34.0396	107.0174	12.00	6.00
82776	81528.49	34.0091	107.0647	10.60	7.10
90276	125137.40	34.1436	106.8552	7.70	10.50
90376	64629.73	33.9717	107.0037	7.50	6.20
90376	152927.10	34.0842	107.0210	7.10	4.80
100576	192608.47	34.0320	106.9610	6.50	11.10
100776	232109.56	34.0128	107.0366	9.90	9.80
12177	616.33	33.9950	107.0607	7.00	10.20
12177	164228.18	33.9913	107.0680	7.70	11.10
12277	42405.17	34.0151	107.0540	7.80	7.50
20977	13616.79	34.0293	107.0257	12.20	3.40
20977	110713.59	34.0038	107.0082	6.00	9.90
21077	73328.10	34.1379	106.9314	7.00	7.20
21177	115445.23	34.2753	106.8043	11.30	12.70
21677	144449.69	34.0127	107.0481	11.20	6.70
22577	708.38	34.0144	107.0482	8.50	6.90
30877	45506.17	34.0035	107.0588	9.00	7.50
30977	115016.01	34.0030	107.0620	9.40	7.50
30977	114902.53	34.0084	107.0607	9.10	7.70
30977	112544.52	34.0036	107.0603	8.70	7.40
31077	132733.31	33.9877	107.0699	8.30	10.20
40577	193431.13	34.0116	107.0356	8.90	8.30
41277	32503.26	34.0591	107.0357	10.10	3.50
41377	123952.13	34.0350	107.0218	10.60	6.40
42677	20820.67	34.0569	107.0308	8.80	6.10
42677	165608.00	34.0369	107.0554	8.80	7.20
42777	121556.32	34.0107	107.0592	9.10	8.00

DATE	ORIGIN TIME	LATITUDE	LONGITUDE	REFLECTION DEPTH	ITERATIVE DEPTH
42877	105910.81	34.0489	107.0505	9.10	5.40
42877	110331.25	34.0445	107.0509	9.70	5.90
50677	104318.52	34.1766	106.9256	10.80	5.60
51277	61914.45	34.0747	107.0318	10.20	0.00
60177	64045.08	34.0043	107.0575	9.10	6.40
60277	65024.36	34.0118	107.0635	8.90	8.00
60277	173008.27	34.0027	107.0612	10.20	6.30
60377	34901.59	34.0097	107.0602	9.30	7.70
60377	193829.82	34.2280	106.8883	4.30	12.50
60377	204502.97	34.2284	106.8973	8.60	11.00
60377	230119.24	33.9809	107.0094	9.20	7.40
60777	122528.61	34.0119	107.0534	9.40	6.80
60877	33223.37	34.1967	106.9304	4.80	11.90
60877	53029.67	34.0251	107.0524	8.10	10.80
61077	40444.94	34.0141	107.0620	9.20	8.00
71177	235234.88	34.1179	107.0364	10.50	6.30
71477	23402.03	34.1590	106.8814	7.20	5.30
71577	122625.73	34.0064	107.0611	7.50	8.50
71977	61654.87	34.1535	106.8721	9.30	4.30
72177	31227.43	34.0412	107.0448	8.30	0.00
72777	120730.54	33.9656	106.9443	8.00	0.00
72777	155315.12	34.0056	107.0568	7.90	0.00
72777	171729.49	34.1571	106.9072	9.60	0.00
72977	120722.72	34.1457	106.9045	9.10	0.00
81777	22020.68	34.2882	107.0497	8.10	7.80
81777	60319.97	34.1671	106.8721	7.30	6.70
81777	153722.00	34.2628	106.9233	7.10	5.70
81977	92822.91	34.0105	107.0613	10.30	8.40
82477	112235.90	34.0123	107.0512	9.60	7.80
82677	103258.00	34.0093	107.0599	9.20	8.50
83077	183728.97	34.0391	107.0013	6.20	2.40
90177	182002.11	34.0548	106.7526	3.00	3.00
90177	215848.71	34.0139	107.0456	10.00	7.50

DATE	ORIGIN TIME	LATITUDE	LONGITUDE	REFLECTION DEPTH	ITERATIVE DEPTH
91577	5335.40	34.0371	107.0595	8.20	7.70
91577	64517.00	34.3401	106.8883	6.20	0.50
91577	114334.47	34.3068	106.9246	9.40	0.40
91677	80408.23	34.0593	106.9885	8.70	0.00
92077	12008.81	34.0352	107.0511	7.30	10.10
92077	81923.32	34.1615	106.8804	5.00	3.80
92277	52127.96	34.3340	106.8907	7.70	5.30
92277	191916.59	34.3329	106.8897	7.70	11.30
101877	81632.86	34.0353	107.0603	8.10	7.70
111577	190241.73	34.1391	106.8857	9.90	5.50
111777	25417.59	34.3807	107.0541	7.00	11.10
111877	65812.49	34.4121	107.0703	12.40	0.90
111877	124249.40	34.3902	107.0540	6.70	3.30
120577	205719.47	34.4084	107.0783	7.10	5.50
121477	174833.18	34.0949	107.0234	2.50	4.60
121477	205727.46	34.2846	106.8770	7.50	12.50
121577	171540.41	34.3225	107.0596	7.50	11.20
122077	122118.72	34.0121	107.0556	7.80	6.40
122377	13739.40	34.0927	107.0444	10.50	8.90
122377	35144.35	34.3202	107.1322	11.60	0.00
10678	151237.02	34.4097	107.0465	7.60	0.01
10678	151237.02	34.4097	107.0465	8.50	0.01
11178	72247.55	34.0281	107.0682	6.90	4.50
11178	103919.18	34.0284	107.0054	6.90	4.60
11778	50501.02	34.3102	106.7201	7.10	10.70
11778	231421.22	34.3463	106.8731	7.00	8.15
11878	122432.84	34.1661	106.8587	7.50	4.50
11878	124942.99	34.1721	106.8656	5.10	4.60

Appendix 3

Appendix 3 contains the basic versions of the computer programs used in this study. Matrix manipulations and power spectrum determination (main program not included) used the IMSL subroutine package maintained by the N. M. Tech Computer Department as a source. A very brief description of each program will be given for each program.

REFIN.FOR. This is the basic least squares inversion program used for this study. It reads in the data (travel times, station locations epicenter locations and depths of focus), calculates the real and theoretical travel times of the S_zS reflection, calculates the epicentral distances, calculates the $\underline{A}$ matrix and calls the subroutine INVER.FOR for the inversion. Simple changes in calculating the $\underline{A}$ matrix and theoretical travel times are required for each different model used. Up to 50 unknowns and 300 data can be used.

```
TYP REFIN2.FOR
00100    C
00200    C
00300    C         TSS IS THE SXS TRAVEL TIME
00400    C         EPLONG IS THE EPICENTER LONGITUDE
00500    C         EPILAT IS THE EPICENTER LATITUDE
00600    C         DEPTH IS THE DEPTH OF FOCUS
00700    C         D ISTHW DIST.NCE FROM THE EPICENTER TOSTATION
00800    C         Z IS THEUNKNOWN
00900    C         DZ IS DELTA Z
01000    C         NUM IS THE NUMBER OF REFLECTIONS
01100    C         LONG IS THE STATION LONGITUDE
01200    C         LAT IS THE SAATION LATITUDE
01300    C         Z(1) IS THE DEPTH TO THE REFLECTOR
01400    C         Z(2), Z(3) IS THE S WAVE VELOCITIES
01500    C         Z(2) IS FOR THE UPPER LAYER
01600    C         Z(3) IS FOR THE LOWER LAYER
01700    C         DT IS DELTA T
01800    C         ZZZ IS THE CALCULATED DEPTH TO THE REFLECTOR
01900    C
02000             DIMENSION A(300,50),DEPTH(300), Z(50),
02100            1DT(300),XT(50),YT(50),TSS(300),EPLONG(300),EPLAT(300),
02200            2DZ(50),ZZZ(300),COEFF(50),DT1(300),COR(50)
02300            3,DIST(300),VAR(50,50),TAO(50),AL1(400),AL2(400)
02400             COMMON/WORK1/MIN,SEC,RATEP,RONEP,DF,PARVL,SS,RONST,
02500            1RATST
02600             REAL LAT(300),LONG(300)
02700             COMPLEX NAME
02800             INTEGER STAT(30),ST(300),P
02900             TAN(A)=SIN(A)/COS(A)
03000             IIII=1
03100    9900     CONTINUE
03200             IF(IIII.EQ.0)STOP
03250             Z(1)=9.2
03300             Z(2)=3.35
03400             Z(3)=3.35
03500             OPEN(UNIT=01,FILE='STAT.DAT')
03600             DO 2 I=1,50
03700             READ(1,1,END=3) STAT(I),YT(I),XT(I),COR(I)
03800    2        NN=I
03900    1        FORMAT(A2,2X,F7.4,1X,F8.4,7X,F4.2)
04000    3        CONTINUE
04100             CLOSE(UNIT=01)
04200             TYPE 9989
04300    9989     FORMAT('0TYPE DATA FILE NAME ')
04400             READ(5,9988)NAME
04500    9988     FORMAT(2A5)
04600             WRITE(5,63)
04700    63       FORMAT('0WRITE P AND SIG')
04800             READ(5,*)P,SIG
04900             XX=(19.20-Z(1))*2.
05000             OPEN(UNIT=01,FILE=NAME)
05100             NUM=1
05200    67       READ(1,4,END=11)MNTH,IDT,IYR,IHR,MIN,SEC,EPLAT(NUM),
05300           1EPLONG(NUM),DEPTH(NUM),PARVL,SS,ST(NUM)
05400    4        FORMAT(3I2,1X,2I2,F5.2,1X,F7.4,1X,F8.4,1X,F4.1, 1X,
05500           1F5.2,1X,F4.2,1X,A2)
05700    16       FORMAT('0DATE  '3(I2,1X)'   TIME IS  'I2':'I2)
05800             STAT(NN+2)=40
05900             DO 7 I=1,NN+2
06000             IF(ST(NUM).EQ.STAT(I)) J=I
06100    7        CONTINUE
06200             ST(NUM)=STAT(J)
06300             LONG(NUM)=XT(J)
06400             LAT(NUM)=YT(J)
06500             SS=SS-COR(J)
06600    C
06700    C        CALCULATE REAL TRAVEL TIME
06800    C
06900             IF(PARVL-SEC)14,12,12
07000    14       TTP=PARVL+60.0-SEC
07100             GO TO 13
07200    12       TTP=PARVL-SEC
07300    13       TSS(NUM)=TTP+SS
```

```
07500    C
07600    C       CALCULATE EPICENTRAL DISTANCE
07700    C
07800            DLTLON=(LONG(NUM)-EPLONG(NUM))*92.387
07900            DLTLAT=(LAT(NUM)-EPLAT(NUM))*110.9192
08000            DIST(NUM)=DLTLON*DLTLON+DLTLAT*DLTLAT
08100            DIST(NUM)=SQRT(DIST(NUM))
08200    C
08300            NUM=NUM+1
08400    5       GO TO 67
08500    11      CONTINUE
08600            NUM=NUM-1
08700            DO 39 IIJ=1,4
08800            DO 27 I=1,NUM
08900    C
09000    C       CALCULATE THEORETICAL TRAVEL TIMES
09100    C
09200    C
09300               CALL INCID(Z(2),Z(3),DEPTH(I),DIST(I),AL1(I),AL2(I),
09400           2XX,Z(I))
09500               G1=COS(AL1(I));G2=COS(AL2(I))
09600               TTH=(XX-DEPTH(I))/(Z(2)*G1)+(2.*Z(1))/(Z(3)*G2)
09625               IF(DEPTH(I).GT.10.)TTH=(10.)/(Z(2)*G1)
09665           2+(2.*Z(1)-(DEPTH(I)-10.))/(Z(3)*G2)
09700               DT(I)=TSS(I)-TTH
09800    27         CONTINUE
09900               AL11=AL1(1)*57.2967;AL22=AL2(1)*57.2967
10000               WRITE(3,68)Z(2),Z(3),DEPTH(1),DIST(1),AL11,AL22
10002    68         FORMAT('0'6(2X,F6.2))
10100               L=2
10200               M=NUM
10300    C
10400
10500    C
10600    C
10700               III=1
10800    C          CALCULATE THE A MATRIX
10900    C
11000    C
11100    C
11200               DO 32 I=1,NUM
11300               G1=COS(AL1(I));G2=COS(AL2(I))
11400               A(I,1)=-(XX-DEPTH(I))/(Z(2)*Z(2)*G1)
11500               A(I,2)=-(2.*Z(1))/(G2*Z(3)*Z(3))
11502               IF(DEPTH(I).GT.10.)A(I,1)=-(10.)/(Z(2)*Z(2)*G1)
11504               IF(DEPTH(I).GT.10.)A(I,2)=-(2.*Z(1)-(DEPTH(I)-10.))/(G2*
11506           2Z(3)*Z(3))
11600    32         CONTINUE
11700    C
11800    C
11900    C          WEIGHT THE A MATRIX AMD THE KNOWNS
12000    C
12100    C
12200               TAO(1)=.01
12300               TAO(2)=1.
12400               TAO(3)=1.
12500               DO 17 J=1,NUM
12600               DT(J)=DT(J)/SIG
12700               DO 17 I=1,L
12800               A(J,I)=A(J,I)/SIG
12900    17         CONTINUE
13000    C
13100    C
13200    C
13300    C          CALCULATE BIG R NUMBER FOR THE PREVIOUS RUN
13400    C
13500               IF(IIJ.EQ.1) GO TO 49
13600               RR=0.
13700               RNUM=NUM
13800               DO 51 I=1,NUM
13900    51         RR=DT(I)**2+RR
14000               RR=SQRT(RR/RNUM)
14100               WRITE(5,52) RR
14200    52         FORMAT('0THE BIG R NUMBER IS 'F10.5)
14300    49         CONTINUE
```

```
14400   C       INVERT THE A MATRIX WITH DT
14500   C
14600           CALL INVERT(A,DT,COEFF,M,L,P,TAO,VAR)
14700           DO 23 I=1,L
15000   23      DZ(I+1)=Z(I+1)+COEFF(I)
15100           DZ(1)=Z(1)
15200           WRITE(5,50) TSS(10),DT(10),(DZ(I),I=1,3)
15300   50      FORMAT(' '5(2X,F9.5))
15400   19      FORMAT('0'///' THE 'I2'  UNKOWN IS   '2F10.5)
15500           DO 40 I=1,L
15600   40      Z(I+1)=DZ(I+1)
16300   46      CONTINUE
16400           WRITE(3,43)
16500   43      FORMAT('0THE NEW PARAMETERS ARE. . . . .')
16600           WRITE(3,61)NAME
16700   61      FORMAT('0THE FILE NAME IS '2A5)
16800           WRITE(3,44)M,P
16900   44     FORMAT('0NUMBER OF DATA IS  'I3'  P NUMBER IS  'I3)
17000           YYX=XX/2.
17100           DO 20 I=1,3
17200   20      WRITE(3,19) I,YYX,Z(I)
17300           WRITE(3,45),(VAR(I,I),I=1,L)
17400   45     FORMAT('0THE STD DEVIATIONS ARE'//////3(2X,F10.5))
17500           WRITE(3,60)RR,(TAO(I),I=1,3),SIG,P
17600   60      FORMAT('0THE BIG R IS  'F6.3/' THE TAOS ARE  '
17700         23(1X,F4.2)/' SIGMA IS   'F4.2/' P IS    'I2)
17701           DO 71 I=1,NUM
17702   71      DT(I)=DT(I)*SIG
17705           WRITE(3,69)(DT(I),I=1,NUM)
17710   69      FORMAT('1THE DELTA TS ARE'40(10(2X,F6.3)/))
17750   39      CONTINUE
17800           WRITE(5,62)
17900   62      FORMAT('0IF YOU WANT TO STOP TYPE 0')
18000           READ(5,*)IIII
18100           GO TO 9900
18200           END
18300           SUBROUTINE INCID(V1,V2,DEPTH,DIST,AL1,AL2,D1,D2)
18400           TAN(A)=SIN(A)/COS(A)
18500           IF(DEPTH.GT.10.)GO TO 4
18600           AL1=0.
18700   2       AL2=ASIN(V2*SIN(AL1)/V1)
18800           X=(D1-DEPTH)*TAN(AL1)+(2.*D2)*TAN(AL2)
18900           IF(X.GT.DIST)RETURN
19000           AL1=AL1+0.005
19100           GO TO 2
19150   4       AL1=0.
19200   3       AL2=ASIN(V2*SIN(AL1)/V1)
19250           X=10.*TAN(AL1)+(2.*D2-(DEPTH-10.))*TAN(AL2)
19300           IF(X.GT.DIST)RETURN
19350           AL1=AL1+0.005
19400           GO TO 3
19800           END
@
```

INVER.FOR. This subroutine inverts the data and the A matrix using the eigen vector - value elimination procedure (Jackson, 1972). M is the number of data, L is the number of unknowns and P is the degrees of freedom. Also calculated are the variances and resolution matrix R.

```
00100           SUBROUTINE INVERT(A,DT,COEFF,M,L,P,TAO,VAR)
00200           DIMENSION A(400,50),C(50,50),R(50,50),D(400),VP1(50,
00300          150),WK(400),VP(50,50),E(400,50),UP(400,50),H(50,400),
00400          2DT(400),COEFF(50),VAR(50,50),S(60,60),TAO(50)
00500           INTEGER P
00600           REAL LAMINV(50,50)
00620           DO341 I=1,L
00630           DO341 J=1,M
00640    341    A(J,I)=A(J,I)*TAO(I)
00700           MM=300
00800           LL=50
00900    C
01000    C       CALCULATE EIGEN VALUES
01100    C
01200         CALL VMULFM(A,A,M,L,L,300,300,C,LL,IER)
01300         CALL VCUTFS(C,L,LL,C)
01400         CALL EIGRS(C,L,1,D,VP1,LL,WK,IER)
01500         DO 14 I=1,L
01600         IF(D(L+1-I).LT.0.00) GO TO 354
01700         GO TO 14
01800      354 D(L+1-I)=0.0000
01900       14 CONTINUE
02100      132 FORMAT('0 EIGEN VALUES'///4(7 (2X,G9.2)/)//)
02200    C
02300    C       CALCULATE LAMBDA INVERSE
02400    C       REARRANGE EIGEN VALUES
02500    C       REARRANGE V VECTOR
02600    C       ALL ARE REARRANGED SO THAT THE SMALLEST EIGEN VALUE
02700    C       IS LAST.  IF THERE ARE ANY NEGATIVE EIGEN VALUES
02800    C       BECAUSE OF ROUNDOFF ERROR THESE ARE SET TO ZERO.
02900    C
03000         DO 133 I=1,L
03100      133 LAMINV(I,I)=1./SQRT(D(L+1-I))
03200    1       CONTINUE
03220           WRITE(3,556)
03240    556    FORMAT('0'////)
03300           WRITE(3,132),(LAMINV(I,I),I=1,L)
03400         DO 134 J=1,L
03500         DO 134 I=1,L
03600      134 VP(I,J)=VP1(I,L +1-J)
03700    2       CONTINUE
04100      135 FORMAT('0'///4(7 (2X,G9.2)/)//)
04300    C
04400    C                       INVERT
04500    C
04800          CALL VMULFF(A,VP,M,L,P,300,LL,E,MM,IER)
04900         CALL VMULFF(E,LAMINV,M,P,P,MM,LL,UP,MM,IER)
05000         CALL VMULFF(VP,LAMINV,L,P,P,LL,LL,C,LL,IER)
05100         CALL VMULFP(C,UP,L,P,M,LL,MM,H,LL ,IER)
05200    4      CONTINUE
05300         CALL VMULFF(H,DT,L,M,1,LL,300, COEFF,LL,IER)
05350           DO 557 I=1,L
05375    557    COEFF(I)=COEFF(I)*TAO(I)
05400    C      WRITE(3,455),(COEFF(K),K=1,LL)
05500    C  455 FORMAT('0THE CHANGES TO THE UNKNOWNS ARE'///3(2X,F10.5)/)
05600    C
05700    C       CALCULATE VARIANCES
05800    C
05900           CALL VMULFP(H,H,L,M,L,LL,LL,VAR,LL,IER)
06100           DO 20 I=1,L
06102    20     VAR(I,I)=SQRT(VAR(I,I))
06200    C       CALCULATE R MATRIX
06300    C
06400         CALL VMULFP(VP,VP,L,P,L,LL,LL,R,LL,IER)
06500         WRITE(3,8),((R(I,J),J=1,3 ),I=1,3 )
06600       8 FORMAT('0THE R MATRIX IS . . .'///5(3 (2X,G9.2)/)//)
06700    C
06800    C       CALCULATE LITTLE R NUMBER
06900    C
07000         DO 16 I=1,L
07100         RR=0.
07200         R(I,I)=R(I,I)-1.
07300         DO 17 J=1,L
07400      17 RR=RR+R(I,J)**2
07450    16     CONTINUE
07500    C    16 WRITE(3,18),I,RR
07600       18 FORMAT('0 THE LITTLE R NUMBER('I2') IS...' 2X,F7.4)
08200    RETURN
```

REFIN.FOR. This main program calculates using REFLP.FOR the areal location of reflection points either assuming a depth to interface or a depth of focus. The reflection point can then be plotted using SUBPL.FOR which uses the COMPLT subroutines maintained by the N. M. Tech Computer Department. SUBPL.FOR also plots a map of the local area including selected stations. SUBPLT.FOR can easily be converted to plot epicenters and the points of interest by simply in putting (FLAT,FLONG) coordinates.

```
TYP REFIN.FOR
01600            DIMENSION DEPTH(400),D(400), Z(50),
01700           1DT(400),XT(50),YT(50),TSS(400),SSLONG(400),SSLAT(400),
01800           2DZ(50),ZZZ(400),DTI(400),COR(50)
01900              COMMON/WORK1/MIN,SEC,RATEP,RONEP,DF,PARVL,SS,RONST,
02000           1RATST
02100              REAL LAT(400),LONG(400)
02200              INTEGER STAT(30),ST,P
02900              TAN(A)=SIN(A)/COS(A)
03000              CALL INITAL(22)
03200    C
03300    C
03400    C         IS THE DATA TO BE READ OFF DATA.DAT, OR IS IT TO BE
03500    C         COMPUTED?
03600    C
04200              OPEN(UNIT=01,FILE='STAT.DAT')
04300              DO 2 I=1,50
04400              READ(1,1,END=3) STAT(I),YT(I),XT(I),COR(I)
04500    2         NN=I
04600    1         FORMAT(A2,2X,F7.4,1X,F8.4,7X,F4.2)
04700    3         CONTINUE
04800              WRITE(5,12)
04900    12        FORMAT(' TYPE 0 FOR INVERT ONLY'/
05000           1'       1 FOR PLOT AND INVERT'/'       2 FOR PLOT ONLY'
05100           2/'       3 FOR TRAVEL TIMES ONLY...NO PLOT OR INVERT')
05200              READ(5,*)IJK
05250              CALL FACTOR(.9)
05300              CLOSE(UNIT=01)
05400              OPEN(UNIT=01,FILE='REFLT.DAT')
05500              DO 5NUM=1,390
05600              READ(1,4,END=11)MNTH,IDT,IYR,IHR,MIN,SEC,RATEP,
05700           1RONEP,DEPTH(NUM),PARVL,SS,ST
05800    4         FORMAT(3I2,1X,2I2,F5.2,1X,F7.4,1X,F8.4,1X,F4.1, 1X,
05900           1F5.2,1X,F4.2,1X,A2)
06000    C         WRITE(3,16),MNTH,IDT,IYR,IHR,MIN
05900           1F5.2,1X,F4.2,1X,A2)
06000    C         WRITE(3,16),MNTH,IDT,IYR,IHR,MIN
06100    16        FORMAT('0DATE  '3(I2,1X)'   TIME IS  'I2':'I2)
06200              DF=DEPTH(NUM)
06300              STAT(NN+2)=40
06400              DO 7 I=1,NN+2
06500              IF(ST.EQ.STAT(I)) J=I
06600    7         CONTINUE
06700              ST=STAT(J)
06800              RONST=XT(J)
06900              RATST=YT(J)
07000              SS=SS-COR(J)
07100              CALLREFLP(TSS(NUM),SSLONG(NUM),SSLAT(NUM),D(NUM)
07200           2,ZZZ(NUM),ANG)
07500              IF(SSLAT(NUM).LT.33.84.OR.SSLAT(NUM).GT.34.55) GO TO 999
7
07600              IF(SSLONG(NUM).GT.106.75.AND.SSLONG(NUM).LT.107.25)
07700           2WRITE(3,36)IYR,MNTH,IDT,ST,SSLONG(NUM),SSLAT(NUM),ZZZ(NUM)
07800           2,DF,DEPTH(NUM),IHR,MIN,PARVL
07900    9997      CONTINUE
07902             IF(SSLAT(NUM).LT.33.90.OR.SSLAT(NUM).GT.34.20)GOTO978
07904             IF(SSLONG(NUM).GT.106.75.AND.SSLONG(NUM).LT.106.84)
07906           2TYPE 976,IYR,MNTH,IDT,IHR,MIN,MIN,ST
07908    976     FORMAT('0'2(3(I2)2X),2X,A2)
07910    978     CONTINUE
08000    36        FORMAT(' '1X,I2,2X,I2,2X,I2,1X,A2,5F10.3,2X,I2,2X,I2
08010           2,2X,F4.1)
08100    C       2 WRITE(3,8)TSS(NUM),SSLONG(NUM),SSLAT(NUM),ZZZ(NUM)
08200    8         FORMAT(' THE REFLECTION TRAVEL TIME IS',2X,F6.2,2X,
08300           1'REFLECTINGAT',3(2X,F10.4))
09400              JJJ=NUM
09600    5         CONTINUE
09800              NUM=NUM-1;JJJ=JJJ-1
09900    11        CONTINUE
10000              DO 14 I=1,NUM
10100              SLAT=SSLAT(I);SLONG=SSLONG(I)
10200              JJJJ=I
10300              IF(IJK.EQ.3)STOP 3
10400              IF(IJK.EQ.1.OR.IJK.EQ.2)CALL SUBPL(SLAT,SLONG,JJJJ)
10500    14        CONTINUE
10600              CALL RSTR(0)
10700              NUM=JJJ
10800              IF(IJK.EQ.2) STOP
10850              STOP
```

```
@TYP REFLP.FOR
00100            SUBROUTINE REFLP(TTSS,RFLONG,RFLAT,DIST,ZZ,ANG)
00200            COMMON/WORK1/MIN,SEC,RATEP,RONEP,DF,PARVL,SS,RONST,RATST
00300            TAN(A)=SIN(A)/COS(A)
00400          DLTLON=RONST-RONEP
00500          DLTLAT=RATST-RATEP
00600          DDLONG=DLTLON*92.387
00700          DDLAT=DLTLAT*110.9192
00800          DISSQ=DDLAT**2+DDLONG**2
00850            IF(DISSQ.LT.0)TYPE *,MIN,SEC,RATEP,RONEP
00860            IF(DISSQ.LT.0) STOP 4
00900          DIST=SQRT(DISSQ)
01000          IF(PARVL-SEC)11,12,12
01100    11    TTP=PARVL+60.0-SEC
01200          GO TO 13
01300    12    TTP=PARVL-SEC
01400    13    TTSS=TTP+SS
01500          DISTSS=TTSS*3.485
01600    C
01700    C.....................CALCULATION OF REFLECTION POINTS.............
.........
01800    C
01900          RR=(DISTSS**2-DIST**2)/4.0
01950            IF(RR.LE.0.)TYPE *,MIN,SEC,RATEP,RONEP
01960            IF(RR.LE.0.)STOP 5
02000            ZZ=19.3
02100            DF=(ZZ-SQRT(RR))*2.
02200          SN=DIST/DISTSS
02300          ALPHA=ASIN(SN)
02350            ANG=ALPHA*57.29577951
02400          RLNTH=TAN(ALPHA)*(ZZ-DF)
02500          AB=DDLONG/DDLAT
02600          TN=ABS(AB)
02700          PHI=ATAN(TN)
02800          RDLAT=COS(PHI)*(DIST-RLNTH)
02900          RDLONG=SIN(PHI)*(DIST-RLNTH)
03000          RLAT=RDLAT/110.9192
03100          RLON=RDLONG/92.387
03200          IF(0.0-DLTLAT)1,2,3
03300    1     RFLAT=RATST-RLAT
03400          GO TO 10
03500    2     RFLAT=RATST
03600          GO TO 10
03700    3     RFLAT=RATST+RLAT
03800          GO TO 10
03900    10    IF(0.0-DLTLON)4,5,6
04000    4     RFLONG=RONST-RLON
04100          GO TO 20
04200    5     RFLONG=RONST
04300          GO TO 10
04400    6     RFLONG=RONST+RLON
04500       20 CONTINUE
04600            RETURN
04700            END
```

```
@TYP SUBPT.FOR
00100           SUBROUTINE SUBPL(FLAT,FLONG,KIJ)
00200         DIMENSION XX(100),YY(100),XT(100),YT(100),ST(100)
00300         REAL PTX(50),PTY(50)
00400           IF(KIJ.GT.1) GO TO 205
00500         NUM=12
00600         PTY(1)=34.50
00700         PTY(2)=34.5000
00800         PTY(3)=33.9167
00900         PTY(4)=33.9167
01000         PTY(5)=34.5000
01100         PTY(6)=34.5000
01200         PTY(7)=33.9167
01300         PTY(8)=33.9167
01400         PTY(9)=34.00
01500         PTY(10)=34.00
01600         PTY(11)=34.25
01700         PTY(12)=34.25
01800         PTX(1)=107.25
01900         PTX(2)=106.75
02000         PTX(3)=106.75
02100         PTX(4)=107.25
02200         PTX(5)=107.25
02300         PTX(6)=107.00
02400         PTX(7)=107.00
02500         PTX(8)=107.25
02600         PTX(9)=107.25
02700         PTX(10)=106.75
02800         PTX(11)=106.75
02900         PTX(12)=107.25
03000         DO201 I=1,NUM
03100         CALL TRNFM1(PTX(I),PTY(I))
03200         PTY(I)=(PTY(I)+20.0)/6.3492
03300         PTX(I)=(PTX(I)+62.5)/6.3660
03400     201 CONTINUE
03500           CALL PLOT(-3.,0.0,0)
03600           CALL MARKER(2)
03700           CALL PLOT(PTX(1),PTY(1),3)
03800         DO 202 I=2,NUM
03900         CALL PLOT(PTX(I),PTY(I),2)
04000     202 CONTINUE
04600         CALL PLOT(0.0,0.0,3)
04700         OPEN(UNIT=01,FILE='PLOTZ.DAT')
04800         READ(1,204) NUM
04900     204 FORMAT(I3)
05000         DO 200 I=1,NUM
05100         READ(1,206)ST(I),YT(I),XT(I)
05200     206 FORMAT(A4,2F8.4)
05300           CALL TRNFM1(XT(I),YT(I))
05400           XT(I)=(XT(I)+62.5)/(6.3660)
05500           YT(I)=(YT(I)+20.0)/(6.349)
05600           CALL PLOT(XT(I),YT(I),3)
05700           CALL PLOT(XT(I)-.1,YT(I)-.1,3)
05800           CALL PLOT(XT(I),YT(I)+.1,2)
05900           CALL PLOT(XT(I)+.1,YT(I)-.1,1)
06000           CALL PLOT(XT(I)-.1,YT(I)-.1,1)
06100           CALL SYMBOL(XT(I)+.2,YT(I)-.07,.14,ST(I),0.,3)
06200     200 CONTINUE
06300           CLOSE(UNIT=01)
06400   205     CONTINUE
```

```
86500          IF(FLAT.GT.34.46.OR.FLAT.LT.33.98) GO TO 207
86600           IF(FLONG.GT.107.25.OR.FLONG.LT.106.75)  GO TO 207
86700           CALL TRNFM1(FLONG,FLAT)
86800           XPLOT=(FLONG+62.5)/(6.3660)
86900           YPLOT=(FLAT+20.0)/(6.349)
87000           CALL PLOT(XPLOT,YPLOT,3)
87100           CALL MARKER(2)
87200           GO TO 209
87300    207    PRINT 208, FLAT,FLONG,KIJ
87400    208    FORMAT(' CAN NOT PLOT'//2(2X,F10.4)/' EVENT NUMBER'
87500         22X,I3)
87600    209    CONTINUE
87700           RETURN
87800          END
87900         SUBROUTINE TRNFM1(X,Y)
88000         TAN(A)=SIN(A)/COS(A)
88100         PI=3.14159265
88200         A=2.382585
88300      301 FN=6.8051586*A
88400         RM=6.8031292*A
88500         RM= EXP (RM)/1000.
88600         FN= EXP (FN)/1000.
88700      302 FLATO=34.076*2.*PI/360.
88800         FLONGO=106.943*2.*PI/360
88900         FLONG=X*2.*PI/360.
89000          FLAT=Y*2.*PI/360.
89100         X=FN*(FLONGO-FLONG)* COS(FLAT)
89200      304 Y=RM*(FLAT-FLATO)+(X**2* TAN(FLATO))/(2.*FN)
89300      305 RETURN
89400         END
@
```

Appendix 4.

Appendix 4 contains reproductions of 11 outstanding MEQ-800 seismograms and one LRSM record. All of the included records were used to qualitatively determine the predominate frequency content of the reflected and direct S-wave phases. Dates, origin times to the last minute and recording stations are also given.

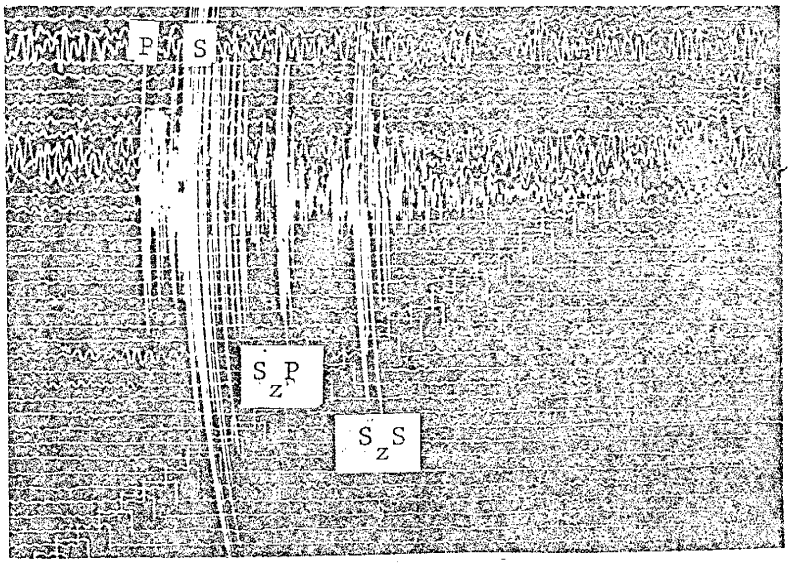

January 23, 1976
O. T. 02:53
Station WT

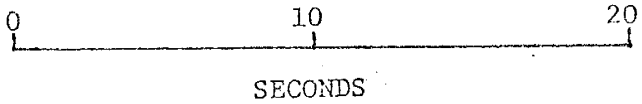

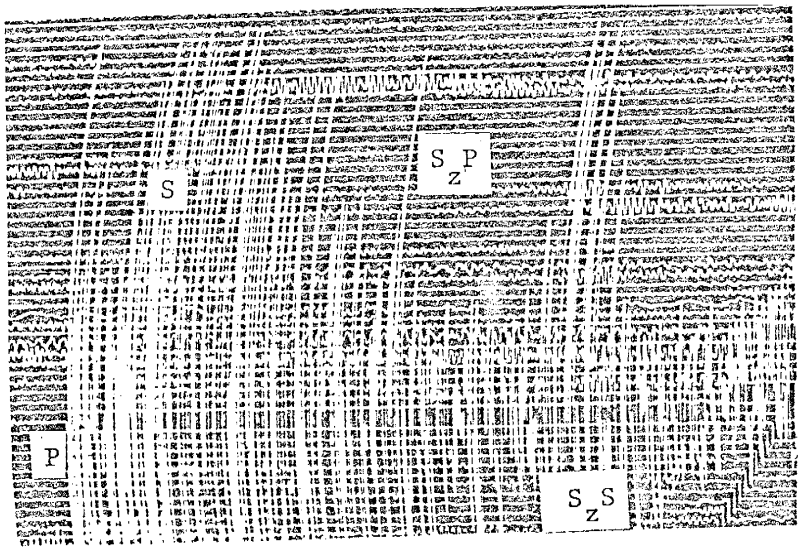

August 30, 1978
O. T. 22:53
Station WM
(Not located)

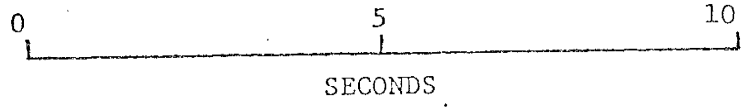

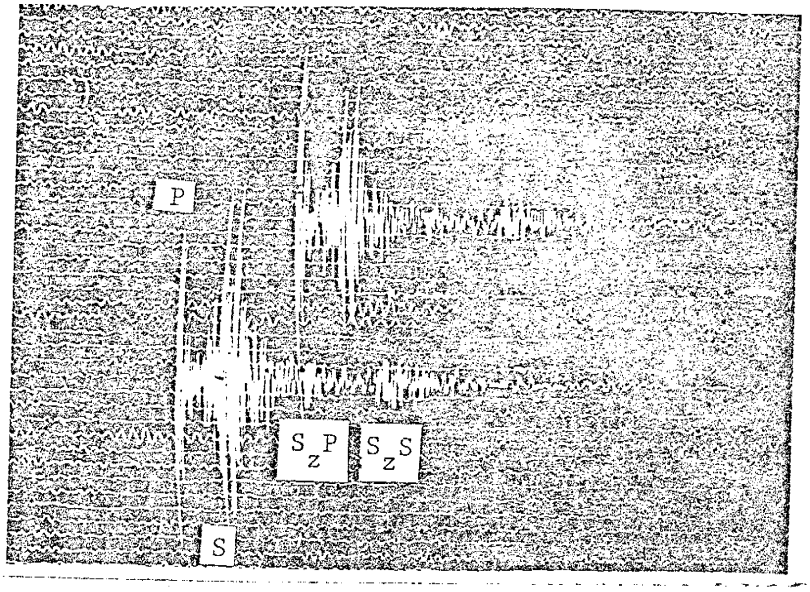

August 12, 1976
O. T. 00:51
Station WT

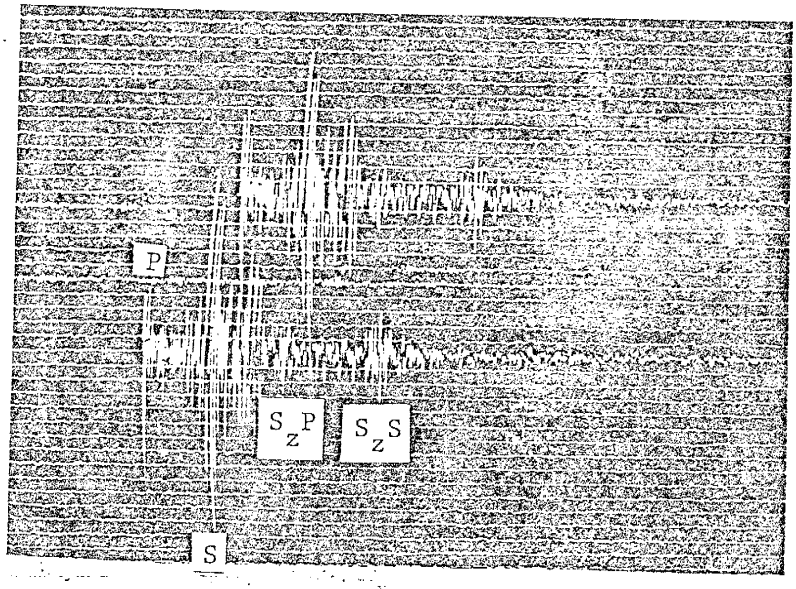

Station SC

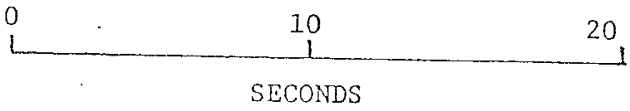

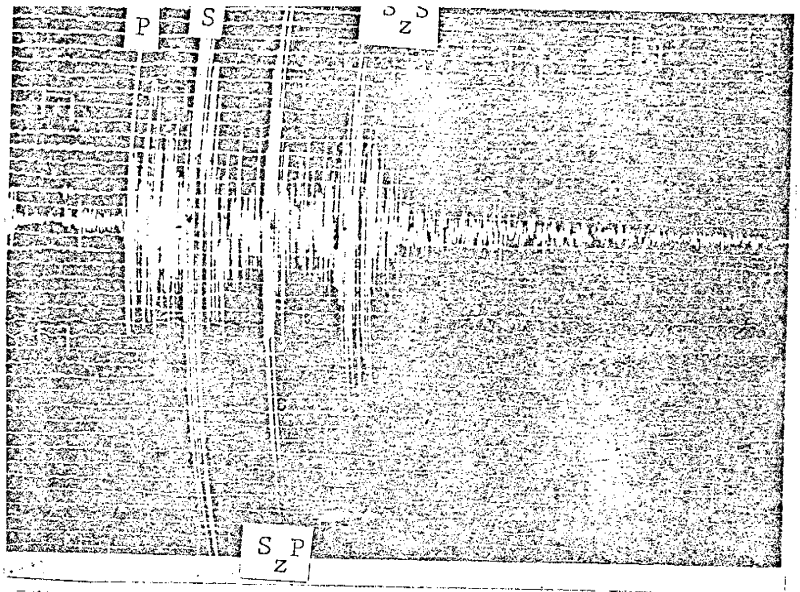

November 05, 1975

O. T. 22:28

Station CC

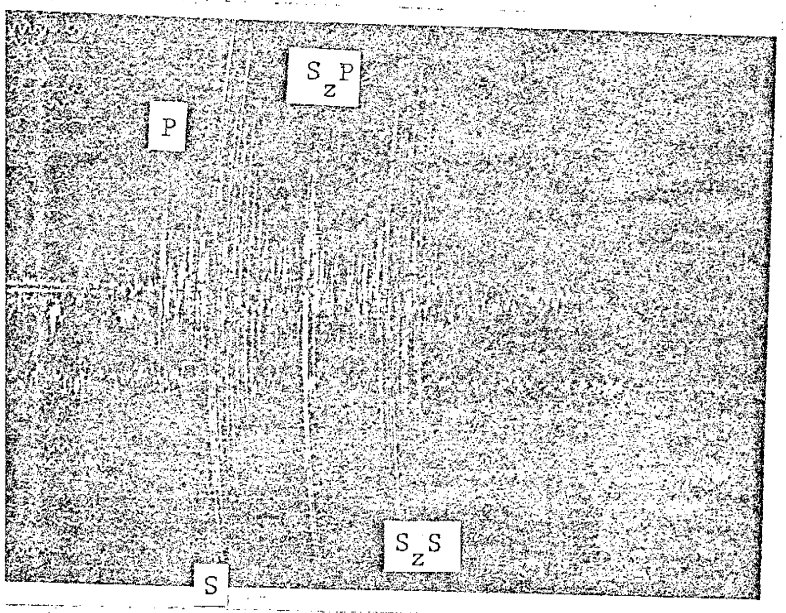

Station WT

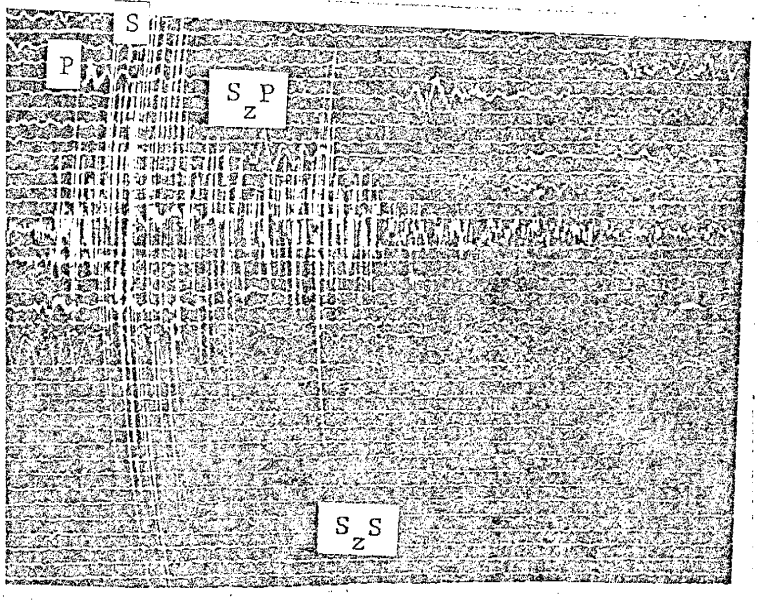

Station SC

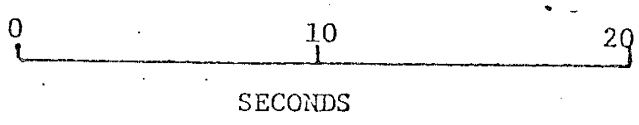

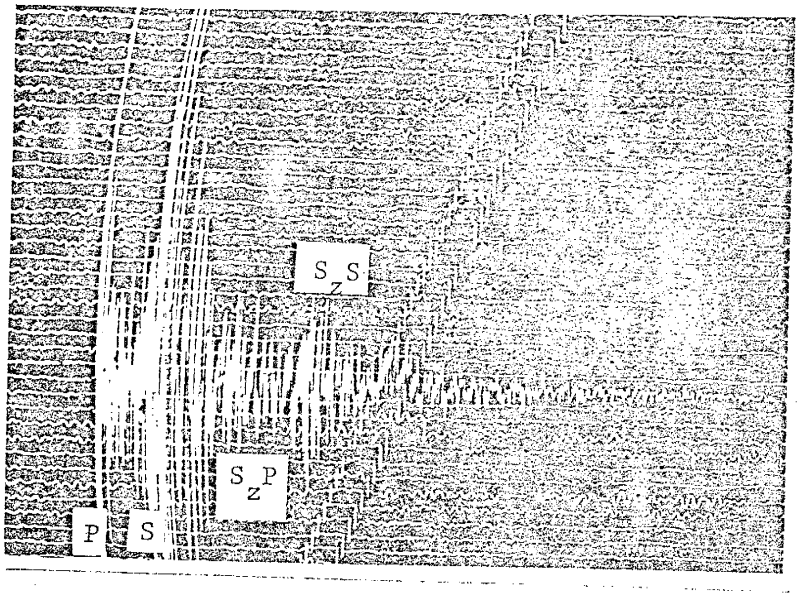

August 21, 1975
O. T. 03:44
Station WT

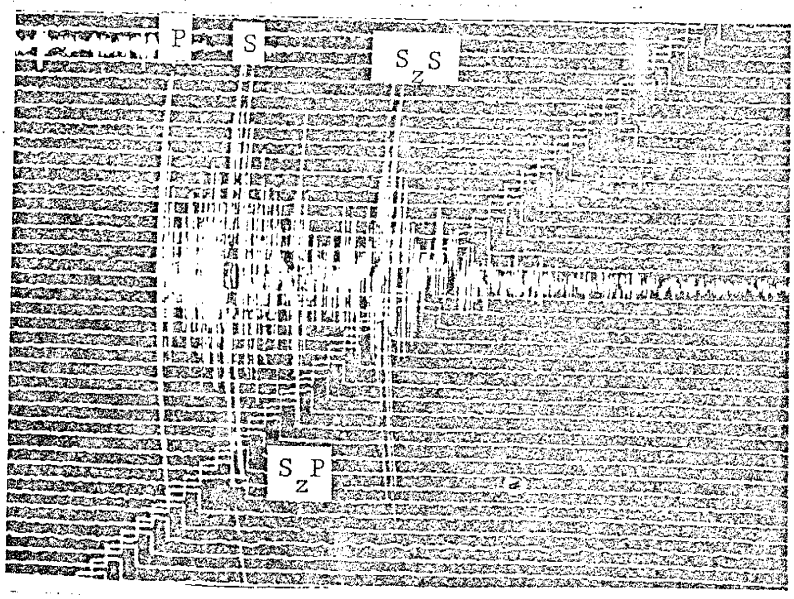

Station CC

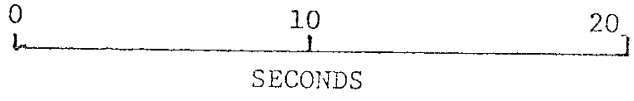

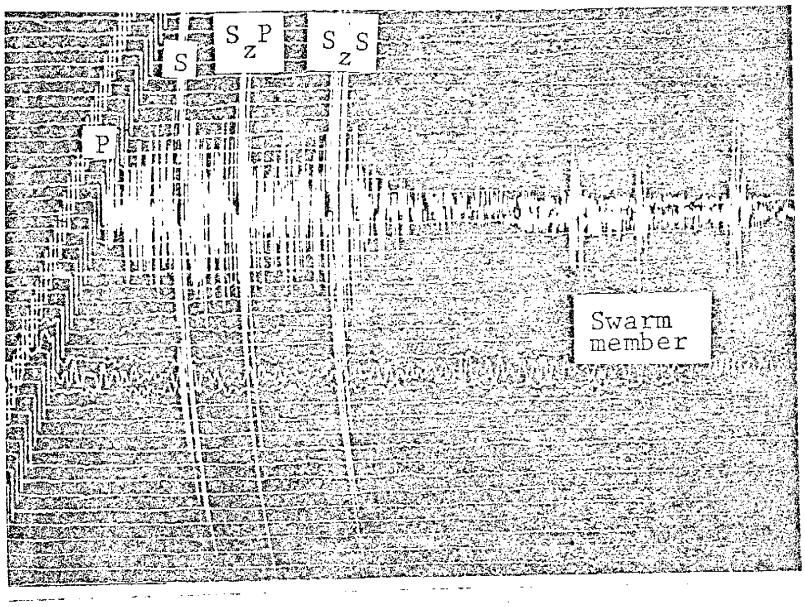

August 26, 1977
O. T. 10:32
Station CC

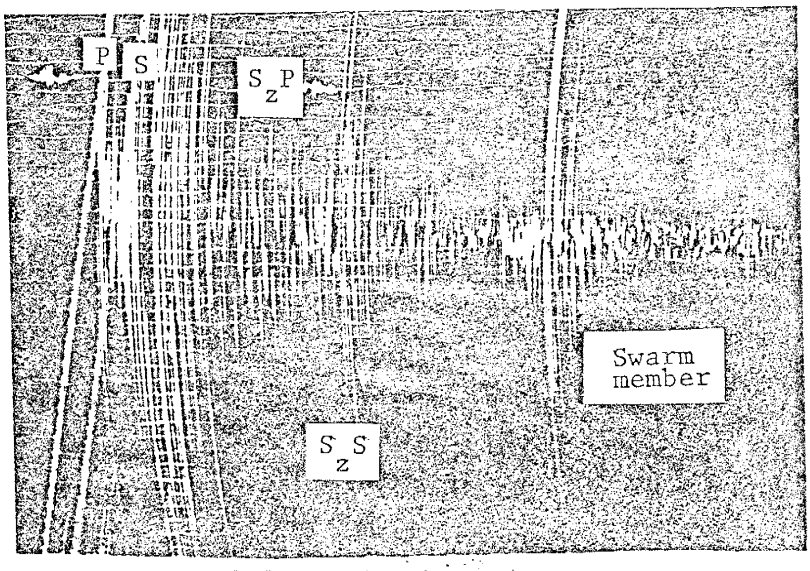

Station SC

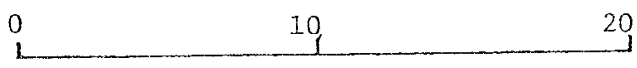

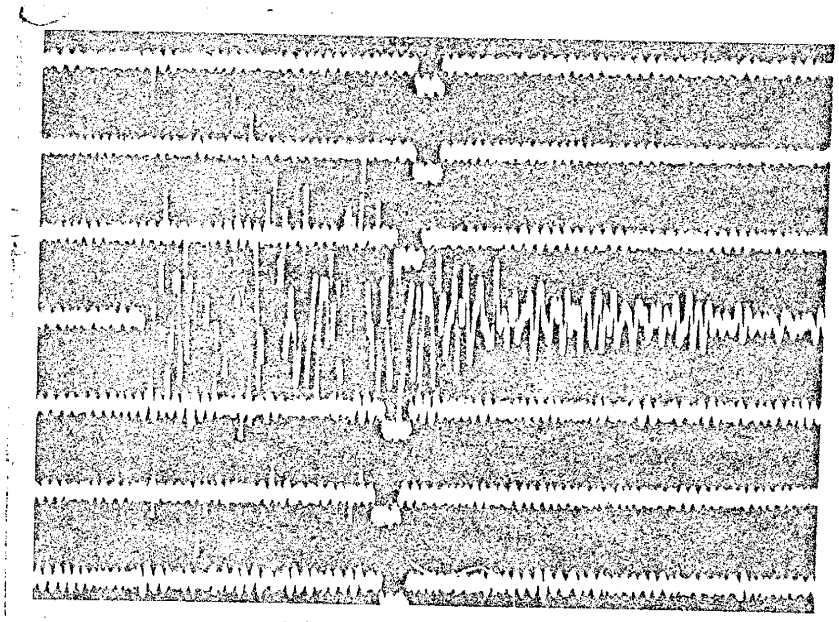

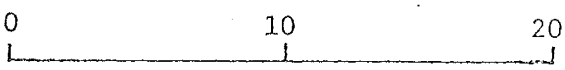

SECONDS

August 30, 1978
O. T. 22:53
SNM

This thesis is accepted on behalf of the faculty of the Institute by the following committee:

Allan R. Sanford

John Wm Schlaer

W. T. Budding

Wm C. Chapman

Date July 6, 1979